MIDWESTERN UNIVERSITIES RESEARCH ASSOCIATION

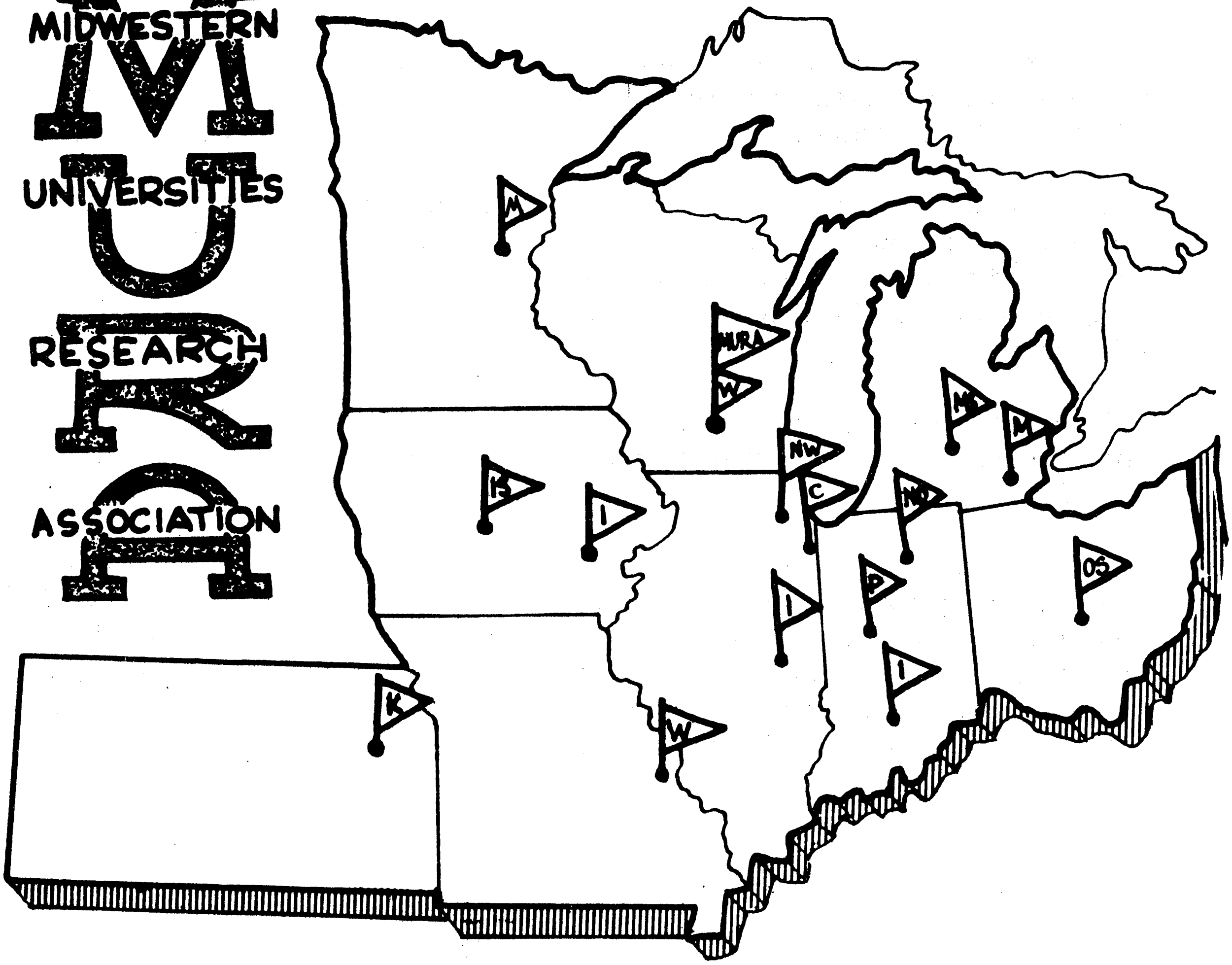

THE DESIGN OF PROTON LINEAR ACCELERATORS FOR ENERGIES UP TO 200 MEV

B. Austin, T. W. Edwards, J. E. O'Meara,
M. L. Palmer, D. A. Swenson, and D. E. Young

REPORT **NUMBER** 713

LEGAL NOTICE

Printed in USA. Price $5.00. Available from the

Clearinghouse for Federal Scientific and Technical Information
National Bureau of Standards, U. S. Department of Commerce
Springfield, Virginia

MURA-713
UC-28: Particle Accelerators and
High-Voltage Machines
TID-4500 (43rd Edition)

MIDWESTERN UNIVERSITIES RESEARCH ASSOCIATION[*]
P. O. Box 6, Stoughton, Wisconsin

THE DESIGN OF PROTON LINEAR ACCELERATORS FOR ENERGIES UP TO 200 MEV

B. Austin, T. erry W. Edwards, J. E. O'Meara,
M. L. Palmer, D. A. Swenson,[**] and D. onald E. dward Young

July 1, 1965

ABSTRACT

A study of proton linear accelerators of energy up to 200 MeV using drift tube loaded cavities resonant at 200 Mc is described. Such an accelerator is useful as an injector for a high energy synchrotron. Two computer programs have been used extensively in this study; one is used to calculate the resonant frequency and rf fields in the appropriate linear accelerator geometry, the other is used to calculate particle motion in the accelerator. From the field computational program a variety of resonant cavity configurations have been investigated, and an optimum structure has been chosen on the basis of minimizing the rf power costs and the structure length costs. Several optimized sets of parameters for a linear accelerator are given. More detailed studies were done on one of the sets of parameters including particle dynamics studies. Tables of drift tube dimensions are given. From the specification of parameters, mechanical engineering studies have been made to evolve a design which can be fabricated and from which realistic construction costs can be estimated. Some details of mechanical models constructed to test design features are given.

---

[*] AEC Research and Development Report. Supported by the U. S. Atomic Energy Commission through ANL by Subcontract 31-109-38-1707.

[**] Now at Los Alamos Scientific Laboratory, Los Alamos, New Mexico.

TABLE OF CONTENTS

FIGURES

FIGURES (continued)

I. INTRODUCTION

The study of proton linear accelerators of energy up to 200 MeV was initiated at MURA in 1959 at the suggestion of Dr. J. P. Blewett during a summer study session dealing with the acceleration of high intensity beams. It had been recognized even earlier[1] that there existed no fundamental limitation for the extension of the Alvarez rf structure up to at least these energies. The MURA studies were directed toward the use of the 200 MeV linac as an injector for a 10 BeV synchrotron. Such a linac is well suited as a high intensity injector. Linacs have high beam current capability, little difficulty in obtaining a beam external to the accelerator of good quality, and beam pulse lengths of sufficient duration so as to "fill" the synchrotron ring.

More recently the linac studies have been redirected towards a possible new injector for the Zero Gradient Synchrotron at Argonne National Laboratory. A set of suitable parameters has been selected for such a linac and more detailed design studies have been carried out, including preliminary engineering studies. This report contains some of the considerations that have gone into this study. Undoubtedly, further study will modify and expand some of the details of this report, but they are included so that others may benefit from the studies so far completed.

Studies are more useful when they can be implemented with an experimental modelling program formulated to test questionable features of the design. Three cavities have been constructed at MURA. The first consists of one-half unit cell adjustable for all energies in the linac so as to allow precise frequency and field measurements to be made. The second cavity is a complete unit cell accommodating energies from 5 to 130 MeV capable of operation at the highest power levels anticipated in the design. The third cavity is a three-unit cell model at 200 MeV also allowing operation at full power. Some of the mechanical engineering problems associated with the fabrication of these cavities have been included in this report as they bear directly upon the design of 200 MeV linacs.

A computer program for the calculation of fields in appropriate linac geometry is a valuable aid in linac design. At MURA such a program was initiated in the spring of 1960 following techniques used by Professor J. Van Bladel[2] and by late 1961 was operational. This program called MESSYMESH is described as well as the application of the program for linac design. A large number of computer runs for a variety of linac geometry at many energies have been made with this program.

A particle dynamics program has also been used in the study. This program called PARMILA treats the phase and radial motion of the particles in the linac and allows the motion of the protons to be analyzed when they are subjected to the rf fields between drift tubes and the focusing action of the quadrupoles in the drift tubes. Such a program is necessary so that the linac design can be investigated being cognizant of beam quality and beam loss.

The use of these computer programs has allowed a suitable set of parameters to be selected for three possible linac designs; two being linacs for high beam current, short duty factor injector application, and a third for smaller beam current, larger duty factor application, possibly as the low energy portion of a linear accelerator meson facility. The parameter selection was made on the basis of optimization with respect to power and length costs and with due consideration to accelerating gradients, reliability, mechanical feasibility, and other restrictions to be enumerated more fully. One of these sets of parameters was selected as being more suitable as a new injector for the Zero Gradient Synchrotron. A more detailed design was made for this choice including drift tube tables, mechanical engineering design, and a particle dynamics study.

II. COMPUTER PROGRAMS

MESSYMESH Program

The mathematical details of the field computational program, MESSYMESH,[3] are summarized in Appendix A.

For ϕ-independent transverse magnetic modes, in linac-type geometry, Maxwell's equations reduce to

$$\frac{\partial^2 F}{\partial r^2} - \frac{1}{r}\frac{\partial F}{\partial r} + \frac{\partial^2 F}{\partial z^2} + k^2 F = 0$$

where $F = r H_\phi$, and $k = \omega/c$. F is chosen so that the boundary conditions are simple. The solution of this equation is written in terms of an eigenfunction expansion; the eigenvalue is calculated from a variational principle. A convergent iterative process is possible with each new eigenvalue giving a better value of F. For digital computation, these equations are reduced to finite difference relations and the calculation carried out over a mesh defined by the linac unit cell as shown in Fig. 1. The solutions are obtained by a (over) relaxation process which treats the boundary conditions exactly, and which neglects (as error terms) only quantities which vanish as the discreteness of the eigenfunction vanishes.

The field values calculated by MESSYMESH are normalized both with respect to the field intensity and with respect to the physical dimensions of the geometry. From these field values auxiliary electromagnetic quantities may be calculated which are useful in linac design. These quantities include the energy stored per unit volume, the power lost to the cavity walls per unit area, the Q, the average axial accelerating field, the shunt impedance, the transit

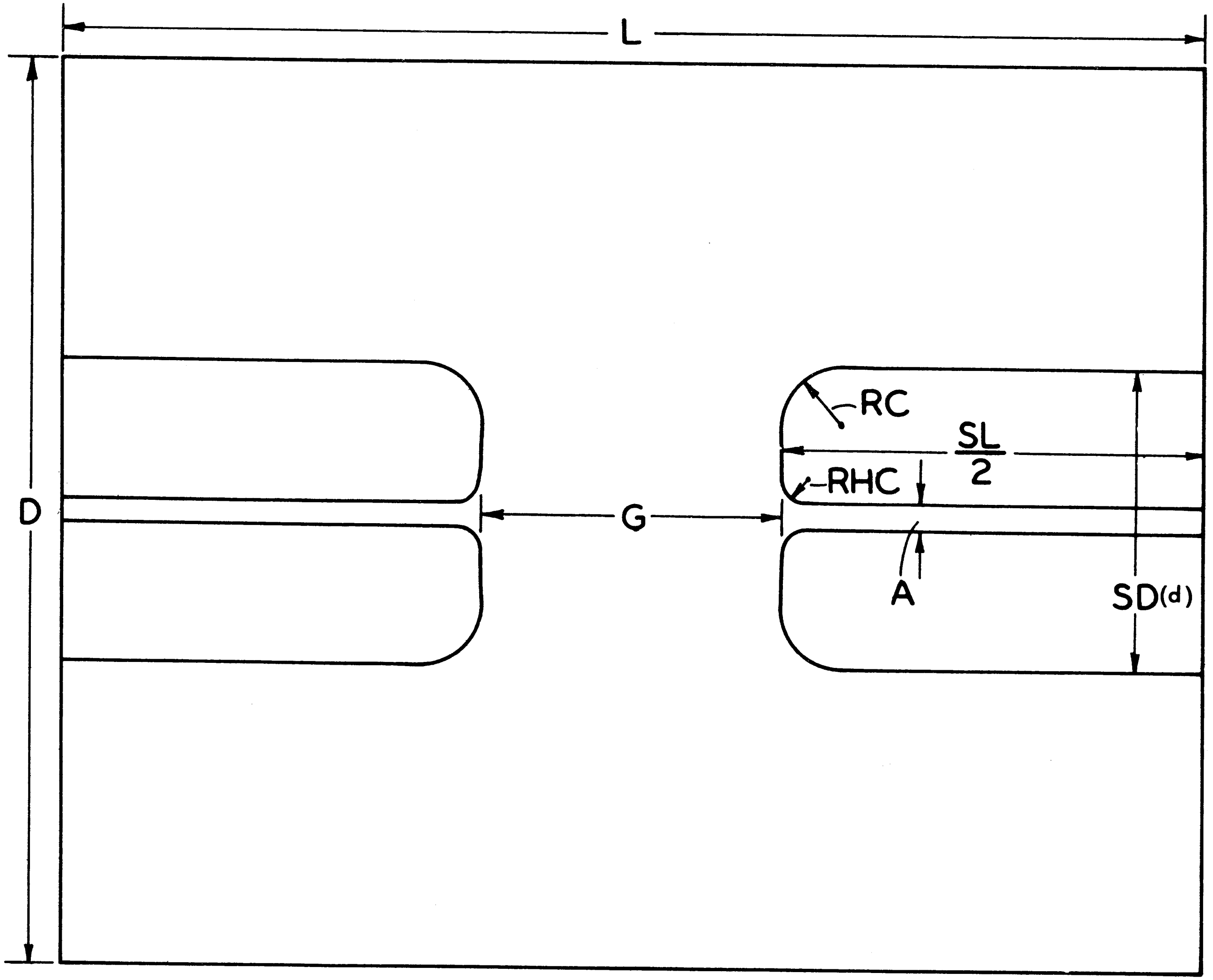

Fig. 1 Unit Cell Geometry (Cylindrical Drift Tube)

time factor, and the coupling coefficient. To allow more extensive use of these quantities, the results of MESSYMESH for a single description of the linac cavity geometry have been renormalized and summarized on a single page by another computer program called SUMMARY to be described.

A large repertoire of geometries have been calculated with MESSYMESH and the results retained on magnetic tape in an easily accessible form so as to permit subsequent use as initial trial eigenvectors for new geometry specifications. A good initial trial eigenvector can considerably reduce computing time. These stored results can also be used for an investigation of field gradients or any other problems which later become apparent.

The program has been developed so that greatest accuracy is achieved for cylindrical-shaped drift tubes with end caps of rounded corners and with bore holes (Fig. 1). In order to investigate drift tube shapes other than this, another computer program has been written which allows drift tubes of arbitrary shape. Several other drift tube shapes have been investigated with this program including drift tubes of ellipsoidal shape. Some results of this investigation are given in Section III of this report. Since for this structure there appeared to be little gain in a more complicated drift tube shape with the added fabrication complexity, this program has not been extensively developed in favor of greater effort on improvements to the MESSYMESH program.

The input to MESSYMESH includes the specification of the geometry from which the frequency and fields are calculated. Currently integral mesh dimensions are required which imposes a restriction on the physical dimensions as integral multiples of the mesh dimension. For a specified frequency, interpolation is necessary between runs differing in one of the geometry variables by a mesh dimension. In order to be able to run each unit cell in a cavity at a fixed frequency, it would be desirable to not be limited to an integral mesh unit. This program limitation is being removed.

Although it is very difficult to be absolutely certain of the accuracy of any finite difference calculation, approximate error bounds have been established on the basis of comparison of results obtained for the same or similar geometries from analytic and finite difference methods.[4] This comparison was done for nearly square or square corner drift tubes with the results:

Accuracy of Eigenvector Values	$\sim 1\,\%$
Accuracy of Eigenvalues	$< 0.1\,\%$
Accuracy of Auxiliary Quantities	$< 0.5\,\%$.

The frequency and field values have also been checked in the laboratory on a precision frequency cavity model, i.e., the one-half unit cell model. The results were in agreement with the computed values to better than 1% in the field values and better than 0.1 % in the frequency. Power loss measurements have been checked on the one-cell power cavity with no disagreements noted.

The MESSYMESH program is limited to geometry with azimuthal symmetry with the calculation performed in the meridian plane over one-quarter of the unit cell as shown in Fig. A-1. Drift tube stems, tuners, and asymmetry of the unit cell in an actual accelerating structure are not considered. It is possible to calculate corrections to the resonant frequency for these. In practice where rf contacts, bellows, loops, pump-out ports, etc. must be included in the design, it is necessary to make provisions in the design for fixed tuning. Under these circumstances, the MESSYMESH results are sufficiently accurate to allow drift tube tables and the cell-to-cell geometry to be specified. However, even more important at this stage is a program which will allow a variety of linac geometry to be investigated so that optimum geometry may be selected.

SUMMARY Program

A computer program (SUMMARY) has been written which reduces the MESSYMESH output to a single page which contains the essential information for a single description of the linac cavity geometry. This summary program converts the MESSYMESH output from mesh units to centimeters (or meters) and also normalizes the auxiliary computed quantities to an average axial electric field of one million volts per meter.

Figure 2 shows two summary sheets. At the top of the sheet is the geometric dimensions of the cell (see Fig. 1 for the definition of these dimensions). L is the cell length, D, the cavity diameter, G, the gap length, SL the drift tube length, SD (d), the drift tube diameter, RC, the radius of the drift tube corner, A, the diameter of the hole, and RHC, the radius of the hole corner. The resonant frequency of the cell is given next followed by the particle velocity and energy calculated from the geometry and the frequency.

In order to normalize to an average axial electric field of one million volts per meter, a normalization or scaling factor is calculated from the average axial electric field given by MESSYMESH. The stored energy per unit volume is normalized by the square of this factor. The power losses calculated by MESSYMESH are also normalized by the square of the normalization factor and are given on the summary sheet in both watts and watts per square meter for various sections of the cavity.

```
MURA LINAC CAVITY CALCULATIONS                          RUN NO. 30635

CYLINDRICAL DRIFT TUBE, WITH HOLE   (DIMENSIONS IN CENTIMETERS)
  L =  47.00          SL = 32.00        A = 3.0000          A/L =0.0638
  D =  88.00          SD = 16.00      RHC = 1.0000          G/L =0.3191
  G =  15.00          RC =  4.00

FREQUENCY = 199.09 MC/SEC.       BETA = .3121       ENERGY =  49.34 MEV


NORMALIZATION FACTOR            FACTOR =  572.28

AVERAGE AXIAL EFIELD             EO = 1.000            MILLION VOLTS/METER

STORED ENERGY/UNIT VOL.         W/V =     1.66         JOULES/CUBIC METER

POWER DISSIPATION                    WATTS             WATTS/SQUARE METER
  TO OUTER WALLS                PW1 =   3889.37        PW1 =   2993.29
  TO END PLATE                  PW2 =   2338.72        PW2 =   3845.23
  TO DRIFT TUBE PLATE           PW3 =   3476.84        PW3 =   5911.93
  TO DRIFT TUBE                 PW4 =   3574.52        PW4 =  16988.76

QUALITY FACTOR
  FOR LINAC CAVITY               Q1 =  77616.6
  FOR LAB CAVITY                 Q2 =  30338.4

SHUNT IMPEDANCE
  FOR LINAC CAVITY              ZS1 =  62.89           MEGOHMS/METER
  FOR LAB CAVITY                ZS2 =  24.58                 ''

RATIO                          ZS/Q =  810.26          OHMS/METER

TRANSIT TIME FACTOR               T = 0.8020

COUPLING COEFFICIENT              S = 0.0588

PRODUCT ZS1*T**2                ZTT = 40.449           MEGOHMS/METER

QUOTIENT ZTT/Q1                 Z/Q =  521.14          OHMS/METER

PEAK ELECTRIC FIELD            EMAX =  5.050           MILLION VOLTS/METER

PEAK FIELD LOCATION             5.53CM. FROM AXIS OF DRIFT TUBE
                                0.30CM. FROM END OF DRIFT TUBE

COST ESTIMATE  .00393 * A + 6.297 * B + 20.176 * C + D  MILLION $/MEV
```

```
MURA LINAC CAVITY CALCULATIONS                          RUN NO. 30470

CYLINDRICAL DRIFT TUBE, WITH HOLE   (DIMENSIONS IN CENTIMETERS)
  L =  47.00          SL = 31.00        A = 3.0000          A/L =0.0638
  D =  88.00          SD = 16.00      RHC = 1.0000          G/L =0.3404
  G =  16.00          RC =  4.00

FREQUENCY = 202.82 MC/SEC.       BETA = .3180       ENERGY =  51.36 MEV


NORMALIZATION FACTOR            FACTOR =  562.01

AVERAGE AXIAL EFIELD             EO = 1.000            MILLION VOLTS/METER

STORED ENERGY/UNIT VOL.         W/V =     1.60         JOULES/CUBIC METER

POWER DISSIPATION                    WATTS             WATTS/SQUARE METER
  TO OUTER WALLS                PW1 =   3829.46        PW1 =   2947.18
  TO END PLATE                  PW2 =   2283.04        PW2 =   3753.68
  TO DRIFT TUBE PLATE           PW3 =   3396.60        PW3 =   5775.48
  TO DRIFT TUBE                 PW4 =   3353.98        PW4 =  16406.04

QUALITY FACTOR
  FOR LINAC CAVITY               Q1 =  79291.5
  FOR LAB CAVITY                 Q2 =  30717.0

SHUNT IMPEDANCE
  FOR LINAC CAVITY              ZS1 =  65.34           MEGOHMS/METER
  FOR LAB CAVITY                ZS2 =  25.31                 ''

RATIO                          ZS/Q =  824.11          OHMS/METER

TRANSIT TIME FACTOR               T = 0.7786

COUPLING COEFFICIENT              S = 0.0652

PRODUCT ZS1*T**2                ZTT = 39.609           MEGOHMS/METER

QUOTIENT ZTT/Q1                 Z/Q =  499.54          OHMS/METER

PEAK ELECTRIC FIELD            EMAX =  4.901           MILLION VOLTS/METER

PEAK FIELD LOCATION             5.53CM. FROM AXIS OF DRIFT TUBE
                                0.30CM. FROM END OF DRIFT TUBE

COST ESTIMATE  .00401 * A + 6.295 * B + 19.797 * C + D  MILLION $/MEV
```

Fig. 2 Sample Summary Sheets

The wall losses (PW1) are taken for a cylinder of length L and diameter D. The end plate losses (PW2) are calculated for a conducting disk placed in the plane of symmetry at the center of the gap. The drift tube plate (in PW3) refers to a disk placed in the plane of symmetry of the drift tube. The surface area of only one plate is used in the calculation for the power loss in watts for the end plate and the drift tube plate. The surface area of one drift tube of length SL and diameter SD is used for the power dissipation to the drift tube in watts (PW4). The curvature of the corners and the drift tube hole is considered in the calculation of the drift tube power losses.

Both the quality factor (Q) and the shunt impedance (ZS) are evaluated for the linac cavity and the laboratory cavity. The former consists of an outer wall of length L and two half drift tubes while the latter is of length L/2 with an end plate and a drift tube plate supporting a half drift tube.

Neither the transit time factor nor the coupling coefficient are affected by the normalization process. Both of these quantities are used in particle dynamics studies (see Appendix B). The quantity ZT^2 (ZTT) is calculated as a cavity figure of merit (see Section III, this report). The ratio of the shunt impedance to the Q (ZS/Q or Z/Q) is useful for laboratory cavity measurements being independent of the power losses.

In order to calculate the peak electric field along the surface of the drift tube, the electric field is calculated at a finite number of points along the surface. A polynomial is fit to the points in the region where the electric field is the greatest. From this polynomial and through a curve smoothly process, the peak electric field is evaluated and its location computed. The electric field is normalized to an average axial field of one million volts per meter.

At the bottom of the summary sheet a cost estimate is given for the cell geometry. This formula is derived in Section III where the symbols are defined (Eq. (3-13)), i.e.,

$$\frac{1}{\Delta W}\left[\frac{C - C_f}{1 - \eta t}\right] - C_P\, I_B = C_P \left[\frac{k\, E_{SL}\, T}{Z T^2\, \alpha \cos\phi}\right] + C_L \left[\frac{\alpha}{E_{SL}\, T \cos\phi}\right] \qquad (3\text{-}13)$$

where $\alpha = E_{max}$ when $E_o = 1$ MV/m . The cost formula on the summary sheet is of the form

$$\text{Cost} = x\,A + y\,B + z\,C + D$$

and when $C_L = C_{L_1} + C_{L_2}/\beta$

$$x = \frac{T}{ZT^2\alpha}$$

$$y = \frac{\alpha}{T}$$

$$z = \frac{\alpha}{T\beta}$$

and

$$A = \frac{C_P\, k\, E_{SL}}{\cos\phi}$$

$$B = \frac{C_{L_1}}{E_{SL}\cos\phi}$$

$$C = \frac{C_{L_2}}{E_{SL}\cos\phi}$$

so that x, y, z are calculated from the values given on the summary sheet for the specified cell geometry. By substituting in values for A, B and C, a cost estimate can be determined.

Over 2000 cavity calculations for cylindrical drift tubes have been made with the MESSYMESH program near a frequency of 200 Mc. These runs cover a range of energy from 1 MeV to 250 MeV with at least one run for every integer value of L from 26 to 85 cm. About one-third of the total calculations have been done at 50, 100, 150 and 200 MeV. At these energies runs were made with a variety of cavity diameters, drift tube diameters, and corner radii. The results of these runs have been used to do more specific runs at the other energies.

In Fig. 3, the extent of the runs at 50, 100, 150 and 200 MeV is shown. In the first column the cavity diameter D is given in centimeters. In the second column different values of the corner radius are given for a specific D. The lines or dots indicate the range of drift tube diameters or diameter done with each D and RC. For each energy there is a set of information for drift tubes with and without bores. At 50 MeV the diameter of the hole is 3 cm. At 100 MeV most of the runs were done with a hole diameter of 4 cm, but some do have a diameter of 3. A hole diameter of 4 cm is used for all the runs with holes at 150 and 200 MeV.

In all cases the gap G of a cavity is chosen for resonance at approximately 200 Mc. Since the MESSYMESH program only accepts integer dimensions (at the present time) for the cavity dimensions, resonance varies around 200 Mc. Where the exact frequency is required, interpolation (or extrapolation) is required between two runs differing in the gap dimension G by one unit.

PARMILA Program

A particle dynamics program is a necessary "tool" in the design and study of linacs. Even though the rf structure may be adequately described, the cell

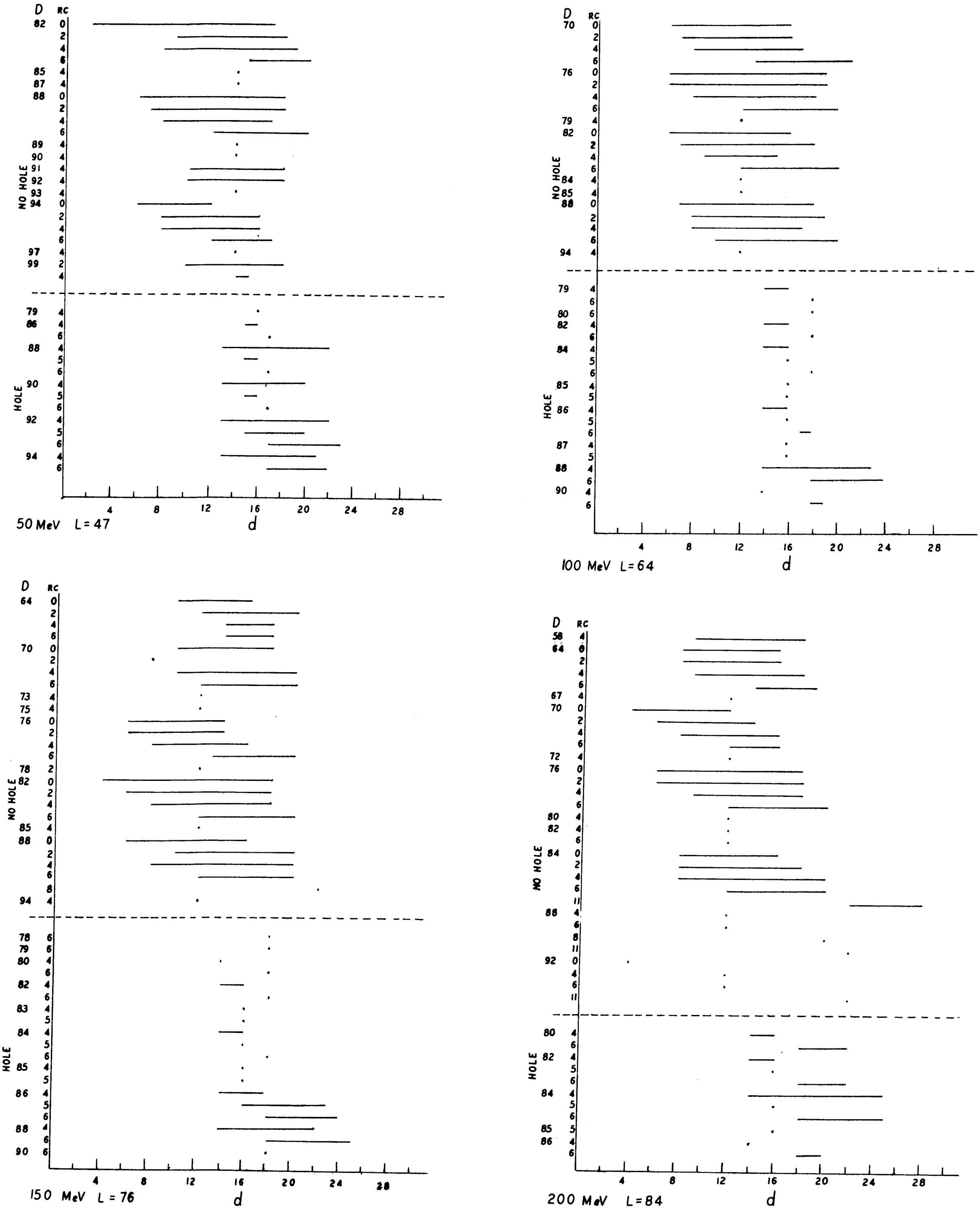

Fig. 3 RANGE OF COMPUTED GEOMETRY

lengths must be chosen on the basis of the behavior of the synchronous particle. However, even the rf structure must be chosen so that adequate space is allowed in the drift tubes for the incorporation of quadrupoles to provide the radial focusing. The quadrupole properties must be determined from particle dynamics considerations, i.e., the acceptance and emittance desired. Even after a linac is in operation, beam properties and linac operating conditions can be best understood with reference to particle dynamics.

It is possible to formulate a dynamics program in different ways depending somewhat upon the information desired and the computing time available. An adequate description of each particle should include the six coordinates, namely x, x', y, y', W and ϕ where x, x', y and y' are the transverse displacements and angles of the particle trajectories in two transverse directions, W is the energy and ϕ is the phase of the particle with respect to the rf accelerating voltage. Particles in the linac are subject to the quadrupole focusing-defocusing fields or the rf accelerating fields. These fields can be handled with various degrees of complexity ranging from a simple impulse approximation to a complete point-by-point description. Tracing particles in six coordinates through the complete fields for many cells in a linac becomes a prodigious task. Since the MESSYMESH program does provide the fields, a program has been written[5] (called LINDY) which traces individual particles through the rf fields in a single cell. Greater utility in linac design is achieved, however, if many particles can be sent through simple approximations to the fields so as to allow acceptance-emittance information to be obtained for a range of design parameters. Such a program called PARMILA has been used in this study and is described in Appendix B. The degree of approximation of such a program is continually being checked by other particle dynamics programs, some treating independently the transverse and phase (W, ϕ) motion, as well as the LINDY program, and also by actual measurements on operating linacs.

The PARMILA program proceeds by transforming the coordinates of a collection of particles through a set of transformations representing a linac of standard design, i. e., a linac composed of a set of resonant cavities, each containing a series of drift tubes, each of which contains a quadrupole focusing magnet. The energy gain for each cell is calculated at the center of the gap. The change in phase is calculated at the same place and in addition at the center of the drift tube to allow examination of the motion at that point. The transverse motion is broken down into a series of transformations. The particles are first transformed through one-half of a quadrupole magnet and then through a drift space. At the center of the gap the effect of the rf is calculated. Another transformation through a drift space and half of a quadrupole magnet completes the calculation of transverse motion for one cell. A special feature of the program is the fact that the phase and transverse motion are not treated independently, but are coupled. The nature of the coupling is described in Appendix B.

A useful feature of the program is the GENLIN subroutine which generates the cellular properties of the linac based on the dynamical properties of the synchronous particle. The information which must be supplied as input is, for example, the initial kinetic energy of the synchronous particle, the resonant frequency, the approximate final kinetic energy of each cavity, the accelerating rf field, the stable phase angle, and transit time information. Using this information the change in momentum for the synchronous particle is calculated and from the new momentum the cell length, particle velocity and energy can be obtained. Using the dynamical properties from the previous cell the next cell is generated until the final energy is reached. This information facilitates the calculation of a drift tube table as described in Section IV. The GENLIN subroutine also generates the cellular quadrupole strength and lengths.

PARMILA allows 500 particles to be sent through the described linac. The position of any two of the six coordinates may be plotted by the computer at the center of a given quadrupole so as to obtain the appropriate phase space plots. If particles become lost because their amplitudes are greater than the bore radius or because their energy is a given amount (usually 2 MeV) behind the synchronous energy, the number, place and reason for the loss is given as output. The coordinates of the particles which are not lost give emittance plots, and their original coordinates ascertained for cavity acceptance information. This allows an investigation of the optimum quadrupole focusing law and optimum operating gradients. Drift spaces and matching quadrupole between cavities can also be handled by the program. Proper cavity matching can be obtained by investigating the effects of drift spaces on the phase space. Section V shows examples of particle dynamics studies of a 200 MeV linac.

Attempts have been made to improve the accuracy of the program. Originally, expressions for the transit time factor and the radial impulse at the gap were used which were derived from the simplest approximation of the field in the gap, that is, a field which is uniform across the geometric length of the gap, and zero in the drift tube bore. However, MESSYMESH calculates a transit time factor based on the actual gap fields. This transit time factor is used in the revised program along with a correction factor for particles not having the synchronous velocity (see Appendix B). Further modifications of the PARMILA program are in progress.

III. SELECTION OF CAVITY GEOMETRY

The MESSYMESH program has been developed so that greatest accuracy is achieved for a geometry using cylindrical shaped drift tubes as shown in Fig. 1. In this case the geometry is specified by the seven dimensions: D, the cavity diameter, G, the gap length, L, the length of the unit cell, d, the drift tube diameter, R_c, the radius of curvature of the outer corner of the drift tube end, R_{hc}, the radius of curvature of the drift tube bore hole corner, and A, the diameter of the bore hole. Criteria must be established so that a selection can be made of these dimensions.

The considerations bearing on the choice of frequency have been discussed in the literature[6] and will be mentioned later. The frequency choice imposes a condition on the geometrical dimensions of the unit cell and in addition specifies the value of L when the energy of the unit cell is prescribed, i.e., $L = \beta \lambda$ in the 2π mode structure. The bore diameter A is a compromise between the desire for maximum transmission of particles consistent with the input beam properties and the need for a large value of the transit-time factor. The difficulty of including a focusing quadrupole in the early drift tubes increases greatly as A is made larger. R_{hc} is chosen to allow high fields to be maintained in the gap and without undue sacrifice in the transit-time factor.

It still remains to make a choice of the geometrical factors D, G, or G/L, d, and R_c consistent with the desired frequency after a decision has been reached for the frequency, A, R_{hc}, and the L under investigation. Further criteria on power losses, accelerating gradient, fabrication costs, and/or practical engineering considerations must be established.

In principle the field computational program allows calculation of an arbitrary drift tube shape. Shapes other than cylindrical have been investigated at several energies.[7] In particular, drift tubes of ellipsoidal shape have been compared with the cylindrical shape in regards to improved values for ZT^2 for economy of rf power. For an ellipsoidal shape with a greater value of ZT^2 and which allows a reasonable diameter bore hole, the maximum electric field on the drift tube surface at the same average axial accelerating field as for a cylindrical drift tube becomes quite large. If the ability of the structure to withstand large accelerating voltages against sparking is based on a peak surface field, then the average accelerating gradient must be reduced for ellipsoidal drift tubes to give the same guarantee against sparking as for cylindrical drift tubes. This results in increased length for a structure based on ellipsoidal drift tubes and the power cost saving is clearly offset by increased length costs.

For a drift tube contour which cannot be expressed analytically in terms of a few parameters, the problem of investigating optimum shape by normalizing to a fixed frequency becomes difficult for a computational program such as MESSYMESH. It is also difficult in such a case to generate a complete set of drift tubes for a single resonant cavity. Further, as the energy increases and correspondingly the drift tube length, a drift tube shape which would allow an internal quadrupole without an excessive surface field in general approaches a cylindrical shape. Finally, fabrication costs are less for a simple cylindrical shape where only a small length change allows resonance in each successively higher energy unit cell. For these reasons, the problem of investigating arbitrary drift tube shapes was not pursued exhaustively, but rather, efforts were concentrated on developing the greatest accuracy and usefulness in MESSYMESH for the cylindrical shape with rounded corners and a bore hole.

The first MESSYMESH runs were taken to develop resonance curves at particular energies of 50, 100, 150 and 200 MeV. Examples of such resonance curves are shown in Figs. 4, 5, 6, and 7. These curves represent choices of D, G (or g), d, and R_c for a particular L (determined from the frequency and energy) which will resonate at a frequency of 201.25 Mc. Most of the data do not include the effect of the bore hole. The bore hole has a small frequency effect and is shown by the dotted line in the figure.

Consider now the problem of making a selection of the geometry based on the economy of rf power.

The energy gain of the particles (ΔW) per length L is:

$$\frac{\Delta W}{L} = E_o T \cos \phi \tag{3.1}$$

where E_o is the peak axial accelerating field averaged over the length L, T is the longitudinal transit-time factor, and ϕ the stable phase angle. The rf power required for the structure is:

$$\frac{P}{L} = \frac{(E_o)^2}{Z} \tag{3.2}$$

where Z is the shunt impedance, so that the power required for energy gain ΔW is:

$$P = \frac{(\Delta W)^2}{ZT^2 \, L \cos^2 \phi} \tag{3.3}$$

For greatest economy of rf power, geometry must be selected to maximize ZT^2. Pursuing only this criterion in cylindrical drift tubes, however, results

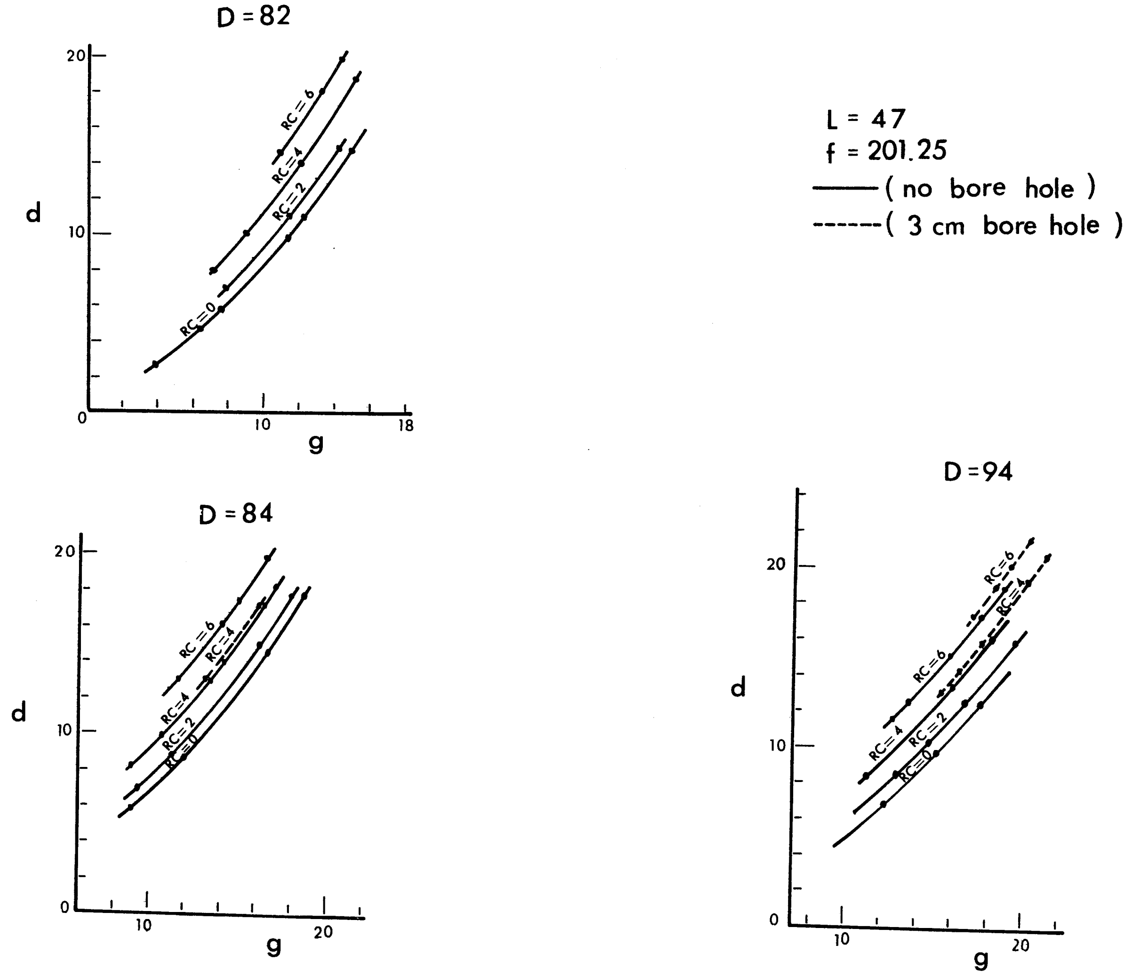

FIG. 4 Resonance Curves For Cylindrical Drift Tubes At 50 MeV

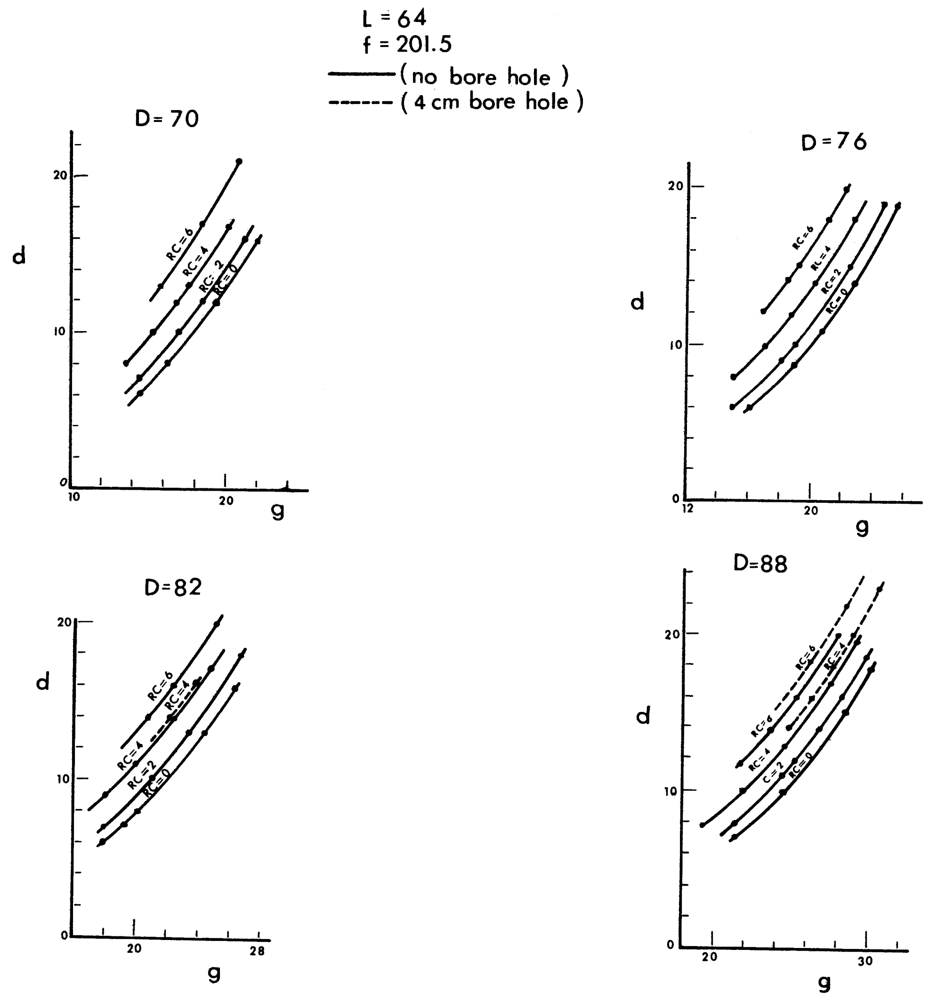

Fig. 5 Resonance Curves For Cylindrical Drift Tubes At 100 MeV

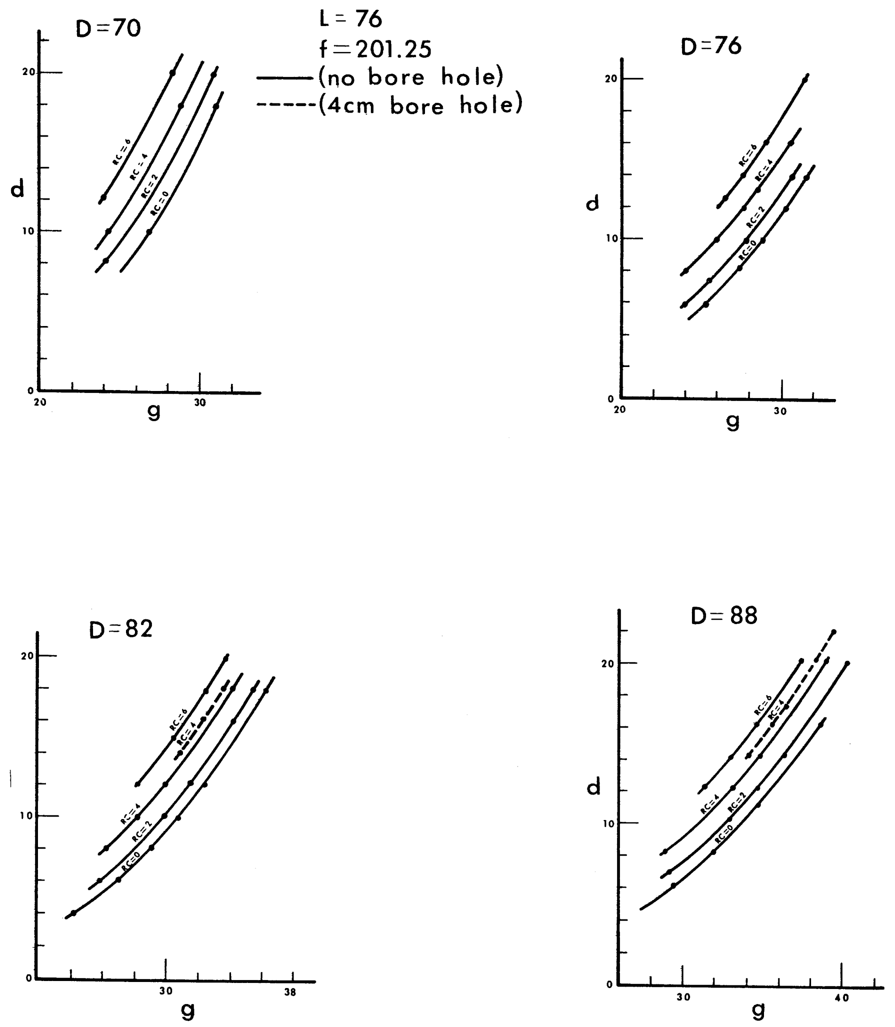

Fig. 6 Resonance Curves For Cylindrical Drift Tubes At 150 MeV

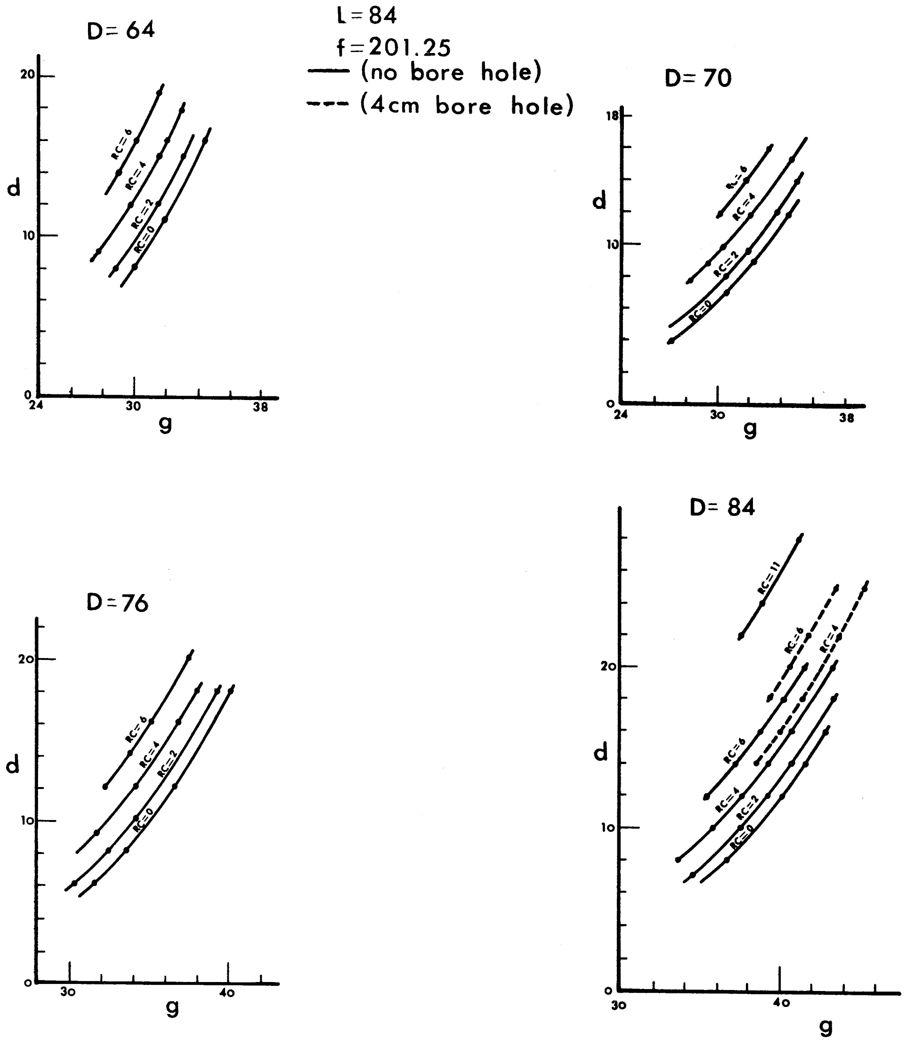

Fig. 7 Resonance Cuves For Cylindrical Drift Tubes At 200 MeV

in long drift tubes of small diameter. This type of drift tube results in a large value of the transit-time factor so that the increase in T^2 is greater than the decrease in Z. Such drift tubes are impractical because the peak fields on the surface become large and any saving in rf power costs are offset by added length costs to give reasonable assurances against sparking. A minimum drift tube diameter must always be specified in order to allow for the bore hole, quadrupoles, and cooling. Clearly a selection of cavity geometry consistent with fabrication and practical considerations must be made being cognizant of power and length costs.

It might be pointed out here that it has been assumed so far that the cost of power is less than the length costs in the linac. If this were not so, then properly one could reduce the accelerating gradient so as to use less power but increase the length and achieve the same acceleration of the particles. These considerations point out the need for a selection of geometry and accelerating gradients based on a cost optimization procedure.[8, 9, 10]

The cost formula for building and operating a linac can be written as

$$C = C_f + C_P\,P + C_{OP}\,Pt + C_L\,L + C_{OL}\,Lt \tag{3.4}$$

where C_f = fixed costs

C_P = power capital costs per unit of power

C_{OP} = power operating costs per unit of power per unit time

C_L = length capital costs per unit of length

C_{OL} = length operating costs per unit of length per unit time

P = total power

L = total length.

The fixed costs do not play a part in choosing structure.

The power capital costs in units of megawatts peak power have been evaluated by an examination of the rf power supply costs (including labor) of present operating linacs[11, 12] and by independently obtaining quotations from commercial suppliers. Estimates for present design purposes were based on a single 5 MW power amplifier tube capable of exciting each cavity.* Power costs range from 82 to 106 thousand dollars per megawatt. For the purpose of the discussion to be given here, a value of 94 (K$/MW) for C_P seems reasonable.

C_L includes the costs of the accelerator cavities, the vacuum system, the building costs which scale with the length of the linac, cavity-cooling costs, and some labor costs. Another part of C_L changes with the energy of the linac. This includes the drift tubes with quadrupoles, quadrupole power supplies, drift tube cooling, lump cavity tuners, and labor associated with these components. It is more difficult to evaluate these factors until a complete engineering design has been done. Some information is available from present operating linacs but different construction methods can influence these costs. A value for C_L of 16.5 thousand dollars per meter for the factors which do not depend on the energy has been used. If a drift tube cost, including the factors enumerated above, of $3000, is taken, C_L would then be $16.5 + 2/\beta$ (K$/MW) where $\beta = v/c$.

Attempts have been made to evaluate the operating costs broken down into those costs associated with the rf power supply (C_{OP}) and those associated with the length (C_{OL}), i.e., electric power costs, spare parts and tube replacement costs, vacuum and water pump replacement and repair, etc. It has been

---

*Using an RCA-7835 amplifier tube.

found that the ratio C_{OL}/C_L is approximately equal to the ratio C_{OP}/C_P. Setting this ratio equal to η, the cost formula becomes:

$$C - C_f = (1 + \eta t) \left[C_P P + C_L L \right] . \tag{3.5}$$

The choice of geometry to minimize $C - C_f$ is independent of η or t, and depends only on the quantity in the square bracket.

The power P per energy gain ΔW is given by:

$$\frac{P}{\Delta W} = \frac{E_o T}{Z T^2 \cos \phi} \tag{3.6}$$

and the length L per energy gain by:

$$\frac{L}{\Delta W} = \frac{1}{E_o T \cos \phi} . \tag{3.7}$$

The power has to be increased over a value computed from the theoretical value of Z to allow for losses on drift tube stems, tuners, end plates, rf contacts and spring rings, pump-out ports, and surface roughness and contamination. The power will thus be increased by a factor k which may have some value greater than about 1.2 depending upon how well one can estimate these practical losses and how conservative one chooses to design with respect to excess power. Reserve power must also be provided to allow for beam loading. For a beam of magnitude I_B, the excess power required for purely resistive beam loading will be $I_B \Delta W$ with a cost $C_P I_B \Delta W$. The cost formula thus becomes

$$\frac{C - C_f}{1 + \eta t} = \frac{C_P k E_o T \Delta W}{Z T^2 \cos \phi} + C_P I_B \Delta W + \frac{C_L \Delta W}{E_o T \cos \phi}$$

or

$$\frac{1}{\Delta W}\left(\frac{C - C_f}{1 + \eta t}\right) - C_P I_B = C_P\left(\frac{k E_o T}{ZT^2 \cos \phi}\right) + C_L \left(\frac{1}{E_o T \cos \phi}\right) \tag{3.8}$$

where the terms on the right are related to the choice of geometry. For any particular description of the geometry which specifies a value for Z and T, a cost can be calculated. It is also necessary however in linac design to specify an accelerating gradient, E_o. The value of E_o which minimizes the cost equation (3.8) is given by:

$$E_o = \left(\frac{Z C_L}{k C_P}\right)^{1/2} . \tag{3.9}$$

This value of E_o is called the optimum accelerating gradient and is the value of E_o which allows the power costs of the linac to equal the length costs. Substitution of (3.9) into (3.8) gives:

$$\frac{1}{\Delta W}\left(\frac{C - C_f}{1 + \eta t}\right) - C_P I_B = \frac{2}{\cos \phi}\left(\frac{C_P C_L k}{ZT^2}\right)^{1/2} \tag{3.10}$$

and in the case where an accelerating gradient given by Eq. (3.9) is possible, a proper criterion for the selection of geometry is to maximize ZT^2.

When E_o is calculated from (3.9) for many different descriptions of the unit cell geometry, it is found that in many cases the optimum E_o results in a value which appears to be in excess of that considered "safe" for reliable operation without sparking. Under these conditions then it is necessary to use a different criterion for determining the accelerating gradient. The basic problem is to choose some value of E_o just below the sparking limit; any smaller value will result in added cost and any larger value will result in unreliable operation. Unfortunately however, the basic mechanism of sparking at these frequencies is not well understood[13] so that one can precisely define this limit. Therefore it is necessary to rely on data obtained from operating linacs, or to use some criteria which will insure "safe" operation.[14] A study is in progress at this laboratory to better define this limit over a range of energies by making experimental measurements in a unit cell cavity.[15]

Suppose that one chooses to set a sparking limit in terms of the peak surface field following the example of Kilpatrick. The advantage of limiting the surface field rather than the average field, E_o, in a cell is that the drift tube shape can be more easily factored out. On the other hand, the advantage of specifying a limit on E_o is that these data are more readily available for operating linacs. Either field can be readily specifed when the fields are available from a computational program.

The MESSYMESH summary program provides for the calculation of the maximum field on the surface of a drift tube for E_o = 1 MV per meter. Actually a factor α is calculated, where

$$\alpha = \frac{E_{max}\text{ (on surface)}}{E_o} \quad . \tag{3.11}$$

Thus if one chooses to limit the peak value of the field on the surface to, say E_{SL}, then the value of E_o can be calculated for the geometry considered. In this case the value of E_o is given by

$$E_o = \frac{E_{SL}}{\alpha} \tag{3.12}$$

and in this case the cost equation (3.8) is given by

$$\frac{1}{\Delta W}\left(\frac{C - C_f}{1+\eta t}\right) - C_P I_B = \frac{C_P k}{\cos\phi}\ \frac{E_{SL}}{ZT\alpha} + \frac{C_L}{\cos\phi}\ \frac{\alpha}{E_{SL}T} \tag{3.13}$$

and the criterion for a selection of geometry subject to the sparking limit is now not merely to maximize ZT^2, one must also consider the quantity α .

The procedure for the evaluation of the unit cell geometry has been to calculate a value for the optimum accelerating gradient, E_o from Eq. (3.9), using the most reliable cost information available and the best estimation of the factor k. This value of E_o however may result in a value for the maximum field on the surface which exceeds E_{SL}, in which case one must then use the value E_o obtained from Eq. (3.12). The most desirable geometry will be the one which results in the lowest cost and with reasonable assurance against sparking.

Figure 8 illustrates cost curves for geometry at 50 MeV. The structure cost as obtained from Eq. (3.13) is plotted as a function of the drift tube diameter for different curvature on the drift tube corner, R_c. Plots for cavity outer diameters of 82, 88, and 94 cm for drift tubes with no hole, $A = 0$, and for $D = 92$, $A = 3$ are shown. Superimposing these plots allows a selection of cavity diameter to be made. When a bore hole is added to the drift tube and allowance made for curvature around the bore hole, it is no longer possible to use as small a drift tube diameter for the indicated R_c as shown in these plots. It should also be observed that the total cost is plotted on an expanded scale so that in the region under consideration in Fig. 8 the cost minima are broad allowing greater flexibility in the design without the penalty of greatly increasing the cost.

Figure 9 illustrates the selection of accelerating gradient in the linac design. The curve is a plot of the optimum accelerating gradient as obtained

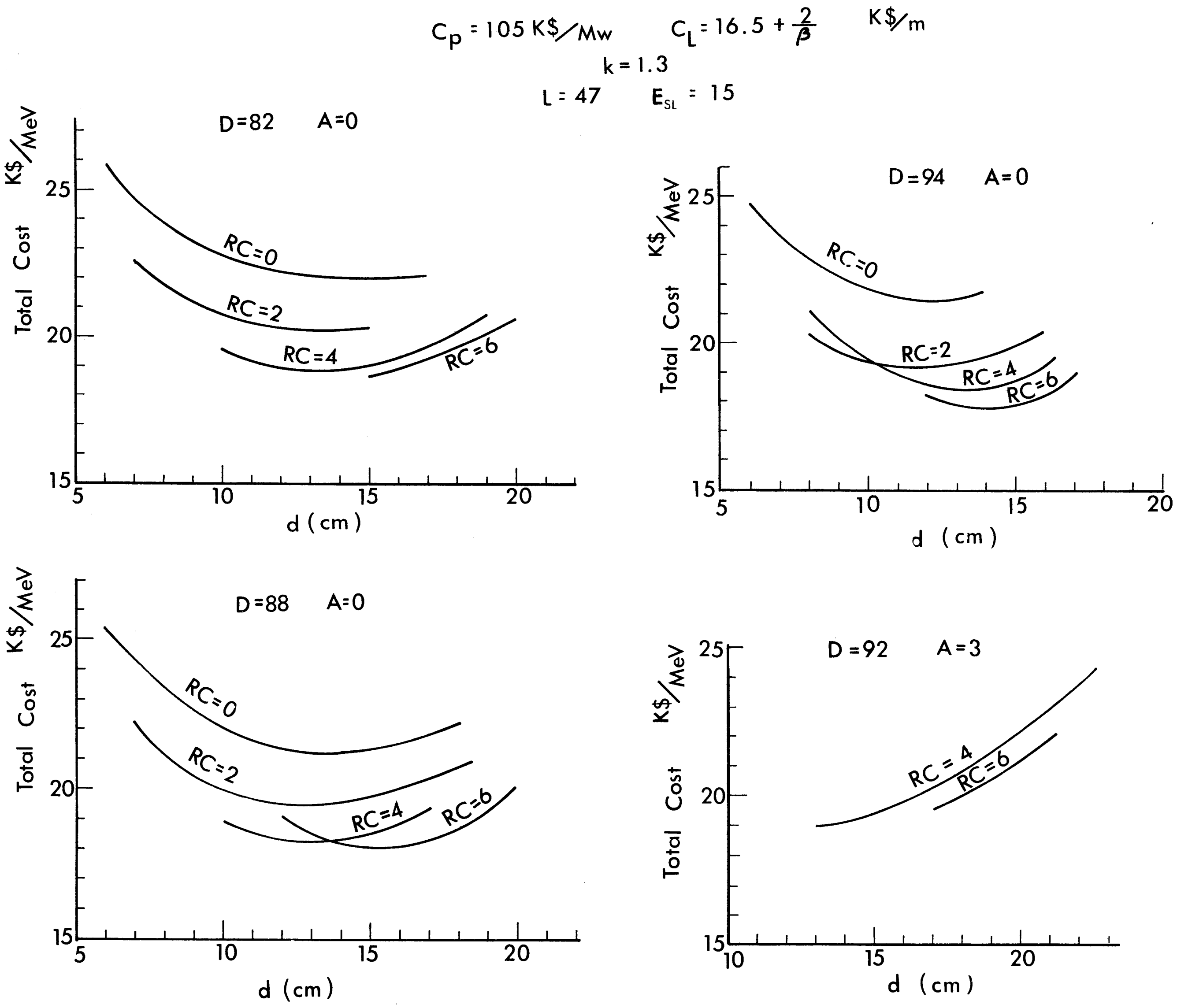

FIG. 8 COST CURVES AT 50 MeV

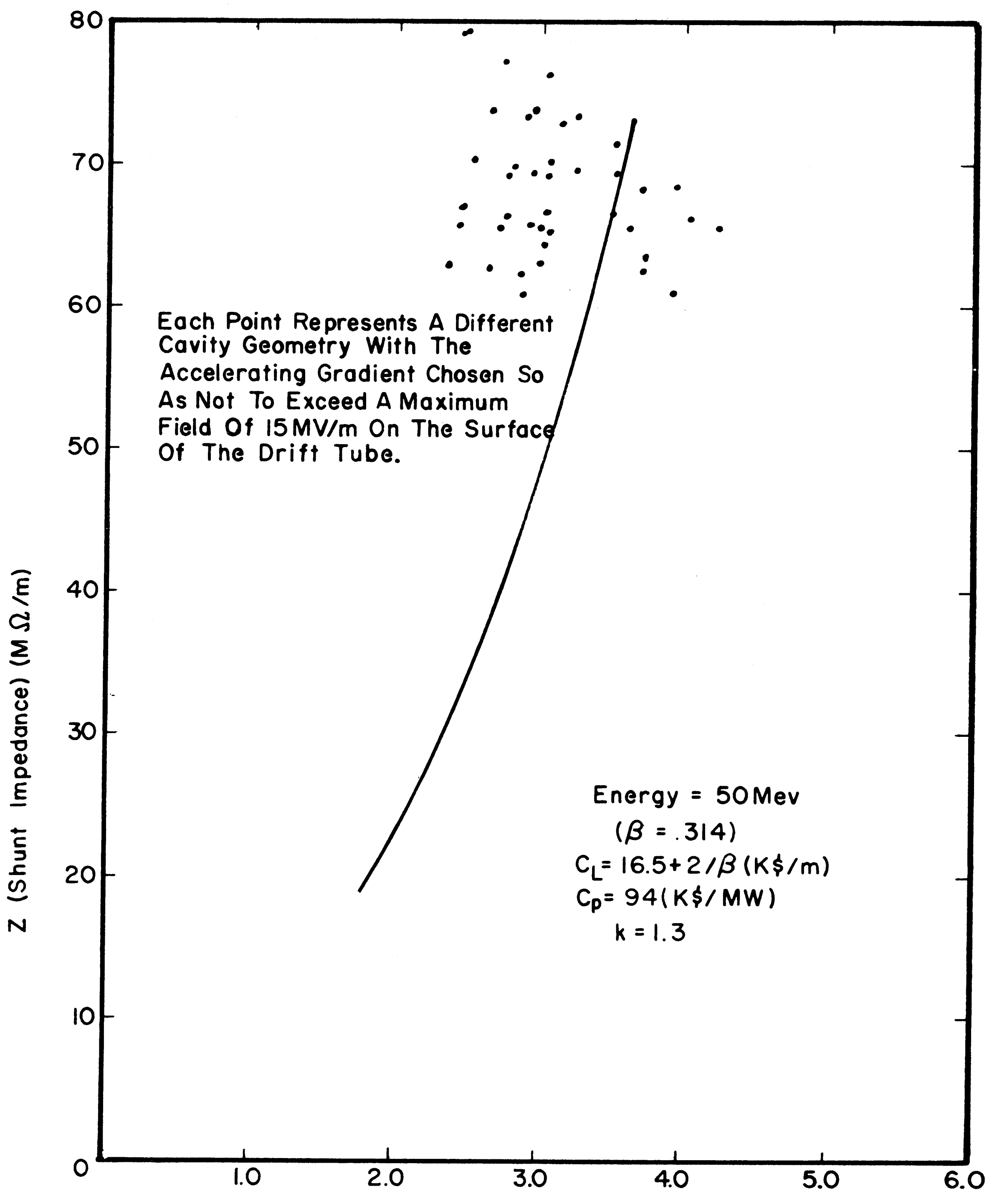

FIG. 9 OPTIMUM ACCELERATING GRADIENT AS A FUNCTION OF SHUNT IMPEDANCE AT 50 MEV

from Eq. (3.9) using the indicated values for C_L, C_P, and k. Each point represents a different selection of cavity geometry resulting in a value of Z which is plotted against an accelerating gradient obtained from Eq. (3.12) where the maximum field on the drift tube surface is taken at 15 MV per meter. Any geometry represented by a point to the left of the curve allows only the accelerating gradient calculated on the basis of a limiting surface field, E_{SL}, from (3.12). Any geometry represented by a point to the right of the curve allows a smaller gradient calculated from the cost optimum, (3.9), to be used with a cost saving and a surface field below the limit, E_{SL} .

When the MESSYMESH runs are evaluated using the cost formula, it is possible to choose an optimum set of parameters that describe the geometry. If each run is plotted on the Z, E_0 diagram with the value of Z corresponding to the geometry and the value E_0 calculated on the basis of an upper limit for the maximum field on the surface, one can observe the importance of the sparking restriction. At 50 MeV money can be saved by raising the gradient closer to the optimum.. At higher energies where the value of Z is smaller, the cost saving in using larger accelerating gradients is not as pronounced.

In addition to the dependence on the unit power and length costs, the drift tube shape, and the peak fields on the surface, a practical design must depart from the optimum because of other design considerations. Cost optimization considerations serve only as a guide for evaluating a great range of different cavity geometries. The cost minima are relatively flat and small departures from the minima do not incur large added costs. In any case practical considerations impose restrictions which bear on the selection of the cavity geometry. Some of these restrictions can be enumerated as follows:

1. Frequency. The cost of power is intimately related to the frequency. In addition, a frequency must be chosen which will allow practical drift tube apertures, drift tube diameters sufficient to incorporate quadrupole focusing, practical tolerances on cavity dimensions, and in copper clad type of construction access to the cavity interior for assembly. A frequency close to 200 Mc is a reasonable choice.[6] A frequency of 201.25 Mc was chosen to minimize interference with existing FCC allotted bands and to be close to the frequency of other accelerators already constructed or contemplated.[16, 17]

2. Length of Cavities. The resonant cavity should not be longer than about 25 m because of difficulty in cavity flattening and/or mode separation. Since it is desirable to excite each cavity from a single power amplifier tube, the peak power limitation on the power amplifier tube is a grater limitation on cavity length in a high current accelerator where sufficient excess power must be provided from the tube to allow for the resistive component of beam loading.

3. Drift Tube Diameter. The drift tube must be of large enough diameter to allow a hole of size to accommodate the full beam and misalignments, to allow a quadrupole of sufficient strength to give good transverse acceptance in each cavity, and to provide cooling for the rf heating of the surfaces and the quadrupole coils. These requirements plus vacuum and rf integrity complicate the mechanical design of drift tubes. Extensive studies outlined later in this report indicate that the minimum diameter requirement is close to 16 cm.

4. Diameter of Cavities. The relation of frequency to cavity diameter has already been mentioned. In copper clad type of construction with entry to the cavity from the ends, sufficient space must be allowed for a person to

assemble and inspect the cavity interior. This imposes a minimum limit of about 82 cm to the diameter of the cavity.

5. Maximum Electric Field. The importance of choosing the maximum accelerating electric field to prevent sparking has already been discussed. Unfortunately there is a lack of information as to the fundamental mechanism and its relation to drift tube shape and materials at all energies to adequately set limits on the electric fields.

6. Reliability. For a linac which is to be used as an injector for a higher energy accelerator where the cost of the linac is a small fraction of the total cost of the big accelerator or installation, reliability is very important. One way reliability can be improved is to provide for more power in the power supply than will be required during normal operation. Reducing the accelerating field will also improve the reliability. There are other ways which do not bear as directly on the choice of cavity geometry.

7. Standardization. Costs can be reduced by fabricating the linac with a number of similar units.

8. X-Ray Levels. As the accelerating field increases, the x-radiation level rises sharply from a threshold value as the fifth or sixth power of the peak surface field. If the accelerating field is chosen at some value above the x-ray threshold, increased shielding will be necessary and radiation damage to accelerator components will result in decreased reliability.

After decisions have been reached on these restrictions and suitable geometry has been selected, it is useful to obtain a table of typical linac parameters with cavity energies, gradients, lengths, and powers specified.

Further MESSYMESH runs in each cavity at intermediate energies and close to the prescribed frequency are helpful in obtaining better estimates for T and ZT^2. Adjustment of the beginning and final energies of each cavity may be necessary so that the cavity lengths, powers, and gradients can be adjusted to stay within the restrictions. An exact specification of the cavity parameters depends upon cell-to-cell particle dynamics considerations and will be discussed in the next section. Such a table of parameters allows design engineering studies to proceed so that further refinements can be initiated.

Typical parameters for three 200 Mc linacs are listed in Tables I, II, and III. Table I gives parameters for a linac of 175 MeV which allows for a beam current of 20 mA. A short first cavity (10 MeV) is provided which allows, (a) greater flexibility in the drift tube design so that quadrupoles with large gradients can be installed, (b) reduced gradients to minimize sparking difficulties in the early gaps, and (c) greater flexibility in tuning. This, of course, causes a deviation from optimum cost in this cavity, but should provide better linac performance. The short first cavity should allow more optimum geometry and gradient to be chosen in later cavities. Four cavities of about 25 m length are prescribed from 10 to 175 MeV with values of the accelerating gradient chosen so that the peak power capability of a 5 MW amplifier tube will not be exceeded and so, hopefully, no sparking difficulties should be encountered.

Table II lists parameters for a 200 MeV linac with reserve rf power to allow 100 mA of beam current. If the rf power including that necessary for beam loading is to be supplied from a single 5 MW power amplifier tube per cavity, the cavity lengths must be reduced. This results in an eight-cavity design with somewhat reduced gradients.

The parameters for another eight-cavity, 200 MeV, 100 mA beam current linac are listed in Table III. In this case the length of the first cavity has been increased to 20 MeV. The longer first cavity design permits a reduction in power in later cavities or alternatively the gradient in the later cavities may be raised without exceeding the power limitation on the amplifier tube with a corresponding decrease in accelerator length in these cavities. Thus, the penalty for the longer first cavity is partially offset and the over-all length and power requirements in design II and design III are nearly the same.

TABLE I

TYPICAL PARAMETERS FOR A 20 mA - 175 MeV LINAC

Cavity No.	1	2	3	4	5
Input Energy, W_i (MeV)	0.75	10	60	103	141
Output Energy, W_o (MeV)	10	60	103	141	175
$\Delta W = W_o - W_i$	9.25	50	43	38	34
D (cm)	94	90	88	86	84
d (cm)	18	16-14	16	16	16
A (cm)	2	2.5	3	3.5	4
R_c (cm	2	4	4	4	4
R_{hc} (cm)	1	1	1	1	1
Range of g/L	.20-.30	.19-.33	.35-.42	.40-.44	.43-.46
E_o (MV/m)	2.0	2.7	2.7	2.6	2.5
E_{max}(surface)(MV/m)	10.0	14.5	14.0	14.0	14.0
E_g(avg)(gap)(MV/m)	10-6.7	14-8.2	7.7-6.4	6.5-5.9	5.8-5.4
T (avg)	0.77	0.84	0.72	0.65	0.60
$\Delta W/\Sigma L$ (MeV/m)	1.38	2.04	1.75	1.52	1.35
Cavity Length (m)	6.7	24.5	24.6	25.0	25.2
ZT^2 (avg)(M Ω /m)	44	49	31	22	18
P (theor) (MW)	0.36	2.6	3.0	3.2	3.2
k	1.3	1.3	1.3	1.3	1.3
P (practical)(MW)	0.65	4.4	4.8	4.9	4.8

Frequency: 201.25 Mc
$\cos \phi_s$: 0.90
Total Power: 19.5 MW
Total Cavity Length: 106 m

TABLE II

TYPICAL PARAMETERS FOR A 100 mA-200 MeV LINAC (10 MeV FIRST CAVITY)

Cavity No.	1	2	3	4	5	6	7	8
Input Energy W_i (MeV)	0.75	10	41	70	98	124.5	150	175
Output Energy W_o (MeV)	10	41	70	98	124.5	150	175	199
$\Delta W = W_o - W_i$	9.25	31	29	28	26.5	25.5	25	24
D (cm)	94	90	88	86	85	84	83	82
d (cm)	18	16-15	16	16	16	16	16	16
A (cm)	2	3	3	3	4	4	4	4
R_c (cm)	2	4	4	5	5	5	5	5
R_{hc} (cm)	1	1	1	1	1	1	1	1
Range of g/L	.20 - .30	.21 - .31	.31 - .37	.34 - .39	.38 - .41	.41 - .43	.43 - .44	.44 .46
E_o (MV/m)	2.0	2.7	2.7	2.6	2.5	2.45	2.4	2.3
E_{max}(surface) (MV/m)	10.0	16.2	13.5	13.5	13.5	13.5	13.4	13.3
E_g (avg)(gap) (MV/m)	10 - 6.7	12.8 - 8.7	8.7 - 7.3	7.6 - 6.7	6.6 - 6.1	6.0 - 5.7	5.6 - 5.4	5.1
T (avg)	0.77	0.85	0.78	0.74	0.69	0.65	0.62	0.59
$\Delta W/\Sigma L$ (MeV/m)	1.38	2.1	1.9	1.7	1.5	1.4	1.3	1.2
Cavity Length (m)	6.7	14.8	15.3	16.5	17.7	18.2	19.2	20.0
ZT^2 (avg) (M Ω /m)	44	51	39	32	26	22	19	16.5
P (theor)(MW)	0.36	1.6	1.7	1.8	1.9	2.0	2.1	2.2
k	1.3	1.3	1.3	1.3	1.3	1.3	1.3	1.3
P (practical)(MW)	1.4	5.2	5.1	5.1	5.2	5.2	5.2	5.2

Frequency:	201.25 Mc
cos ϕ_s:	0.90
Total Power:	37.6 MW
Total Cavity Length:	128.4 m

TABLE III

TYPICAL PARAMETERS FOR A 100 mA - 200 MEV LINAC (20 MeV FIRST CAVITY)

Cavity No.	1	2	3	4	5	6	7	8
Input Energy W_i (MeV)	0.75	20	50	77	104	129	153	177
Output Energy W_o (MeV)	20	50	77	104	129	153	177	200
$\Delta W = W_o - W_i$	19.25	30	27	27	25	24	24	23
D (cm)	94	90	88	86	85	84	83	82
d (cm)	18	16-15	16	16	16	16	16	16
A (cm)	2	3	3	3	4	4	4	4
R_c (cm)	2	4	4	5	5	5	5	5
R_{hc} (cm)	1	1	1	1	1	1	1	1
Range of g/L	.24 - .35	.25 - .32	.33 - .38	.36 - .39	.39 - .42	.41 - .43	.43 - .45	.44 - .46
E_o (MV/m)	2.0	2.8	2.8	2.7	2.6	2.5	2.4	2.3
E_{max} (surface) (MV/m)	10.0	15.1	14.0	14.0	14.2	13.7	13.4	13.3
E_g(avg)(gap) (MV/m)	8.3 - 5.7	11.2 - 8.8	8.5 - 7.4	7.5 - 6.9	6.7 - 6.2	6.1 - 5.8	5.6 - 5.3	5.2 - 5.0
T (avg)	0.76	0.83	0.75	0.72	0.68	0.64	0.62	0.59
$\Delta W/\Sigma L$ (MeV/m)	1.37	2.1	1.9	1.75	1.6	1.45	1.35	1.2
Cavity Length(m)	14.0	14.3	14.2	15.4	15.6	16.6	17.8	19.2
ZT^2 (avg) (M Ω /m)	45	47	36	31	25	21	19	16.5
P (theor)(MW)	0.73	1.65	1.8	1.9	2.0	2.0	2.1	2.1
k	1.3	1.3	1.3	1.3	1.3	1.3	1.3	1.3
P (practical)(MW)	2.9	5.15	5.0	5.2	5.1	5.1	5.1	5.0

Frequency:	201.25 Mc
cos ϕ_s:	0.90
Total Power:	38.6 MW
Total Cavity Length:	127.1 m

IV. GENERATION OF EXACT CAVITY DIMENSIONS

Parameters for three linacs have been listed in Tables I, II, and III. By choosing a given set of parameters, it is possible to proceed with a more detailed design resulting eventually in a complete table of dimensions for the entire accelerating structure. A decision was made to continue the design using the typical parameters of Table III, that is, the 200 MeV design with the 20 MeV first cavity. The longer first cavity design was chosen for the following reasons:

a) The accuracy of the MESSYMESH program in geometry where gaps are short is less than in the higher energy geometry and longer computing times are required. (The program is being modified to correct this deficiency.) However, since an adequate and proven design exists for the low energy cavity* (the present ANL or BNL design), there seems little incentive to redesign this cavity for the present state of the development.

b) The higher power requirements in the 20 MeV cavity forces a power supply design which is similar to the design for the other cavities. In addition to the saving in the multiplicity of design, the power requirement is sufficiently less so that one may use older tubes which are no longer satisfactory for service where full power is required.

c) It is important to keep the drift space between cavities as small as possible since a spread in the phase of the particles between cavities can lead to increased energy spread in the output beam. It is also important to place beam diagnostic equipment, steering, and mechanical hardware between

---

*For example, the LRL Bevatron Injector.

cavities. At 20 MeV, it is possible to allow a longer drift space between cavities for this necessary equipment without causing serious debunching due to energy spread in the beam.

Having made a selection of the geometry of each cavity as given in Table III, precise cell dimensions can be obtained on the basis of the dynamical properties of a "synchronous" particle. The effect of the linac geometry on the dynamics of the synchronous particle can be reduced to a transit time factor, T. T is a function of the distribution of the fields in the linac cell, which, of course, are a function of the geometrical dimensions of the cavity.

In addition to the five geometrical parameters in Table III, i.e., D, d, A, R_c, and R_{hc}, and the resonant frequency, one needs only to specify the cell length L to complete the description of the geometry of that cell. The precise cell length however depends on the average velocity of the synchronous particle within the cell, which is, as yet, unknown.

From the lowest and highest energies of the synchronous particle within a given cavity, the shortest and longest cell lengths for the cavity can be approximately evaluated. After choosing a cell length within this range and with the aid of resonance curves, a gap length G can be chosen which will cause the cell to resonate close to 201.25 Mc.

If the dimensions of this cell are described to the MESSYMESH program, the resonant frequency and the field distribution can be evaluated. At the present time, the MESSYMESH program is restricted to cell dimensions which are integral multiples of some mesh dimension (commonly taken as 0.5 cm/mesh unit). The five geometrical parameters given in Table III are integral multiples of 0.5 cm. Choosing L as an integral multiple of 0.5 cm poses no problem. A problem does arise however in connection with the gap length G. In general, it is impossible to choose a value of G so that the cavity will resonate precisely at 201.25 Mc. It is necessary to make a pair of runs for each value of L ; one with a G which is too short, and one with a G which is too long. On the basis of the resulting resonant frequencies for the pair of runs, a value of G can be interpolated which will cause the cavity to resonate at the proper frequency. From the field distributions for each of the pair of runs, a transit time function T can be evaluated. As T is strongly dependent upon the gap length, it is necessary to interpolate the values of T obtained from the pair of runs to obtain a value of T corresponding to a cavity of the correct gap length.

By choosing other values of L in the appropriate range, and evaluating G and T as above, one may determine the relationships of the ratio G/L and the function T to the cell length L (or the average velocity $\overline{\beta}$). One should note that these relationships are peculiar to the particular set of values given for the five geometrical parameters in Table III. If any of these parameters are changed, the relationships will be affected.

The ratio G/L and transit time function T are plotted in Figs. 12 and 10 as functions of L for cavities 2 - 8 as described in Table III. The discontinuities in the curves are due in part to the change in cell diameter from cavity to cavity.

Given T as a function of L (or $\overline{\beta}$) for a particular cavity, the average axial electric field in the n^{th} cell $E_{o,n}$, and the energy of the synchronous particle at the end of the $n - 1^{st}$ cell, it is possible to evaluate the length of the n^{th} cell and the energy of the synchronous particle after traversing the n^{th} cell.

The energy gained by the synchronous particle in traversing the n^{th} cell is given by

$$\delta W_n = \int_{-L_n/2}^{L_n/2} e\, E_z(z) \cos\left(\phi_s + \frac{2\pi z}{L_n}\right) dz \; ,$$

which can be written

$$\delta W_n = e\, E_{o,n}\, L_n \cos\phi_s \left[\frac{\displaystyle\int_{-L_n/2}^{L_n/2} E_z(z) \cos\frac{2\pi z}{L_n}\, dz}{\displaystyle\int_{-L_n/2}^{L_n/2} E_z(z)\, dz} \right] ,$$

where

$$E_{o,n} = \frac{1}{L_n} \int_{-L_n/2}^{L_n/2} E_z(z)\, dz \; ,$$

and where the quantity in the square brackets is the transit time function T which has been evaluated in the MESSYMESH program and is known as a function of L (or $\overline{\beta}$) .

The change in momentum δp_n for the n^{th} cell is given by

$$\frac{\delta p_n}{m_o c} = \frac{\delta W_n}{m_o c^2 \beta_n} = \frac{e\, E_{o,n}\, \lambda \cos\phi_s}{m_o c^2}\; T(L_n) \; .$$

The only problem in evaluating δp_n is that T is a function of L_n and L_n is not really available until after δp_n has been evaluated. However, this difficulty can easily be overcome by approximating δp_n in order to make a good approximation of L_n, in order to arrive at a precise value of T (L_n). Having done this, δp_n can be evaluated precisely for the n^{th} cell. The momentum p_n is then $p_{n-1} + \delta p_n$ and β_n can be evaluated using the expression

$\gamma_n = \sqrt{p_n^2/m_o^2\,c^2 + 1}$. The precise length of the n^{th} cell is $L_n = (\beta_{n-1} + \beta_n)\,\lambda/2$. The length of the n^{th} gap G_n is obtained from the relation G/L as a function of L and the value of L_n .

The iterative procedure outlined above for generating the parameters of the n^{th} cell from the parameters of the $(n - 1)^{st}$ cell is readily performed by a computer program. This program exists in the GENLIN subroutine of the PARMILA program. The GENLIN subroutine is described in Section IV of Appendix B.

The first 20 MeV cavity in this design is chosen from the present ANL or BNL design with only minor modifications. From 20 to 200 MeV, the range of L is from 30 to 84 cm. Cavity number 2, from 20 to 50 MeV, covers a range in L from 30 to 47 cm. In cavities beyond the second, i.e., above 50 MeV, resonance can be achieved by a simple G/L change, with other geometric dimensions constant throughout the cavity. In this energy range, from L = 47 to 84, two computer runs have been made at each integral G which brackets the frequency of 201.25 Mc.

For the second cavity covering the range from 20 to 50 MeV, i.e., L = 30 to 47 cm, a simple G/L change alone would have incurred a larger variation in the transit time factor than was considered desirable for good rf efficiency, and therefore a variation in the drift tube diameter was also taken. A minimum drift tube diameter at 50 MeV to allow the quadrupole cooling and assembly with a 3-cm bore hole was 15 cm. With the two parameters which can be varied to satisfy the resonance condition, i.e., drift tube diameter, d, and gap, G, the cell-to-cell variation is still an arbitrary choice. It was decided to take a linear variation in the drift tube diameter from L = 30, d = 16 to L = 47, d = 15. The additional G/L variation required to satisfy the resonance condition is then calculated. In this cavity, four computer runs at each integer L value, for a d of 16 and 15 and for two values of g, allow accurate interpolation.

The accurate values of the transit time factor interpolated from the pairs (or quartets) of MESSYMESH runs at each L value for each cavity are fitted to an equation of the type:

$$T = A + B\overline{\beta} + C\overline{\beta}^2 .$$

The constants A, B, and C are used as input data for the GENLIN subroutine of the PARMILA program. The interpolated values of T for each cavity are shown in Fig. 10 and the values of the coefficients given in Table IV.

TABLE IV

Cavity No.	A	B	C
2	0.8102	+0.7452	-2.6554
3	1.0201	-0.49802	-0.73599
4	1.1962	-1.1534	0
5	1.2235	-1.2013	0
6	1.2459	-1.2263	0
7	1.2712	-1.2560	0
8	1.2599	-1.2170	0

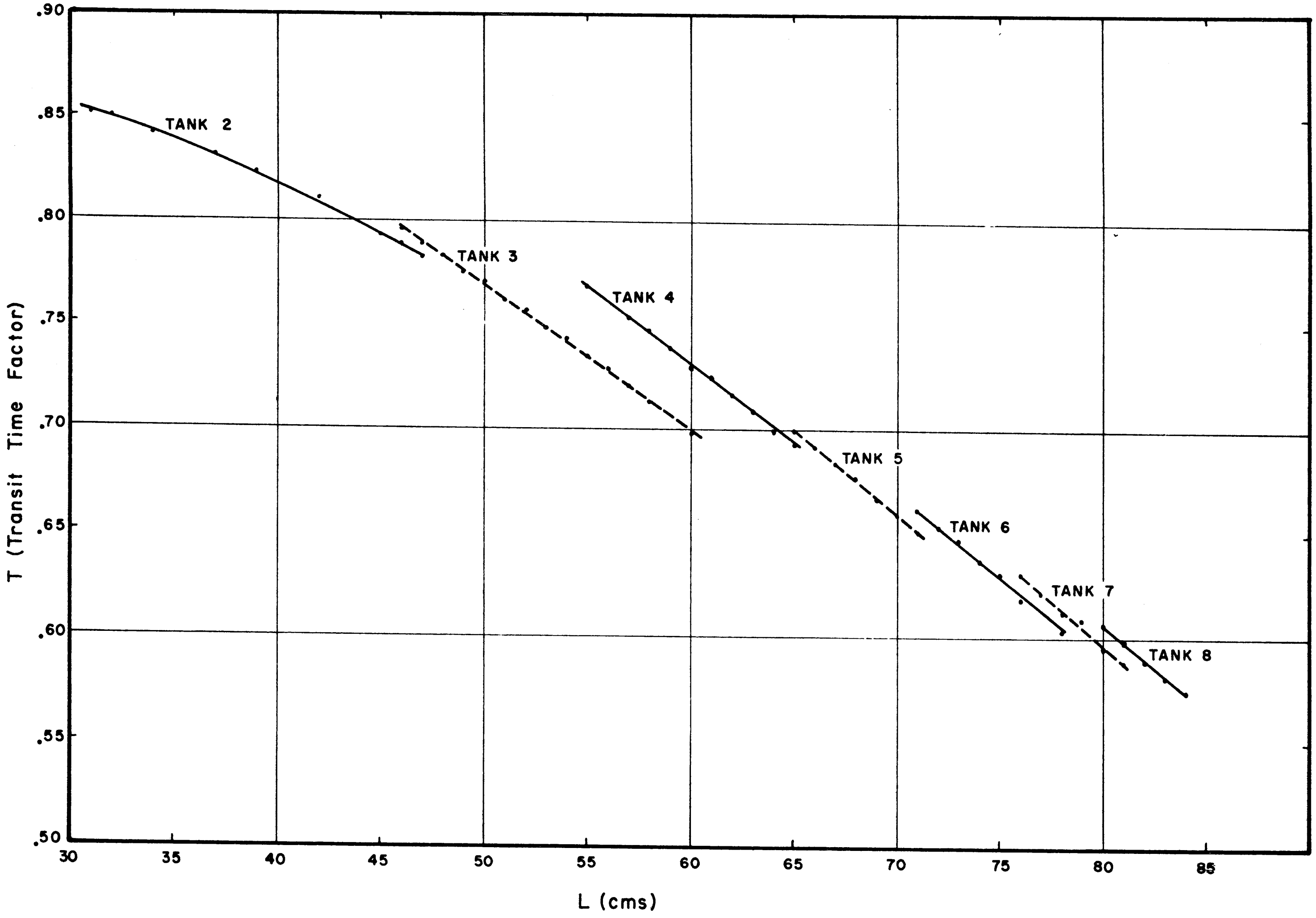

FIG. 10 INTERPOLATED T VALUES

The interpolated values of the coupling coefficient, S (defined in Appendix B) is shown plotted for each cavity in Fig. 11. Values of the coefficients P, Q, and R in the equation:

$$S = P + Q\overline{\beta} + R\overline{\beta}^2 ,$$

which provides a best fit to the data, are given in Table V. These coefficients are used as input to PARMILA.

TABLE V

Cavity No.	P	Q	R
2	+0.04394	-0.1122	0.5574
3	-0.76867×10^{-2}	+0.17319	0.14842
4	-4.5446×10^{-2}	+0.30722	0
5	-4.7371×10^{-2}	+0.30751	0
6	-5.0462×10^{-2}	+0.30868	0
7	-5.5341×10^{-2}	+0.31325	0
8	-4.742×10^{-2}	0.29421	0

With these data and the accelerating field and stable phase angle, the change in the synchronous particle momentum can be calculated as the particle goes through each cell in the cavity. The value of β, γ , the energy, and the cell length can be calculated cell by cell from the particle momentum. This is done in GENLIN. This information is given in the first columns of the drift tube table (see Table VIII). The length of each unit cell allows the drift tube length to be specified.

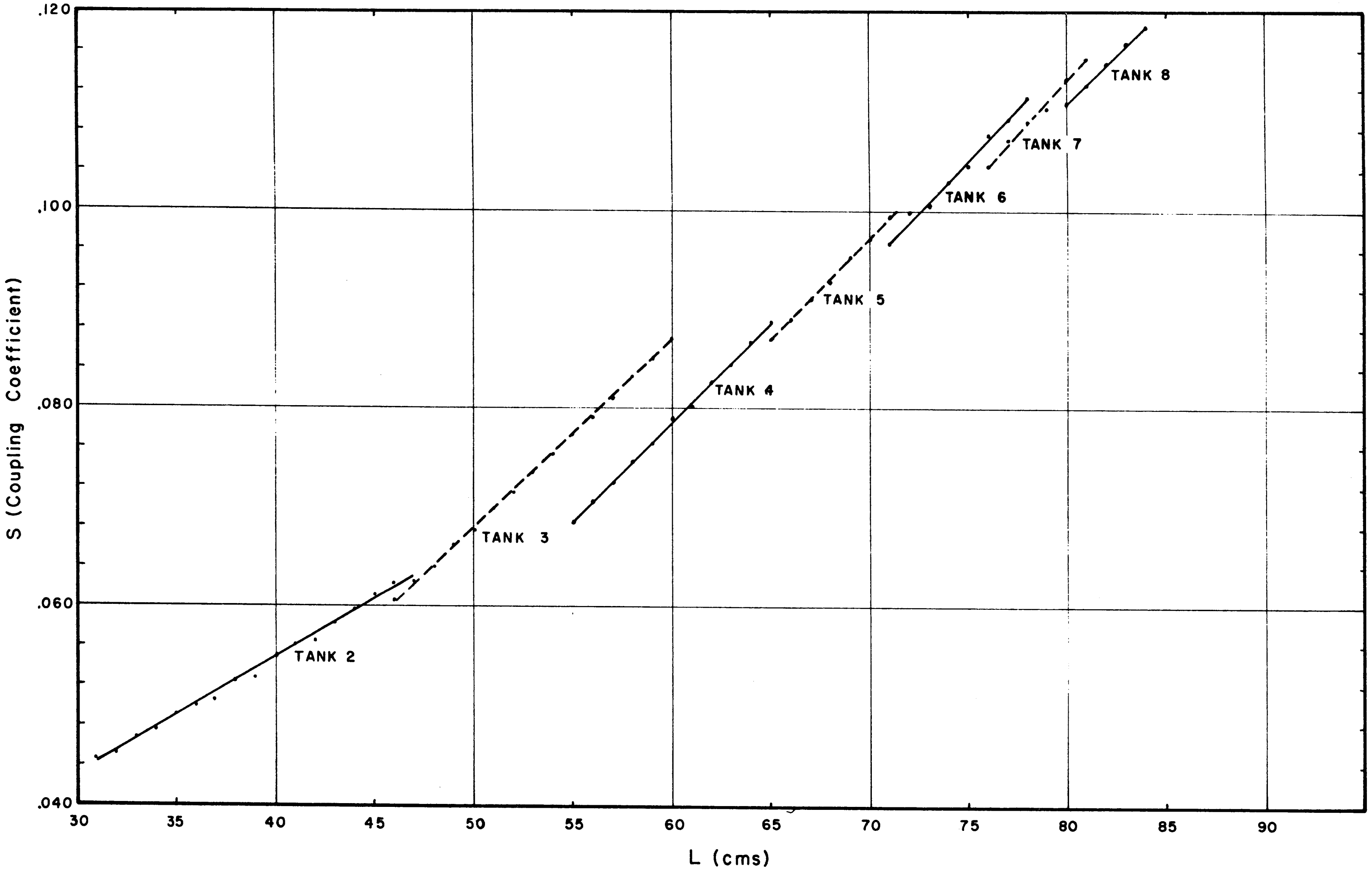

FIG. 11 INTERPOLATED S VALUES

A value of G/L can be interpolated from the pairs (or quartets) of MESSYMESH runs to almost the same accuracy as the frequency is known. These interpolated G/L values are shown in Fig. 12. These values are then fitted by a least-square analysis to the quadratic equation:

$$G/L = DL^2 + EL + F .$$

TABLE VI

Cavity No.	D	E	F
2	-6.97505×10^{-6}	5.64061×10^{-3}	$+8.40275 \times 10^{-2}$
3	-2.36795×10^{-5}	7.82868×10^{-3}	$+1.57196 \times 10^{-2}$
4	-2.03096×10^{-5}	7.63313×10^{-3}	-1.35519×10^{-2}
5	-1.99583×10^{-5}	7.58942×10^{-3}	-1.96904×10^{-2}
6	-2.09946×10^{-5}	7.74800×10^{-3}	-3.25078×10^{-2}
7	-2.60411×10^{-5}	8.59510×10^{-3}	-7.41143×10^{-2}
8	-7.01500×10^{-5}	1.59641×10^{-2}	-3.87549×10^{-2}

The coefficients D, E, and F for this design are listed in Table VI. Thus for the value of the n^{th} cell length, L_n, a value G_n/L_n may be calculated (and a value of G_n). The length of the drift tube, ℓ_n, is:

$$\ell_n = L_n - G_n .$$

Since L_n is calculated for the unit cell geometry illustrated in Fig. 1, as

$$L_n = \left(\frac{\beta_n + \beta_{n-1}}{2} \right) \lambda ,$$

ℓ_n represents one-half the length of the $(n - 1)^{th}$ drift tube and one-half of

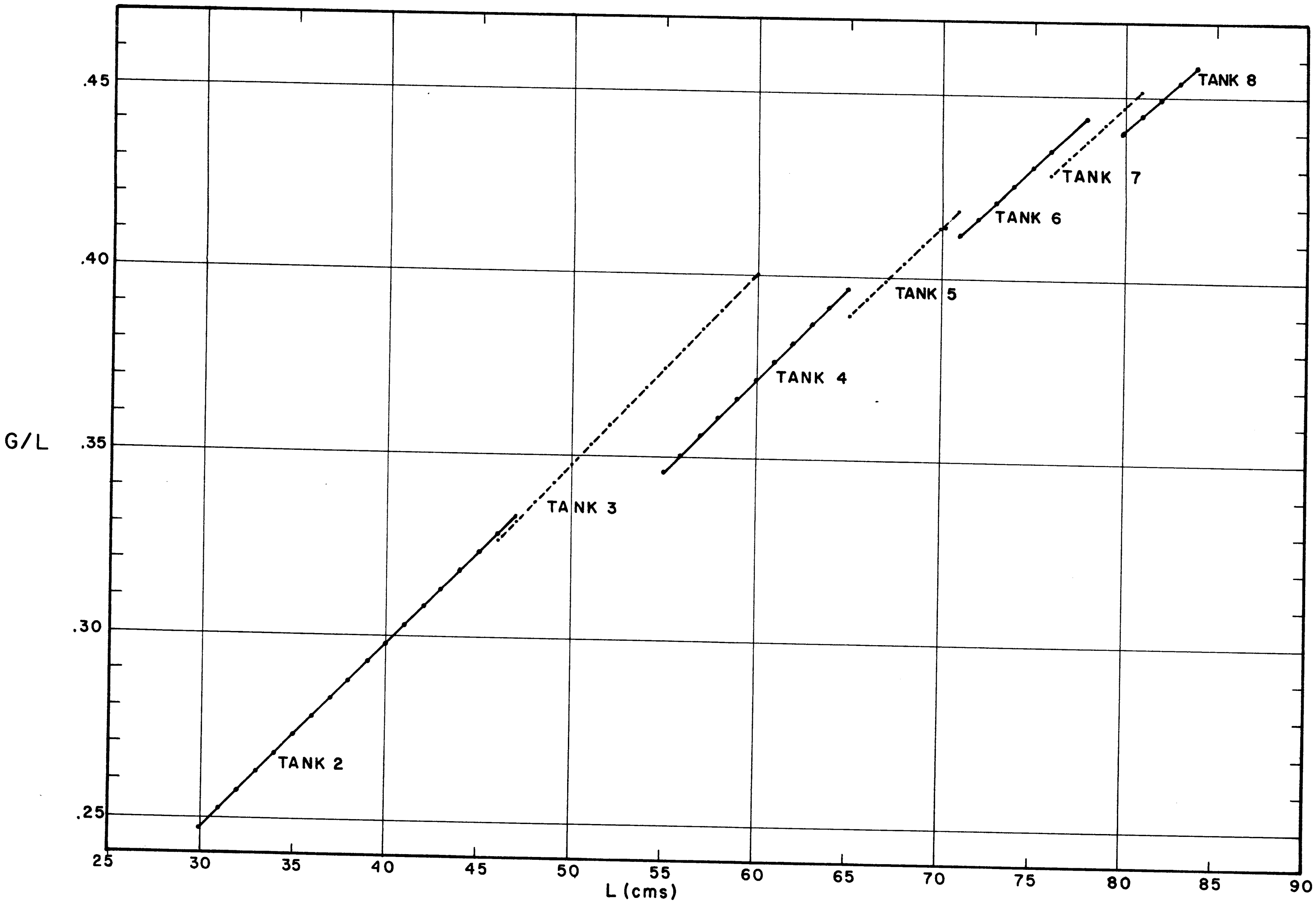

FIG. 12 INTERPOLATED G/L VALUES

the n^{th} drift tube. The length of the n^{th} drift tube is an average of ℓ_n and ℓ_{n+1}.

This drift tube numbering convention is shown in the drift tube table (Table VIII). The gap length, G_n, corresponds to the L_n cell. The drift tube length is the total length of the n^{th} drift tube with one-half of its length in the n^{th} cell and one-half in the $(n+1)^{th}$ cell. Each cavity begins and ends with a complete unit cell and so each end plate contains one-half of a drift tube. The letters A and B are used as the end and beginning half drift tubes of the cavity, respectively, to preserve the cell-drift tube number correspondence.

The considerations bearing on the choice of accelerating gradient in the design have been mentioned in Section III. It is instructive to re-examine this question for the specific design considered here especially in view of the larger number of computer runs available for this geometry specification. Table VII summarizes the results of this analysis.

TABLE VII

Cavity No.	α (From 3-11) Begin	End	$E_o = \frac{E_{SL}}{\alpha}$ (E_{SL} = 15 MV/m) Begin	End	Optimum E_o $E_o = \left[ZC_L/KC_P\right]^{1/2}$	E_o Design Value
2	5.10	5.12	2.94	2.93	3.72	2.8
3	4.96	4.98	3.02	3.01	3.36	2.8
4	5.01	5.11	2.99	2.94	3.15	2.7
5	5.31	5.45	2.82	2.75	3.08	2.6
6	5.41	5.57	2.77	2.69	2.97	2.5
7	5.57	5.66	2.69	2.65	2.89	2.4
8	5.70	5.76	2.63	2.60	2.75	2.3

$k = 1.3$, $C_L = 16.5 + 2/\beta \ (\mathrm{K\$/m})$, $C_P = 94 \ (\mathrm{K\$/MW})$

TABLE VIII DRIFT TUBE DIMENSIONS

Drift Tube No.	Energy	β	Cell Length	Gap Length	Drift Tube Length	d
71B	20.057	0.2035			11.321	15.982
72	20.713	0.2067	30.556	7.635	23.061	15.967
73	21.378	0.2099	31.031	7.831	23.338	15.939
74	22.052	0.2131	31.504	8.028	23.614	15.912
75	22.736	0.2162	31.976	8.226	23.885	15.884
76	23.429	0.2194	32.447	8.426	24.154	15.856
77	24.130	0.2225	32.915	8.628	24.419	15.828
78	24.840	0.2256	33.382	8.831	24.681	15.801
79	25.559	0.2288	33.846	9.035	24.940	15.774
80	26.286	0.2319	34.310	9.241	25.196	15.746
81	27.022	0.2350	34.771	9.448	25.448	15.719
82	27.766	0.2380	35.230	9.656	25.698	15.692
83	28.519	0.2411	35.687	9.865	25.944	15.666
84	29.279	0.2442	36.142	10.076	26.188	15.639
85	30.048	0.2472	36.596	10.288	26.428	15.612
86	30.824	0.2502	37.047	10.500	26.665	15.586
87	31.608	0.2532	37.497	10.714	26.900	15.559
88	32.400	0.2562	37.944	10.928	27.131	15.533
89	33.199	0.2592	38.389	11.144	27.358	15.506
90	34.006	0.2622	38.832	11.360	27.584	15.481
91	34.820	0.2651	39.273	11.578	27.806	15.454
92	35.641	0.2681	39.712	11.796	28.026	15.429
93	36.469	0.2710	40.149	12.015	28.242	15.403
94	37.304	0.2739	40.584	12.234	28.456	15.377
95	38.146	0.2768	41.016	12.454	28.666	15.352
96	38.994	0.2797	41.446	12.675	28.874	15.327
97	39.849	0.2825	41.874	12.897	29.079	15.302
98	40.710	0.2854	42.300	13.119	29.282	15.276
99	41.578	0.2882	42.723	13.342	29.481	15.252
100	42.452	0.2910	43.144	13.565	29.678	15.227
101	43.332	0.2938	43.563	13.788	29.871	15.202
102	44.217	0.2966	43.980	14.012	30.062	15.178
103	45.109	0.2994	44.394	14.237	30.251	15.153
104	46.006	0.3022	44.806	14.462	30.437	15.129
105	46.910	0.3049	45.216	14.687	30.620	15.105
106	47.817	0.3076	45.623	14.912	30.801	15.081
107	48.731	0.3103	46.028	15.138	30.978	15.057
108A	49.649	0.3130	46.431	15.363	15.622	15.034
108B	49.649	0.3130			15.630	16.000
109	50.582	0.3157	46.833	15.475	31.430	↑
110	51.520	0.3184	47.235	15.714	31.601	
111	52.462	0.3211	47.634	15.953	31.760	
112	53.409	0.3238	48.031	16.192	31.917	
113	54.360	0.3264	48.425	16.430	32.072	
114	55.316	0.3290	48.816	16.669	32.224	
115	56.276	0.3316	49.206	16.907	32.373	
116	57.240	0.3342	49.592	17.145	32.520	
117	58.208	0.3368	49.977	17.383	32.666	
118	59.180	0.3393	50.359	17.621	32.809	
119	60.156	0.3419	50.738	17.858	32.950	
120	61.136	0.3444	51.115	18.095	33.088	
121	62.120	0.3469	51.490	18.332	33.225	
122	63.108	0.3494	51.862	18.569	33.360	
123	64.099	0.3519	52.232	18.805	33.493	
124	65.094	0.3543	52.599	19.040	33.624	
125	66.092	0.3568	52.964	19.276	33.753	
126	67.094	0.3592	53.327	19.510	33.880	
127	68.099	0.3616	53.688	19.745	34.005	
128	69.108	0.3640	54.046	19.979	34.128	
129	70.119	0.3664	54.402	20.272	34.250	
130	71.134	0.3688	54.756	20.445	34.370	
131	72.152	0.3711	55.107	20.678	34.488	
132	73.174	0.3734	55.457	20.910	34.604	
133	74.198	0.3758	55.804	21.141	34.719	
134	75.225	0.3781	56.149	21.372	34.832	↓
135	76.255	0.3804	56.491	21.602	34.944	
136A	77.288	0.3826	56.832	21.832	17.528	16.000
136B	77.288	0.3826			18.367	16.000
137	78.331	0.3849	57.172	20.380	36.849	↑
138	79.378	0.3872	57.510	20.604	36.963	
139	80.426	0.3894	57.847	20.827	37.075	
140	81.477	0.3917	58.182	21.050	37.186	
141	82.531	0.3939	58.514	21.273	37.295	
142	83.587	0.3961	58.844	21.495	37.452	
143	84.645	0.3983	59.172	21.716	37.508	
144	85.706	0.4005	59.498	21.937	37.612	
145	86.768	0.4027	59.822	22.158	37.715	
146	87.833	0.4048	60.143	22.377	37.816	
147	88.900	0.4070	60.463	22.596	37.916	
148	89.969	0.4091	60.780	22.815	37.014	
149	91.040	0.4112	61.096	23.033	38.111	
150	92.113	0.4133	61.410	23.250	38.207	
151	93.188	0.4154	61.721	23.466	38.301	
152	94.264	0.4174	62.030	23.682	38.394	
153	95.343	0.4195	62.338	23.898	38.486	
154	96.423	0.4215	62.643	24.112	38.576	
155	97.505	0.4236	62.947	24.326	38.665	
156	98.588	0.4256	63.249	24.540	38.753	
157	99.673	0.4276	63.549	24.752	38.839	
158	100.760	0.4296	63.846	24.964	38.924	
159	101.848	0.4317	64.142	25.176	39.008	
160	102.938	0.4335	64.436	25.386	39.091	↓
161A	104.029	0.4355	64.729	25.596	19.587	16.000
161B	104.029	0.4355			19.830	16.000
162	105.092	0.4374	65.015	25.315	39.740	↑
163	106.155	0.4393	65.296	25.516	39.820	
164	107.220	0.4411	65.575	25.716	39.898	
165	108.286	0.4430	65.852	25.915	39.975	
166	109.352	0.4448	66.127	26.114	40.051	
167	110.420	0.4467	66.401	26.311	40.126	
168	111.488	0.4485	66.673	26.509	40.201	
169	112.558	0.4503	66.943	26.705	40.274	
170	113.628	0.4521	67.211	26.901	40.346	
171	114.670	0.4539	67.478	27.096	40.418	
172	115.772	0.4556	67.744	27.291	40.488	
173	116.844	0.4574	68.007	27.484	40.558	
174	117.918	0.4592	68.269	27.677	40.626	
175	118.992	0.4609	68.529	27.870	40.694	
176	120.067	0.4626	68.788	28.061	40.760	
177	121.143	0.4644	69.045	28.252	40.826	
178	122.219	0.4661	69.301	28.442	40.892	
179	123.296	0.4678	69.555	28.631	40.956	
180	124.374	0.4695	69.807	28.820	41.018	
181	125.452	0.4711	70.058	29.008	41.082	
182	126.530	0.4728	70.308	29.195	41.144	↓
183	127.609	0.4745	70.555	29.381	41.204	
184A	128.688	0.4761	70.802	29.567	20.632	16.000

TABLE VIII DRIFT TUBE DIMENSIONS (CONTINUED)

Drift Tube No.	Energy	β	Cell Length	Gap Length	Drift Tube Length	d
184B	128.688	0.4761			20.873	16.000
185	129.744	0.4777	71.044	29.268	41.805	
186	130.800	0.4793	71.282	29.447	41.864	
187	131.856	0.4809	71.518	29.625	41.922	
188	132.913	0.4825	71.753	29.802	41.980	
189	133.970	0.4840	71.987	29.979	42.036	
190	135.027	0.4856	72.220	30.155	42.092	
191	136.084	0.4871	72.450	30.330	42.148	
192	137.142	0.4887	72.680	30.505	42.202	
193	138.200	0.4902	72.908	30.679	42.256	
194	139.258	0.4917	73.135	30.852	42.310	
195	140.316	0.4932	73.361	31.024	42.362	
196	141.374	0.4947	73.585	31.196	42.415	
197	142.432	0.4962	73.808	31.367	42.466	
198	143.491	0.4977	74.030	31.538	42.517	
199	144.550	0.4992	74.250	31.707	42.568	
200	145.608	0.5006	74.469	31.876	42.617	
201	146.667	0.5021	74.687	32.045	42.666	
202	147.726	0.5036	74.903	32.212	42.715	
203	148.784	0.5050	75.119	32.379	42.763	
204	149.843	0.5064	75.333	32.546	42.811	
205	150.902	0.5078	75.545	32.711	42.858	
206	151.961	0.5093	75.757	32.876	42.904	
207A	153.019	0.5107	75.967	33.040	21.475	16.000
207B	153.019	0.5107			21.718	
208	154.053	0.5120	76.174	32.718	43.479	
209	155.086	0.5134	76.377	32.876	43.522	
210	156.120	0.5148	76.579	33.035	43.566	
211	157.152	0.5161	76.780	33.192	43.609	
212	158.185	0.5174	76.980	33.349	43.652	
213	159.218	0.5188	77.178	33.505	43.694	
214	160.250	0.5201	77.376	33.661	43.736	
215	161.283	0.5214	77.572	33.816	43.776	
216	162.314	0.5227	77.767	33.970	43.818	
217	163.346	0.5240	77.962	34.124	43.858	
218	164.378	0.5253	78.155	34.276	43.898	
219	165.409	0.5266	78.347	34.429	43.938	
220	166.439	0.5279	78.538	34.580	43.976	
221	167.470	0.5291	78.728	34.731	44.016	
222	168.500	0.5304	78.916	34.882	44.054	
223	169.530	0.5316	79.104	35.031	44.092	
224	170.559	0.5329	79.291	35.180	44.130	
225	171.588	0.5341	79.477	35.328	44.168	
226	172.617	0.5354	79.662	35.476	44.204	
227	173.646	0.5366	79.846	35.623	44.240	
228	174.674	0.5379	80.028	35.769	44.277	
229	175.701	0.5391	80.210	35.915	44.313	
230A	176.728	0.5403	80.391	36.060	22.174	16.000

Drift Tube No.	Energy	β	Cell Length	Gap Length	Drift Tube Length	d
230B	176.728	0.5402			22.420	16.000
231	177.731	0.5414	80.569	35.715	44.869	
232	178.733	0.5426	80.743	35.858	44.901	
233	179.735	0.5438	80.917	36.000	44.932	
234	180.737	0.5449	81.090	36.142	44.964	
235	181.738	0.5461	81.262	36.282	44.996	
236	182.740	0.5472	81.433	36,422	45.026	
237	183.741	0.5484	81.604	36.561	45.058	
238	184.742	0.5495	81.773	36.700	45.088	
239	185.743	0.5506	81.942	36.837	45.120	
240	186.743	0.5518	82.110	36.974	45.150	
241	187.743	0.5529	82.276	37.110	45.182	
242	188.743	0.5540	82.443	37.246	45.212	
243	189.743	0.5551	82.608	37.380	45.243	
244	190.742	0.5562	82.773	37.515	45.274	
245	191.742	0.5573	82.936	37.647	45.304	
246	192.740	0.5584	83.099	37.780	45.335	
247	193.739	0.5595	83.261	37.911	45.365	
248	194.737	0.5606	83.423	38.042	45.396	
249	195.735	0.5616	83.583	38.172	45.426	
250	196.733	0.5627	83.743	38.302	45.456	
251	197.730	0.5638	83.902	38.431	45.486	
252	198.727	0.5648	84.060	38.559	45.516	16.00
253A	199.713	0.5659	84.216	38.687	22.773	

The second and third column of Table VII lists the computed value of the maximum surface field for the geometry at the beginning and end of each cavity, i.e., the value α which is the ratio of the maximum field along the surface of the drift tube to the average field on the axis, E_0 . As pointed out earlier, the design accelerating gradient can be chosen either on the basis of a limitation on the peak surface field, or a field which is an optimum between the power and length costs of the design. Accelerating gradients chosen on the basis of these two considerations are shown in the fourth, fifth, and sixth columns of Table VII. The fourth and fifth columns list the gradients at the beginning and end of each cavity such that the peak surface field does not exceed 15 MV/m. The sixth column lists the optimum gradient based on the values: $k = 1.3$, $C_P = 94$ (K\$/MW) , and $C_L = 16.5 + 2/\beta$(K\$/m) . The last column lists the design value of the gradient for comparison. Since the values of the design gradient are less than the values in the fourth and fifth columns, it implies that the peak surface fields at all points are less than 15 MV/m, which gives some assurance against sparking problems. The design gradient has been reduced to stay within the 5 MW limitation of the power amplifier tube on all cavities. This results in less over-all cost than would be the case if an extra cavity and power amplifier tube were required. For this geometry and the values of the cost coefficients, the limitation on the gradient due to the sparking restriction is more restrictive than the gradient specified to optimize the length and power costs.

Figure 13 shows the interpolated values of ZT^2 from which the rf power per cavity may be calculated. The theoretical power losses per cavity were calculated as a sum over the cells of each cavity with added end plate losses.

The specific design parameters for the 200 MeV, 100 mA beam current, linac obtained from these considerations are shown in Table IX.

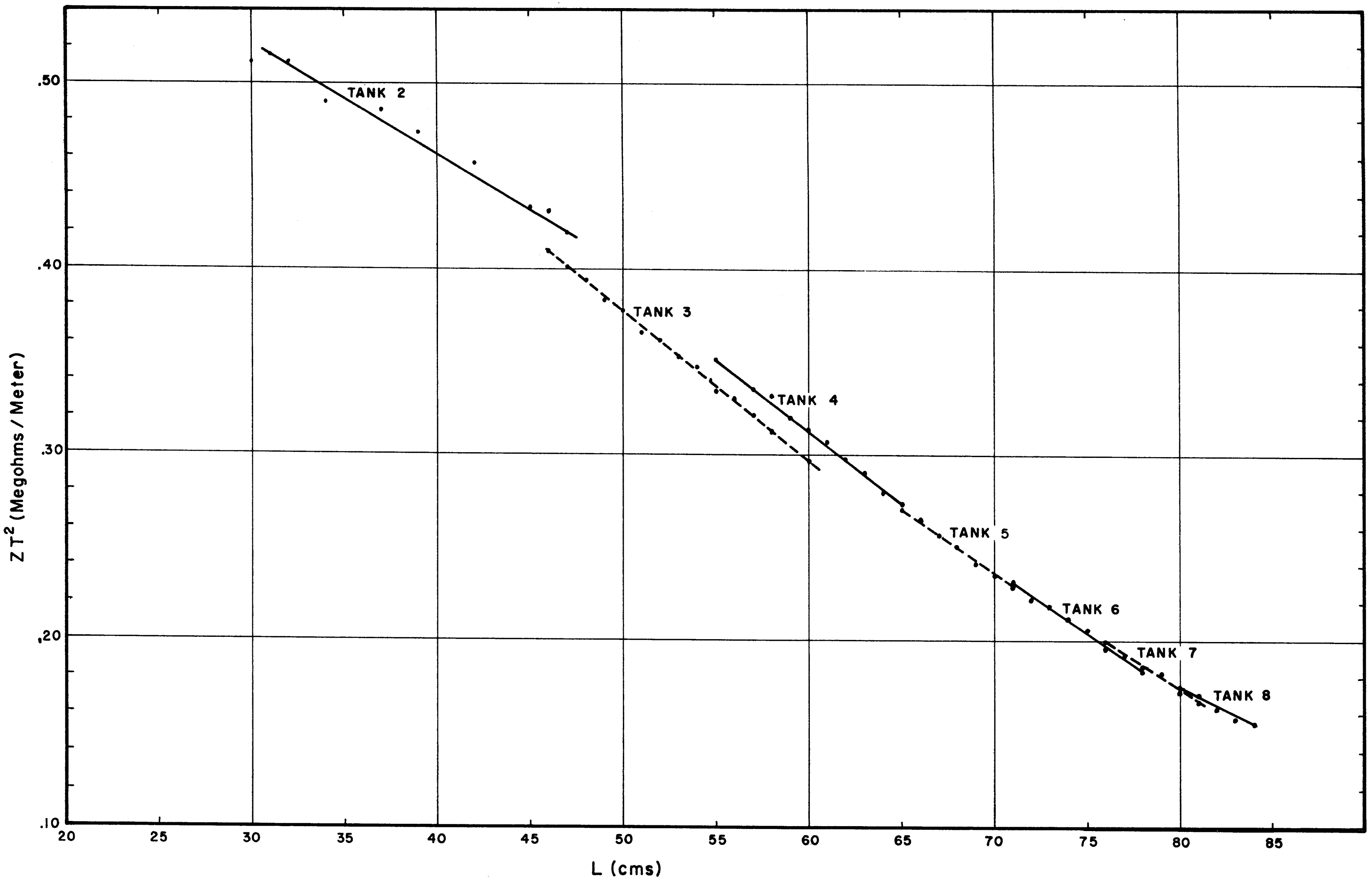

INTERPOLATED ZT^2 VALUES

FIG. 13

TABLE IX

SPECIFIC DESIGN PARAMETERS FOR A 100 mA - 200 MeV LINAC

Cavity Number	1	2	3	4	5	6	7	8
Input Energy W_i (MeV)	0.7594	20.056	49.649	77.288	104.029	128.688	153.019	176.728
Output Energy W_o (MeV)	20.056	49.649	77.288	104.029	128.688	153.019	176.728	199.70
β_{in}	0.0402	0.2035	0.3130	0.3826	0.4355	0.4761	0.5107	0.5403
β_{out}	0.2035	0.3130	0.3826	0.4355	0.4761	0.5107	0.5403	0.5658
$\Delta W = W_o - W_i$ (MeV)	19.297	29.593	27.639	26.741	24.659	24.331	23.709	22.97
Cavity Diameter D (cm)	95	90	88	86	85	84	83	82
Drift Tube Diameter d (cm)	Various	16 to 15	16	16	16	16	16	16
Drift Tube Aperture Diameter, A (cm)	1.3 to 3	3	3	3	4	4	4	4
End Cap Curvature R_c (cm)		4	4	5	5	5	5	5
Range of g/L	0.225 to 0.239	0.250 to 0.331	0.330 to 0.384	0.356 to 0.395	0.389 to 0.418	0.412 to 0.435	0.430 to 0.448	0.443 to 0.459
Number of Cells	71	37	28	25	23	23	23	23
Cavity Length (m)	12.90	14.32	14.55	15.26	15.63	16.92	18.01	18.96
Average Accelerating Gradient, E_o (MV/m)	1.89	2.8	2.8	2.7	2.6	2.5	2.4	2.3
Accel. Rate (MeV/m)	1.50	2.07	1.90	1.75	1.58	1.44	1.32	1.21
Power (Theor., no beam load) MW	0.77	1.67	1.87	1.98	1.99	2.10	2.17	2.18
Power (practical with beam load) MW	2.93	5.13	5.19	5.24	5.06	5.16	5.20	5.13

Total length of cavities - 126.55 m; over-all length including intercavity space - 133.55 m
Total rf power - 39.04 MW

V. PARTICLE DYNAMICS

After an adequate linac description has been obtained as described in the preceding section and by using the GENLIN subroutine of PARMILA, it is possible to investigate particle motion with the program. The usual investigation involves a choice of quadrupole focusing systems, i. e., type or periodicity, gradient, and length, that will preserve beam quality and prevent particle loss in the linac. This problem has been investigated by each laboratory which has built a quadrupole focused linac.[18, 19, 20] A slight complication arises in a multicavity system because of the discontinuity and space between cavities. The PARMILA program not only provides a tool for carrying out the investigation but allows more reliable data to be obtained by using information derived from the actual calculated fields in the gap.

A quadrupole field gradient, B', is chosen with regard to the stability limits. Figure 14 shows a plot of a stability diagram for a +-+- configuration with the line marked $\cos \mu_1 = 1$ showing an approximate stability limit (see reference 19). In this figure, the quadrupole field gradients are chosen for each energy cell according to an operating line given by the equation:

$$\left(\frac{Q/L}{0.5} \right) \theta_o^2 = C_7 + C_8 \Delta$$

where

$$\theta_o^2 = \frac{e\, B' \beta \lambda^2}{m_o\, c^2 \gamma}$$

and

$$\Delta = \frac{\pi e\, E_o\, \lambda\, T_n \sin \phi_s}{m_o\, c^2 \beta\, \gamma^3}$$

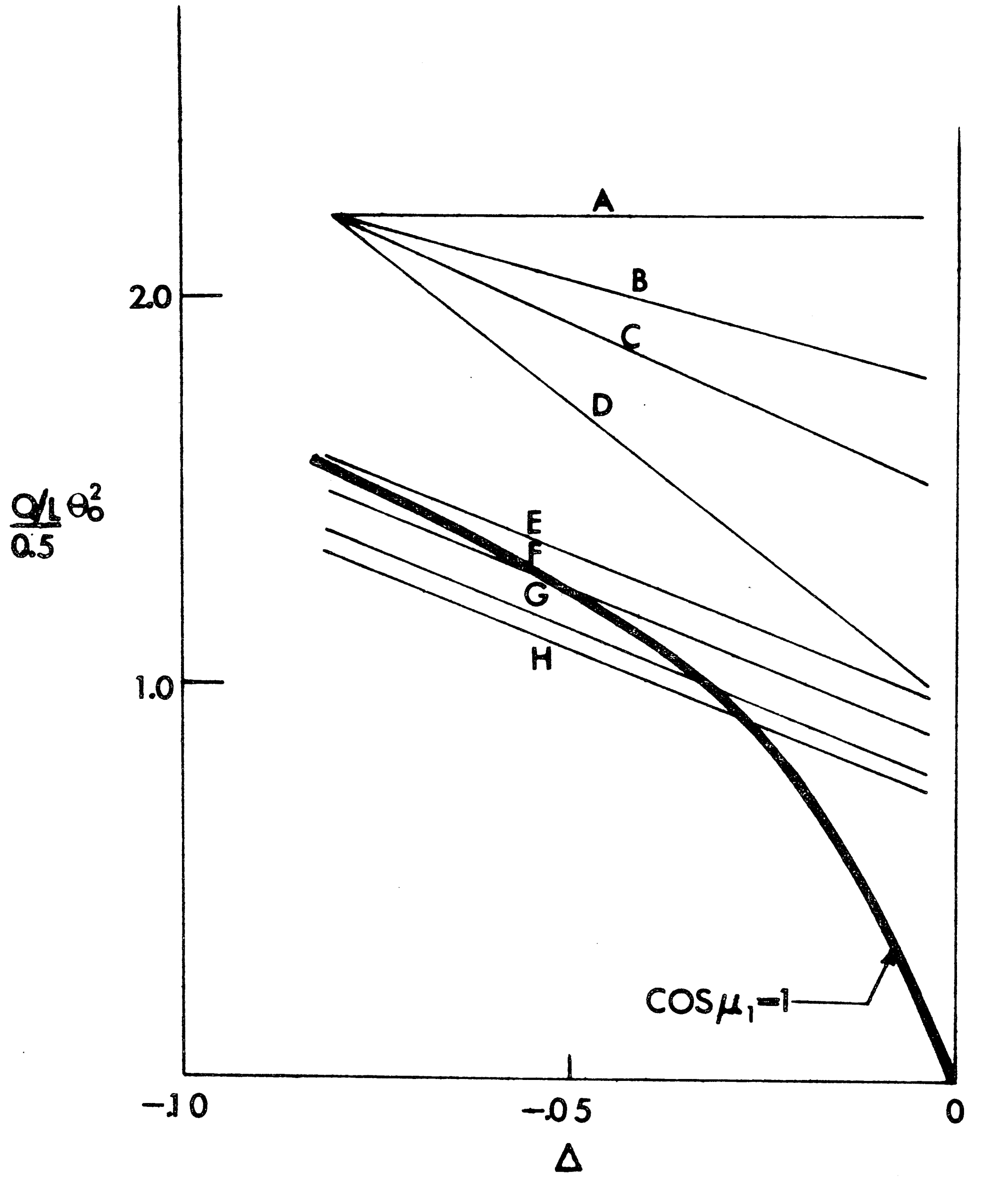

Operation Line Equation	X,X′ Acceptance for Tank 1 in mrad. cm.
A. $\Lambda = 2.28$	21π
B. $\Lambda = 1.77 - 6.1333\Delta$	21π
C. $\Lambda = 1.50 - 9.6154\Delta$	21π
D. $\Lambda = 0.93805 - 16.4166\Delta$	21π
E. $\Lambda = 0.93805 - 7.9396\Delta$	13π
F. $\Lambda = 0.844 - 7.9396\Delta$	10π
G. $\Lambda = 0.75 - 7.9396\Delta$	5π
H. $\Lambda = 0.70 - 7.9396\Delta$	4π

$$\Lambda = \frac{Q/L\,\theta_0^2}{0.5}$$

STABILITY DIAGRAM

Fig 14

so that

$$B' = \frac{0.5}{Q/L} \frac{\gamma}{\beta} \left(\frac{m_o c^2}{e \lambda^2} C_7 + \frac{\pi E_o T_n \sin \phi_s}{\lambda \beta \gamma^3} C_8 \right)$$

in the notation of Appendix B and where Q is the quadrupole length. In this figure, several different operating lines are shown and the x, x' phase-space acceptance for Tank No. 1 corresponding to each operating line. It is observed that the acceptance decreases as operating lines are chosen closer to the stability limit.

The operating line of the present 50 MeV ZGS injector is shown in Fig. 14 as equation D, with $C_7 = + 0.93805$ and $C_8 = - 16.4166$. This system has been investigated in some detail.[20] It was decided to continue this system (System I) throughout the linac described in this report. Beyond 50 MeV the requirements of the quadrupole system become easier to meet and it is possible to consider alternate systems. One configuration (System II) was examined in which alternate quadrupoles are turned off, i.e., +0-0, with the gradients for the magnets left on determined from the same operating line. Although this system does not lose particles, the resulting beam quality is not as good as that for System I. Further study may lead to improved results.

In order to continue along the chosen operating line for System I, it is necessary to use a matching quadrupole in the one-meter drift space between T-1 and T-2. (A one-meter drift space is allowed between successive cavities.) The drift spaces between the other cavities can be bridged without undue sacrifice of beam or quality by using quadrupoles of one-half length, same strength (or one-half strength, same length) in the half drift tubes at the end

TABLE X DRIFT TUBE QUADRUPOLE STRENGTHS

Drift Tube Number	A/2 (cm)	Q (cm)	Quadrupole Gradient (B') gauss/cm System I	Quadrupole Gradient (B') gauss/cm System II
0	0.6350	3.0163	+8245.15	
1	0.6350	3.0163	-7950.06	
2	0.6350	3.0163	+7808.32	
3	0.6350	3.0163	-7599.87	
4	0.6350	3.0163	+7421.50	
5	0.6350	3.0163	-7255.23	
6	0.6350	3.0163	+7100.07	
7	0.6350	3.0163	-6955.16	
8	0.9525	4.4450	+4493.56	
9	0.9525	4.4450	-4424.90	
10	0.9525	4.4450	+4359.80	
11	0.9525	4.4450	-4297.57	
12	0.9525	4.4450	+4238.14	
13	0.9525	4.4450	-4181.39	
14	0.9525	4.4450	+4127.20	
15	0.9525	4.4450	-4075.46	
16	0.9525	4.4450	+4026.06	
17	0.9525	4.4450	-3978.88	
18	1.270	6.035	+2846.39	
19	1.270	6.035	-2819.60	
20	1.270	6.035	+2793.85	
21	1.270	6.035	-2768.96	
22	1.270	6.035	+2744.92	
23	1.270	6.035	-2721.70	
24	1.270	6.035	+2699.27	
25	1.270	6.035	-2677.62	
26	1.270	6.035	+2656.71	
27	1.270	6.035	-2636.51	
28	1.270	6.035	+2617.01	
29	1.270	6.035	-2598.17	
30	1.270	6.035	+2579.97	
31	1.270	6.035	-2562.39	
32	1.270	6.035	+2545.40	
33	1.5875	8.7300	-1731.02	
34	1.5875	8.7300	+1721.21	
35	1.5875	8.7300	-1711.70	
36		8.7300	+1702.45	
37	↑	8.7300	-1693.47	
38		8.7300	+1684.74	
39		8.7300	-1676.25	
40		8.7300	+1668.00	
41		8.7300	-1659.99	
42		8.7300	+1652.20	
43		8.7300	-1644.63	
44		8.7300	+1637.27	
45		8.7300	-1630.11	
46		8.7300	+1623.15	
47		8.7300	-1616.39	
48		8.7300	+1609.81	
49		8.7300	-1603.42	
50		8.7300	+1597.19	
51		8.7300	-1591.14	
52		8.7300	+1585.25	
53		8.7300	-1579.53	
54		8.7300	+1573.95	
55		8.7300	-1568.53	
56		8.7300	+1563.25	
57		8.7300	-1558.11	
58		14.2876	+ 948.98	
59		14.2876	- 946.01	
60		14.2876	+ 943.11	
61		14.2876	- 940.29	
62		14.2876	+ 937.55	
63		14.2876	- 934.87	
64		14.2876	+ 932.27	
65		14.2876	- 929.73	
66		14.2876	+ 927.26	
67	↓	14.2876	- 924.85	
68		14.2876	+ 922.51	
69	1.5875	14.2876	- 920.22	
70	1.5875	14.2876	+ 918.00	
71A	1.5875	14.2876	- 915.83	
Matching Quad.		14.2876	+ 688.07	+ 688.07
71B	1.50	14.2876	-1000.90	
72	1.50	14.2876	+ 996.22	
73	1.50	14.2876	- 991.52	
74		14.2876	+ 986.98	
75	↑	14.2876	- 982.58	
76		14.2876	+ 978.33	
77		14.2876	- 974.22	
78		14.2876	+ 970.24	
79		14.2876	- 966.38	
80		14.2876	+ 962.65	
81		14.2876	- 959.03	
82		14.2876	+ 955.52	
83		14.2876	- 952.13	
84		19.050	+ 711.65	
85		19.050	- 709.25	
86		19.050	+ 706.93	
87		19.050	- 704.68	
88		19.050	+ 702.49	
89		19.050	- 700.37	
90		19.050	+ 698.31	
91		19.050	- 696.31	
92		19.050	+ 694.37	
93		19.050	- 692.49	
94		19.050	+ 690.66	
95		19.050	- 688.89	
96		19.050	+ 687.17	
97		19.050	- 685.49	
98		19.050	+ 683.87	
99		19.050	- 682.29	
100		19.050	+ 680.76	
101		19.050	- 679.28	
102		19.050	+ 677.83	
103		19.050	- 676.43	
104		19.050	+ 675.07	
105	↓	19.050	- 673.74	
106	1.50	19.050	+ 672.46	
107	1.50	19.050	- 671.21	
108A	1.50	9.525	+ 670.00	
108B	1.50	9.525	+ 671.22	+ 671.22
109	1.50	19.050	- 670.21	0
110	1.50	19.050	+ 669.02	- 669.02
111		19.050	- 667.88	0
112	↑	19.050	+ 666.78	+ 666.78
113		19.050	- 665.71	0
114		19.050	+ 664.68	- 664.68
115		19.050	- 663.68	0
116		19.050	+ 662.72	+ 662.72
117		19.050	- 661.79	0
118		19.050	+ 660.89	- 660.89
119		19.050	- 660.03	0
120		19.050	+ 659.19	+ 659.19
121		19.050	- 658.38	0
122		19.050	+ 657.60	- 657.60
123		19.050	- 656.85	0
124		19.050	+ 656.12	+ 656.12
125		19.050	- 655.42	0
126		19.050	+ 654.75	- 654.75
127		19.050	- 654.10	0
128		19.050	+ 653.48	+ 653.48
129		19.050	- 652.88	0
130		19.050	+ 652.30	- 652.30
131		19.050	- 651.74	0
132	↓	19.050	+ 651.21	+ 651.21
133		19.050	- 650.70	0
134	1.50	19.050	+ 650.20	- 650.20
135	1.50	19.050	- 649.73	0
136A	1.50	9.525	+ 649.28	+ 649.28
136B		9.525	+ 649.89	+ 649.89
137		19.050	- 649.59	0
138	1.50	19.050	+ 649.15	- 649.15
139	1.50	19.050	- 648.73	0
140	1.50	19.050	+ 648.34	+ 648.34

TABLE X DRIFT TUBE QUADRUPOLE STRENGTHS (CONTINUED)

Drift Tube Number	A/2 (cm)	Q (cm)	Quadrupole Gradient (B') gauss/cm System I	Quadrupole Gradient (B') gauss/cm System II
141	1.50	19.050	-647.96	0
142	1.50	19.050	+647.60	-647.60
143	1.50	19.050	-647.26	0
144		19.050	+646.93	+646.93
145		19.050	-646.63	0
146		19.050	+646.34	-646.34
147		19.050	-646.06	0
148		19.050	+645.80	+645.80
149		19.050	-645.56	0
150		19.050	+645.33	-645.33
151		19.050	-645.12	0
152		19.050	+644.92	+644.92
153		19.050	-644.74	0
154		19.050	+644.57	-644.57
155		19.050	-644.41	0
156		19.050	+644.27	+644.27
157		19.050	-644.14	0
158		19.050	+644.02	-644.02
159	1.50	19.050	-643.91	0
160	1.50	19.050	+643.82	+643.82
161A	1.50	9.525	-643.73	0
161B (Sys.I)	2.0	9.525	-641.68	
161B (Sys.II)	2.0	19.050		-641.68
162	2.0	19.050	+641.74	0
163		19.050	-641.69	+641.69
164		19.050	+641.65	0
165		19.050	-641.62	-641.62
166		19.050	+641.61	0
167		19.050	-641.60	+641.60
168		19.050	+641.60	0
169		19.050	-641.61	-641.61
170		19.050	+641.63	0
171		19.050	-641.66	+641.66
172		19.050	+641.70	0
173		19.050	-641.74	-641.74
174		19.050	+641.80	0
175		19.050	-641.86	+641.86
176		19.050	+641.93	0
177		19.050	-642.01	-642.01
178		19.050	+642.09	0
179		19.050	-642.19	+642.19
180		19.050	+642.29	0
181		19.050	-642.39	-642.39
182	2.0	19.050	+642.51	0
183	2.0	19.050	-642.63	+642.63
184A	2.0	9.525	+642.76	0
184B (Syst.I)	2.0	9.525	+641.42	
184B (Syst.II)	2.0	19.050		-641.42
185	2.0	19.050	-641.64	0
186		19.050	+641.79	+641.79
187		19.050	-641.94	0
188		19.050	+642.10	-642.10
189		19.050	-642.26	0
190		19.050	+642.43	+642.43
191		19.050	-642.61	0
192		19.050	+642.79	-642.79
193		19.050	-642.97	0
194		19.050	+643.17	+643.17
195		19.050	-643.36	0
196		19.050	+643.56	-643.56
197		19.050	-643.77	0
198		19.050	+643.98	+643.98
199		19.050	-644.19	0
200		19.050	+644.41	-644.41
201		19.050	-644.64	0
202		19.050	+644.87	+644.87
203		19.050	-645.10	0
204		19.050	+645.34	-645.34
205	2.0	19.050	-645.58	0
206	2.0	19.050	+645.82	+645.82
207A	2.0	9.525	-646.07	0
207B (Sys.I)	2.0	9.525	-644.93	
207B (Sys. II)	2.0	19.050		-644.93
208	2.0	19.050	+645.25	0
209		19.050	-645.50	+645.50
210		19.050	+645.76	0
211		19.050	-646.03	-646.03
212		19.050	+646.30	0
213		19.050	-646.57	+646.57
214		19.050	+646.84	0
215		19.050	-647.12	-647.12
216		19.050	+647.40	0
217		19.050	-647.69	+647.69
218		19.050	+647.98	0
219		19.050	-648.27	-648.27
220		19.050	+648.56	0
221		19.050	-648.86	+648.86
222		19.050	+649.16	0
223		19.050	-649.46	-649.46
224		19.050	+649.76	0
225		19.050	-650.07	+650.07
226		19.050	+650.38	0
227		19.050	-650.69	-650.69
228	2.0	19.050	+651.01	0
229	2.0	19.050	-651.33	+651.33
230A	2.0	9.525	+651.65	0
230B (Syst.I)	2.0	9.525	+650.64	
230B (Syst.II)	2.0	19.050		-650.64
231	2.0	19.050	-651.01	0
232		19.050	+651.34	+651.34
233		19.050	-651.67	0
234		19.050	+652.00	-652.00
235		19.050	-652.33	0
236		19.050	+652.67	+652.67
237		19.050	-653.00	0
238		19.050	+653.34	-653.34
239		19.050	-653.69	0
240		19.050	+654.03	+654.03
241		19.050	-654.37	0
242		19.050	+654.72	-654.72
243		19.050	-655.07	0
244		19.050	+655.42	+655.42
245		19.050	-655.77	0
246		19.050	+656.12	-656.12
247		19.050	-656.48	0
248		19.050	+656.84	+656.84
249		19.050	-657.20	0
250	2.0	19.050	+657.56	-657.56
251	2.0	19.050	-657.92	0
252	2.0	19.050	+658.28	+658.28
253A	2.0	9.525	-658.65	0

and beginning of each cavity. In System II the matching between cavities is dependent upon the terminating element in the focusing period in each cavity. If the cavity terminates in a + (or -) quadrupole, then the same system of one-half lengths, same strength, used in System I is satisfactory. However, if a cavity terminates in a 0 (off) quadrupole, then the beginning drift tube in the next cavity contains a full, + or - , quadrupole.

Table II lists the quadrupole length and strength for System I and System II for each drift tube including the matching quadrupole between the first and second cavities. For ease and economy of fabrication the quadrupoles are made in sets of fixed length.

In the PARMILA program each particle may have six coordinates, i.e., x, x', y, y', W, and ϕ , where x, x', y and y' are transverse displacements and angles of the particle trajectories, W is the particle energy and ϕ is the phase of the particle with respect to the rf accelerating voltage. Five hundred particles may be sent through the described linac and their positions plotted by the computer at the center of given quadrupoles in the linac so as to obtain the appropriate phase-space plots. If particles are lost, the number and place lost is given as output. The coordinates of particles which are not lost readily give emittance plots and their initial coordinates likewise give cavity acceptance information. Figure 15 shows x, x' acceptance-emittance plots obtained in this way for quadrupole System I.

The first cavity in this design is a special case and must be handled separately in the dynamics program. The actual gap fields of this cavity are not readily available so that the radial and longitudinal transit-time factors

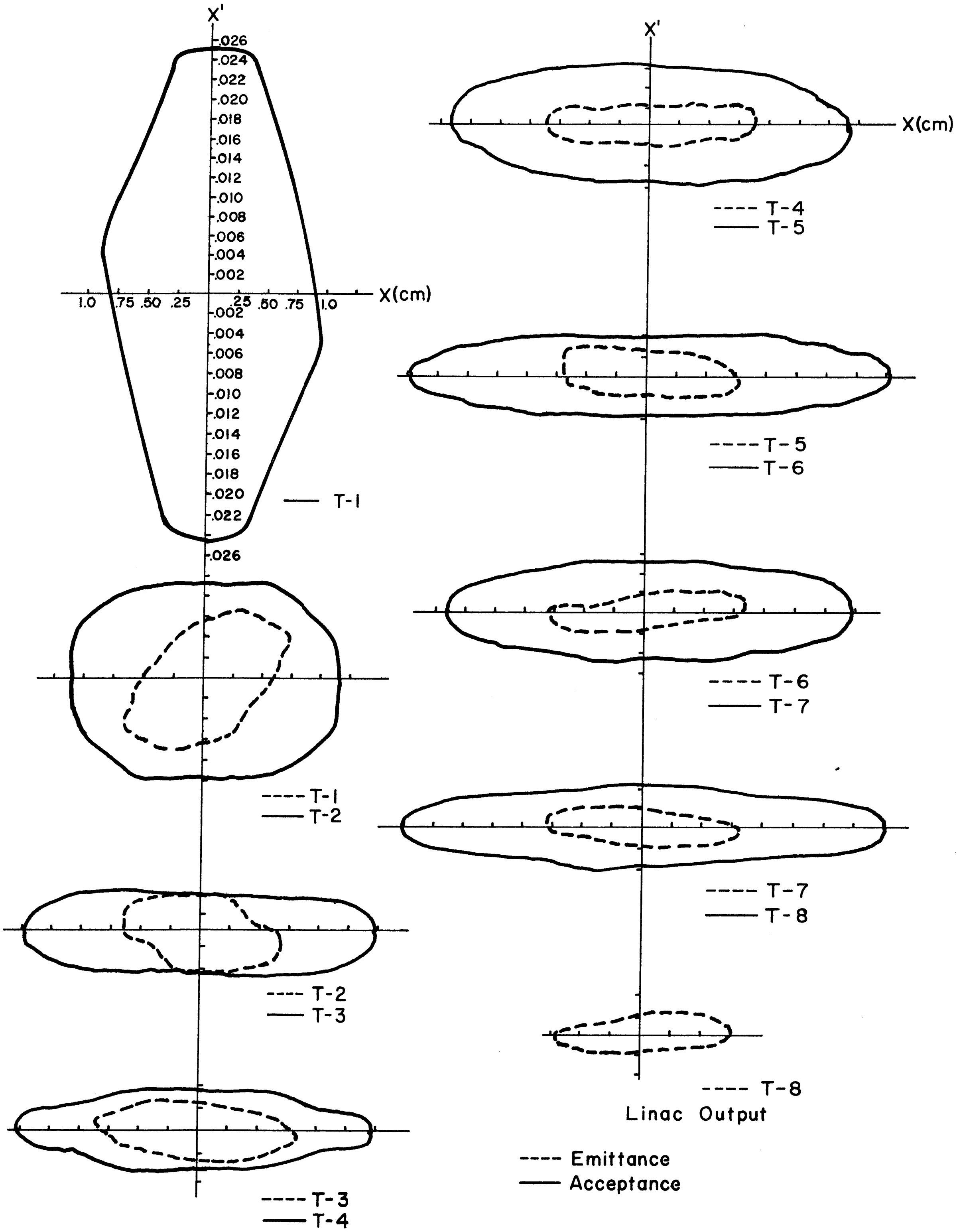

FIG.15 X, X' ACCEPTANCE - EMITTANCE PLOTS FOR EACH CAVITY

must be calculated for each cell from the analytical expressions involving the G/L and A/L ratios. The 50 MeV ZGS injector linac generated from the GENLIN subroutine of PARMILA using these transit-time factors agreed with the actual linac to better than one-half cell length in the 124 total. A beam of particles sent through a linac described in this way with output at 20 MeV allows the beam properties to be described. The output beam at 20 MeV serves as the input beam to the other cavities.

Figure 15 shows the x, x' acceptance-emittance plots for each cavity, being the circumscribed line around the points plotted by the computer. The particles in x, x' space which manage to get through the first cavity, T-1, originate from the area shown plotted in the upper left diagram, giving the acceptance of the linac with an area of about 20 π millirad-cm. This block of particles transform through quadrupole System I into the emittance curves at the end of each cavity as shown by the dotted areas. The final output from cavity T-8 has an area of about 1.4 π millirad-cm, which is about the area expected from adiabatic damping considerations. The acceptance area of each cavity is obtained by uniformly covering x, x' space into each cavity and observing the area covered by those particles not lost in traversing the cavity. If there is large area between the emittance and acceptance curves, misalignments of quadrupoles and drift tubes can be tolerated more easily. The "fit" in cavity T-3 indicates that a larger drift tube bore in this cavity would be desirable. Future work may well take cognizance of this fact.

Figure 16 shows the y, y' acceptance and emittance for the linac with quadrupole System I. The areas are slightly different from those in the x, x' space, but no problems are encountered at any point along the linac.

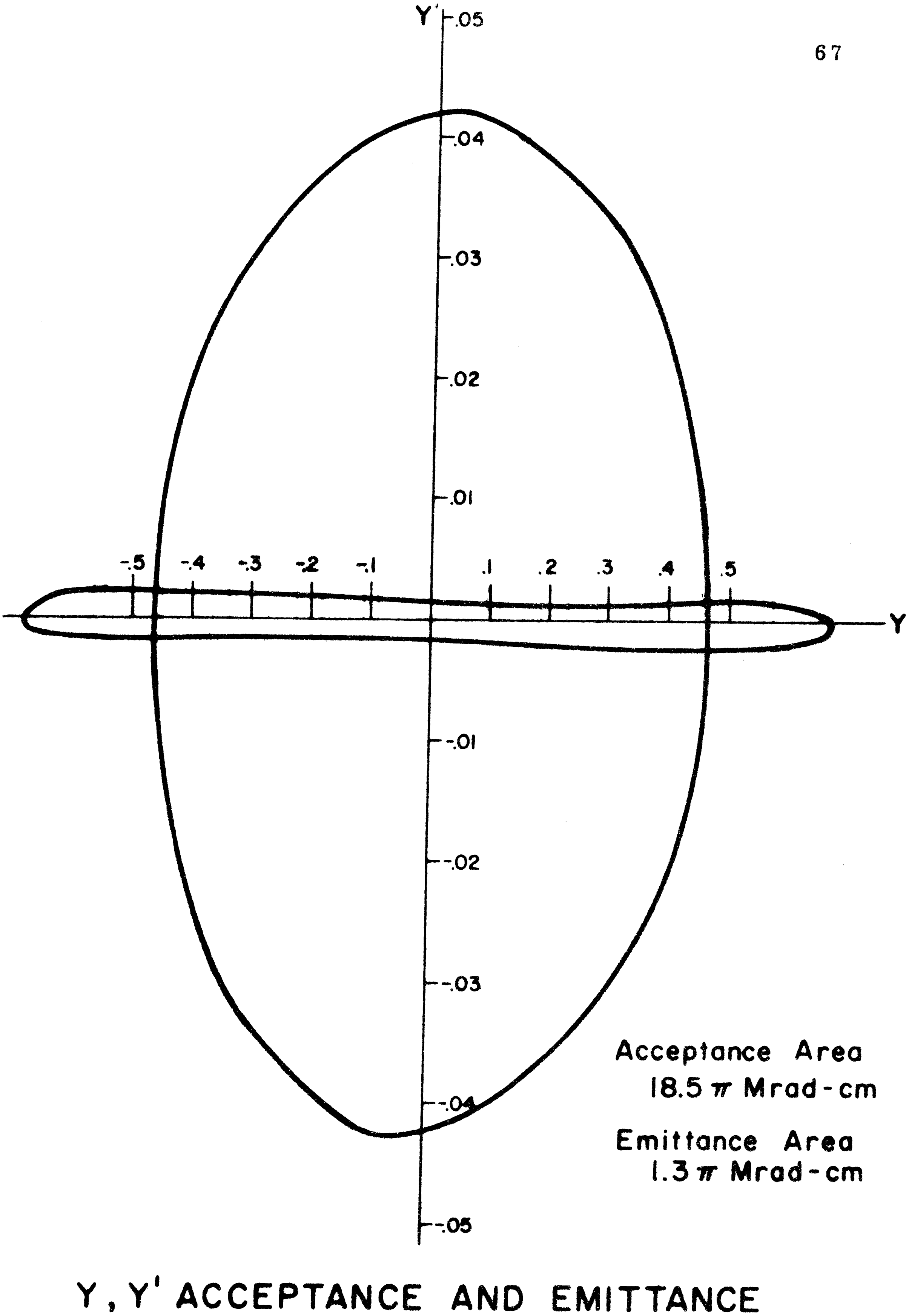

Y, Y' ACCEPTANCE AND EMITTANCE

Fig. 16

The emittances for quadrupole System II are shown in Fig. 17. If these emittance areas are compared with those for System I, it is observed that although no particles are lost the ellipse orientation may not be optimum with respect to the cavity acceptance, and alignment would be more critical. The linac output emittance is about the same. Further study with possible use of intercavity matching lenses may improve this system.

The longitudinal (W, ϕ) acceptance and final longitudinal emittance of the linac is shown in Fig. 18. In this case a block of particles with W, ϕ coordinates (x, x', y, y' equal zero) are sent into the first cavity. Those accepted into the linac originate in the area shown at the left. The emittance of these particles from the final cavity has the area shown at the right. Thus, the energy spread of the beam from the linac is + 0.65 to - 0.4%. If these particles had been sent through a linac with no drift spaces between cavities, the energy spread of the final beam would have been + 0.50 to - 0.4%. The increase in ΔW is attributed mainly to the one-meter drift between cavities 1 and 2 which results in an increase in the phase spread of the beam at this point.

Figure 19 shows the effect of the coupling of the longitudinal and transverse motion of the particles. The same "block" of particles in W, ϕ space is sent into the linac, but now with the values for x, x' shown by the points A, B, C and D in the figure at the left. Case A (x = x' = 0) is that shown in Fig. 18 and is repeated here for comparison. Case B (x = 0.5, x' = 0), Case C (x = 0.5, x' = 0.006), and Case D (x = 0.5, x' = 0.014) show how the longitudinal acceptance is affected by the transverse motion. Thus, alignment of the beam into the linac is important.

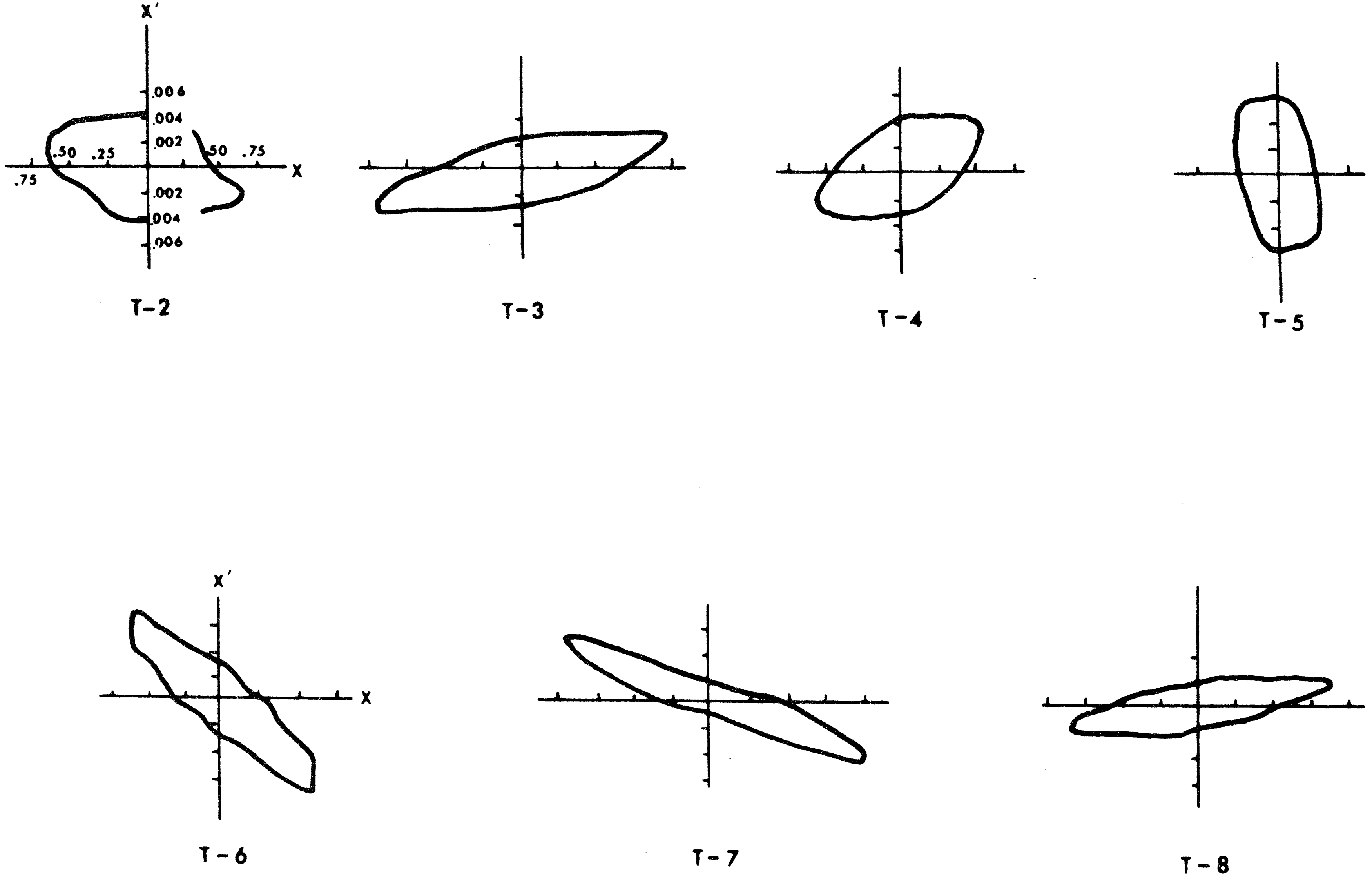

FIG. 17 X, X' EMITTANCES FOR SYSTEM II

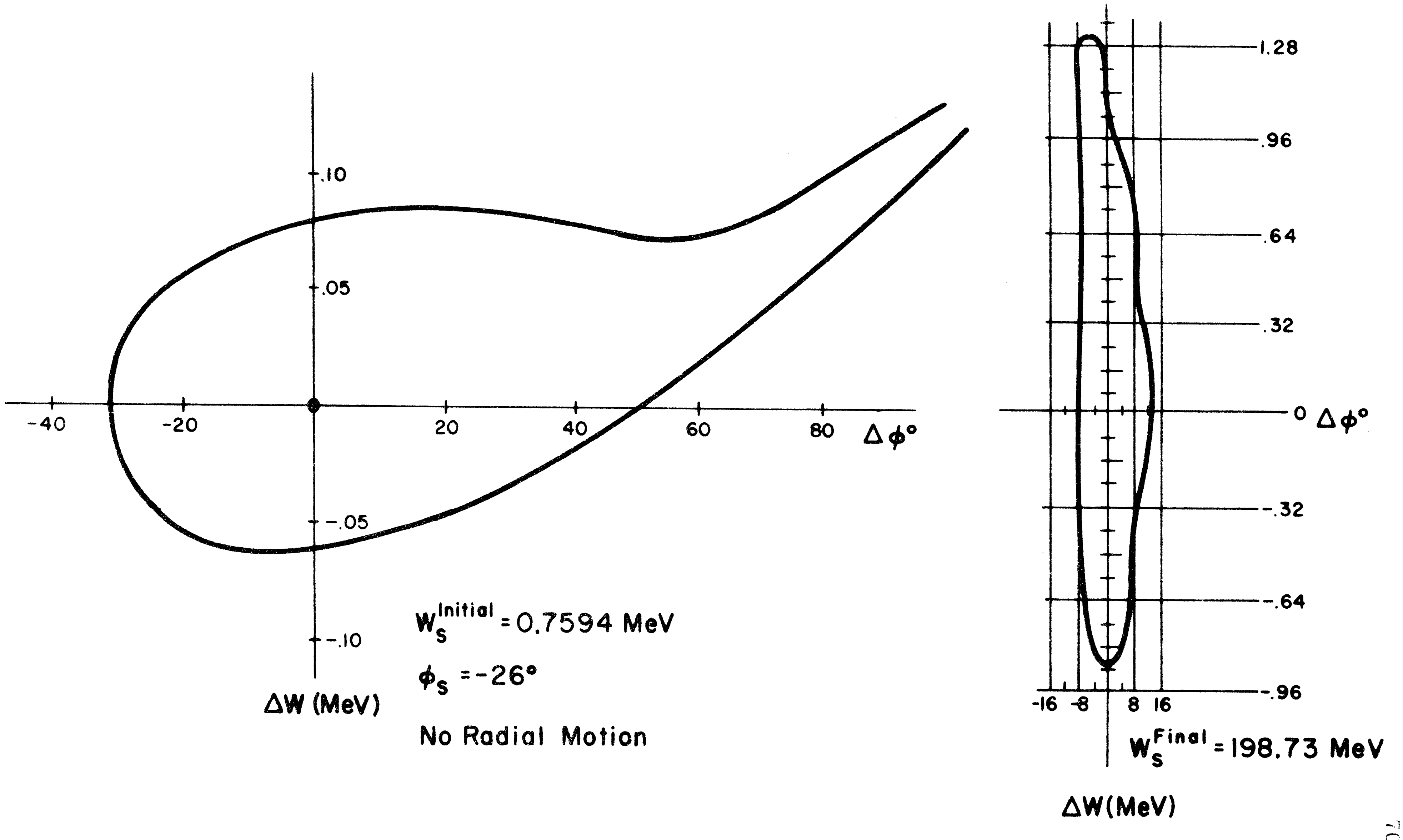

LONGITUDINAL ACCEPTANCE

LONGITUDINAL EMITTANCE

FIG. 18

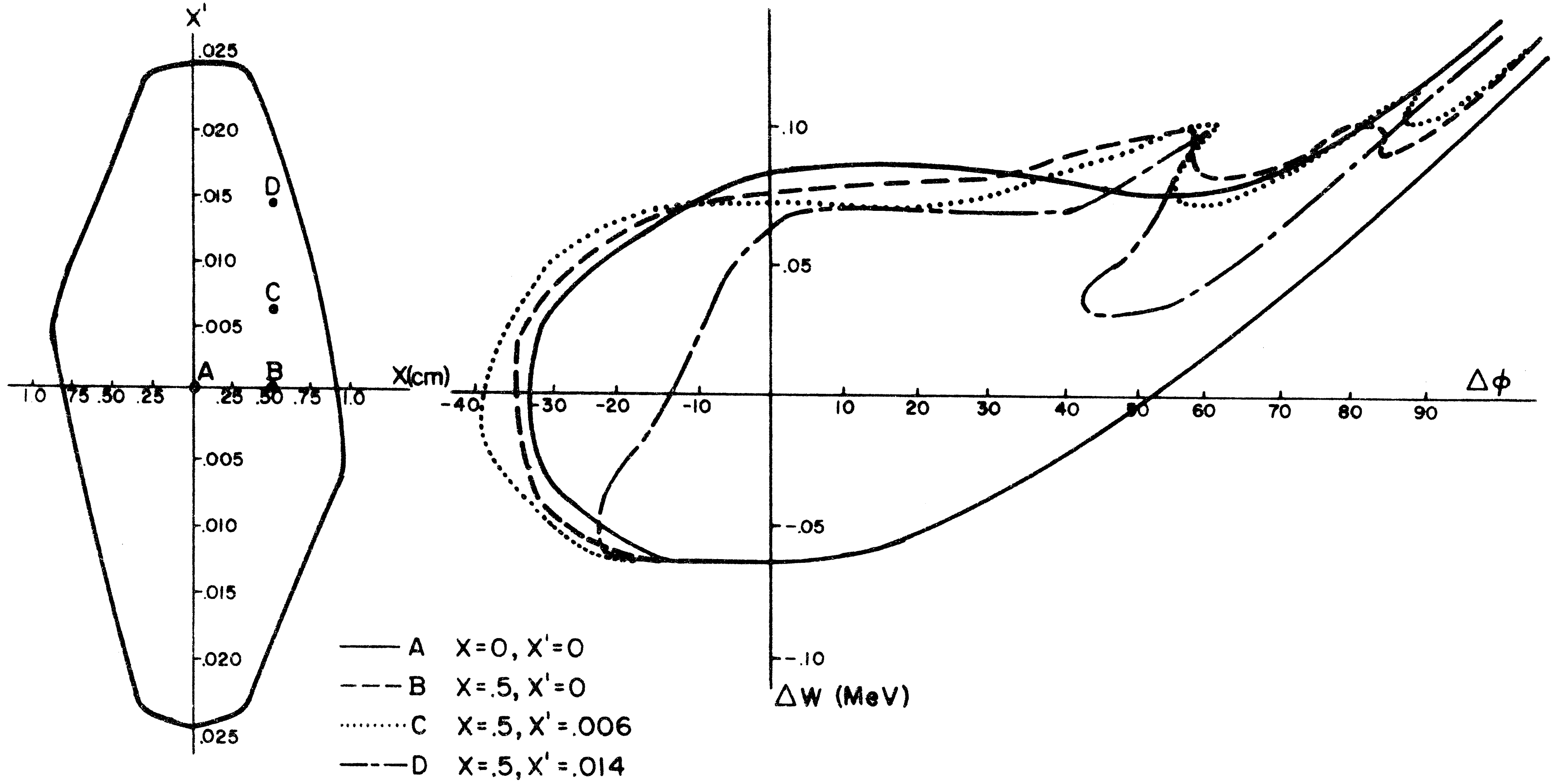

EFFECT ON LONGITUDINAL ACCEPTANCE
OF COUPLING TO TRANSVERSE MOTION.

FIG. 19

The longitudinal and transverse motion may also be represented continuously through the linac. This is shown in Figs. 20 and 21 where the motion of a single particle is plotted vs. the cell number. The ordinate value for each cell number is obtained in the center of the drift tube bearing the same number as the cell, i.e., the final half drift tube in the cell. In Fig. 20 showing the transverse motion for quadrupole System I and quadrupole System II, only the x value is plotted, although the x' value is used to aid in constructing the curve from the sparse x data. Figure 21 shows the longitudinal motion in ΔW and the longitudinal motion in ϕ . The bottom graph in Fig. 21 shows the effect of the coupling of the transverse motion to the longitudinal motion. In this case a particle of synchronous energy and phase, but with non-zero values for x, x' ($x = 0.5$, $x' = 0.014$), is investigated. The value of ΔW represents the energy change of the particle resulting from the transverse motion.

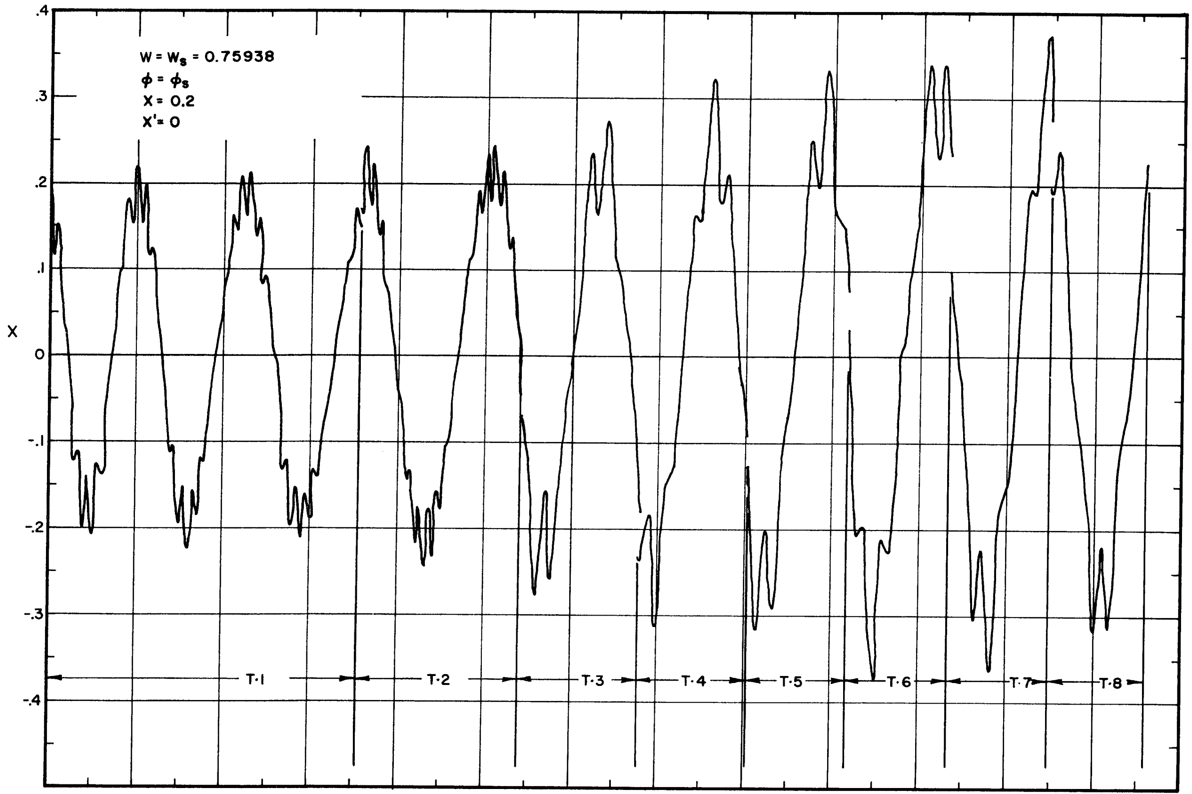

SYSTEM II

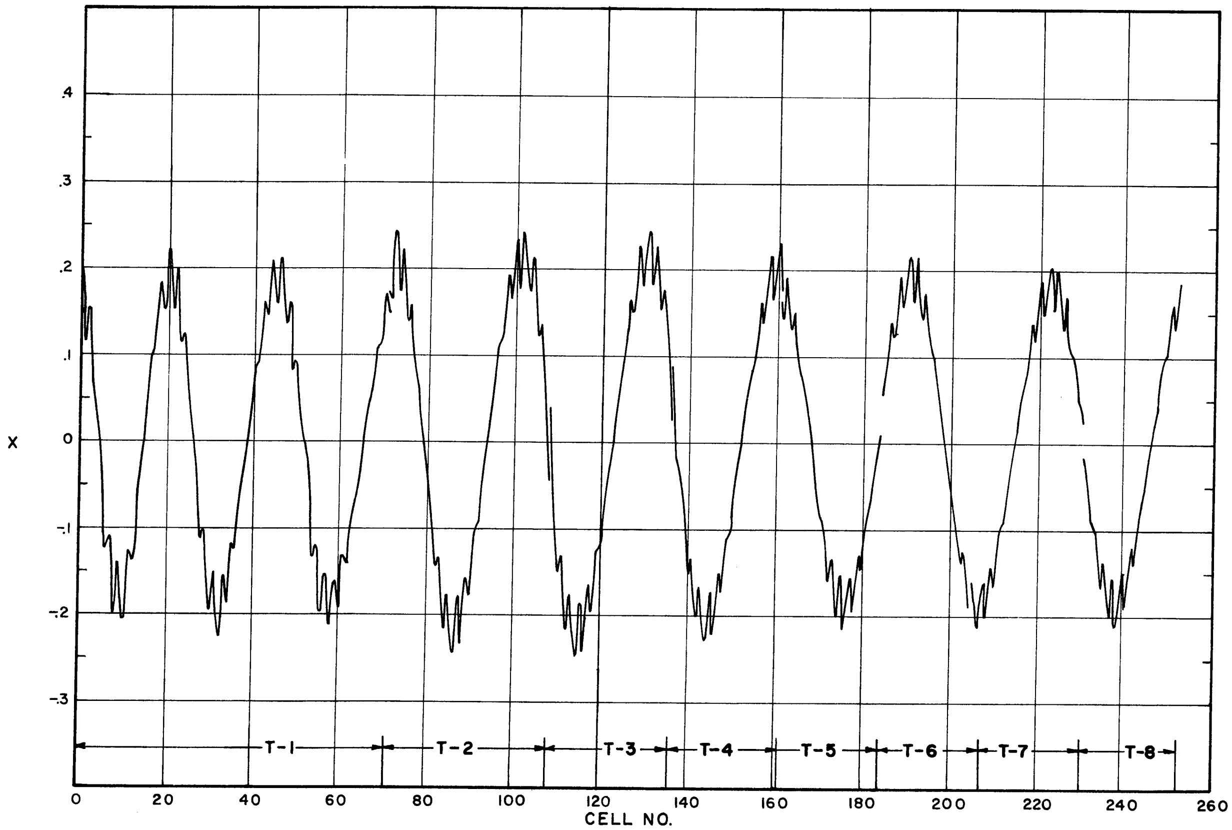

Fig. 20 TRANSVERSE MOTION (QUADRUPOLE SYSTEM I)

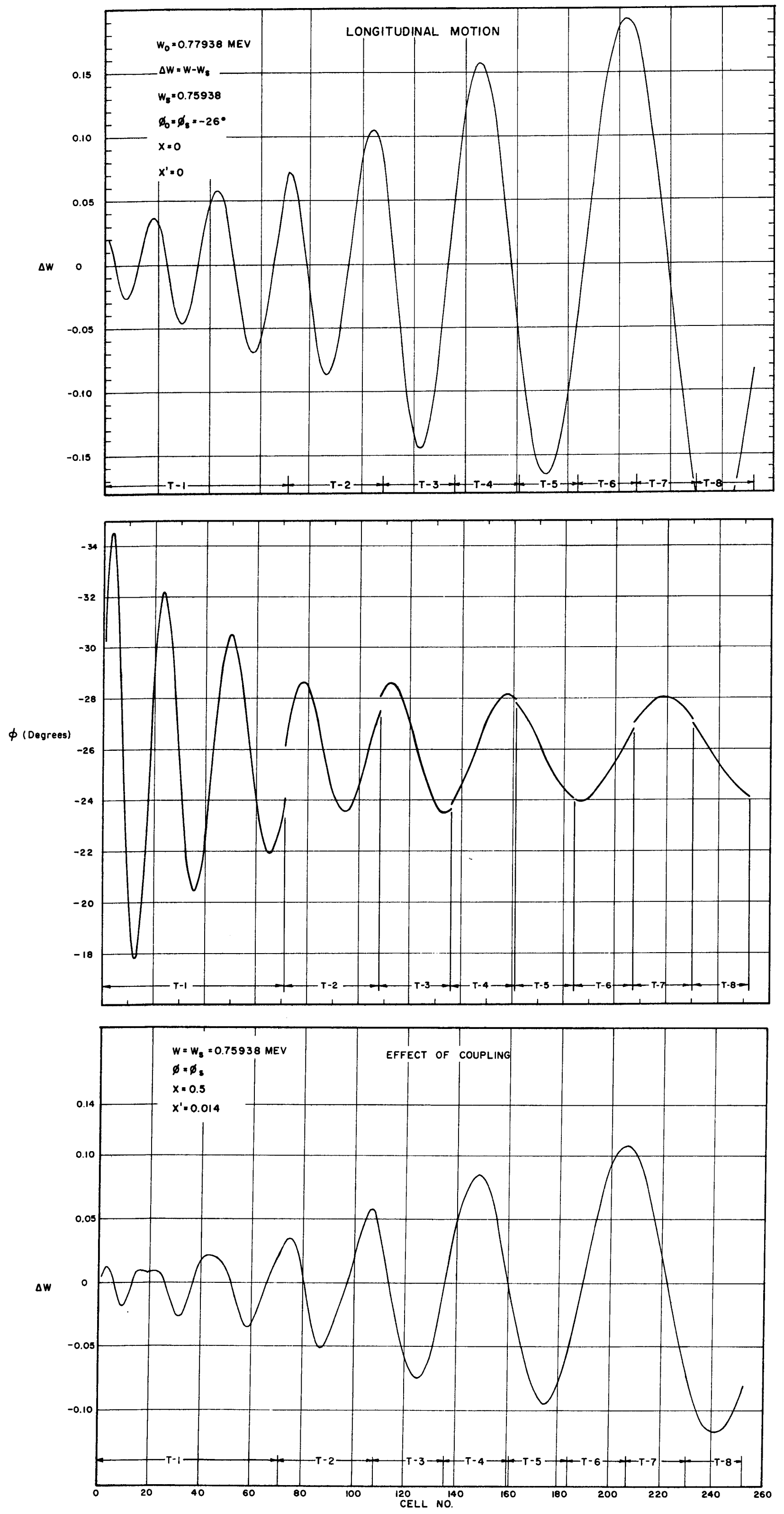

Fig. 21 LONGITUDINAL MOTION

VI. MECHANICAL ENGINEERING CONSIDERATIONS

Several different designs have been investigated for cylindrical drift tubes, their support stems, and adjusting mechanisms. A complete cost analysis has been made for one drift tube design. In addition, three copper clad cavities have been constructed. The experience gained in the cavity design and construction has led to some recommendations regarding vacuum systems and cooling requirements. These will be discussed. Appendix C includes calculations for cavity stresses, quadrupole design, and cooling.

Drift Tube, General

The effort in drift tube design has been directed towards a shape that would be common to many drift tubes. There are approximately 260 drift tubes in a 200 MeV linac and, therefore, a sufficient number to warrant a study of the mechanical design using interchangeable parts to reduce cost of component fabrication and assembly.

A large range in the bore size, outside diameter, length and curvature is required in the range of 0.75 MeV injection to 20 MeV. It appears that most components change from drift tube to drift tube. Thus it would be better to utilize the design and fabrication techniques that have been used on the linacs at BNL and ANL for the drift tubes in this range. This design effort was therefore confined to drift tubes for the range from 20 MeV to 200 MeV and having a 16 cm O.D. cylindrical shape. The cross-sectional shape is the same for all of these drift tubes and the variables are length and bore size. A slight modification of this analysis is required if, in fact, it is necessary to vary the drift tube diameter from 16 cm to 15 cm in cavity two, i.e., from 20 to

50 MeV. An alternative is to taper the cavity diameter and maintain a 16-cm diameter drift tube. This cavity taper is feasible and, if only a small taper is required, it is recommended.

The design then will be concerned with a cylindrical shaped drift tube of constant outside diameter. The end caps can be of simple contour and interchangeable for a large number of drift tubes. This permits volume production techniques to be utilized. A drift tube design was developed as shown in Fig. 22. This drawing is for all drift tubes with the only variables being length and bore to suit any energy position in the cavity. The outer body is a 16-cm copper tube that is cut to a length such that, with two end caps electron beam welded on, it will be the specified length. Inside the outer body is another tube that has cooling passages milled in for cooling the drift tube body. The depth of these passages can be varied to suit the duty cycle and to provide the proper turbulent cooling water flow. The inlet and outlet tubes (11) and cooling passages can be fabricated to provide cooling capacity for a 6% duty factor.

The quadrupole magnet coil is copper tubing (7) that has been wound on an adjustable mandrel of the right length for the drift tube body. After the mandrel is removed, the iron stampings (6) are inserted by halves (alternating the joint)to make the required length and then four rods are inserted and riveted to hold the assembly together. The space between the coil and iron is potted to make a complete magnet. This is then inserted into the machined seat on the inside of the cooling body while the leads are threaded up through the stem adapter (5). When in position, the magnet is held by a retaining ring (9). The quadrupole cooling is internal in the winding.

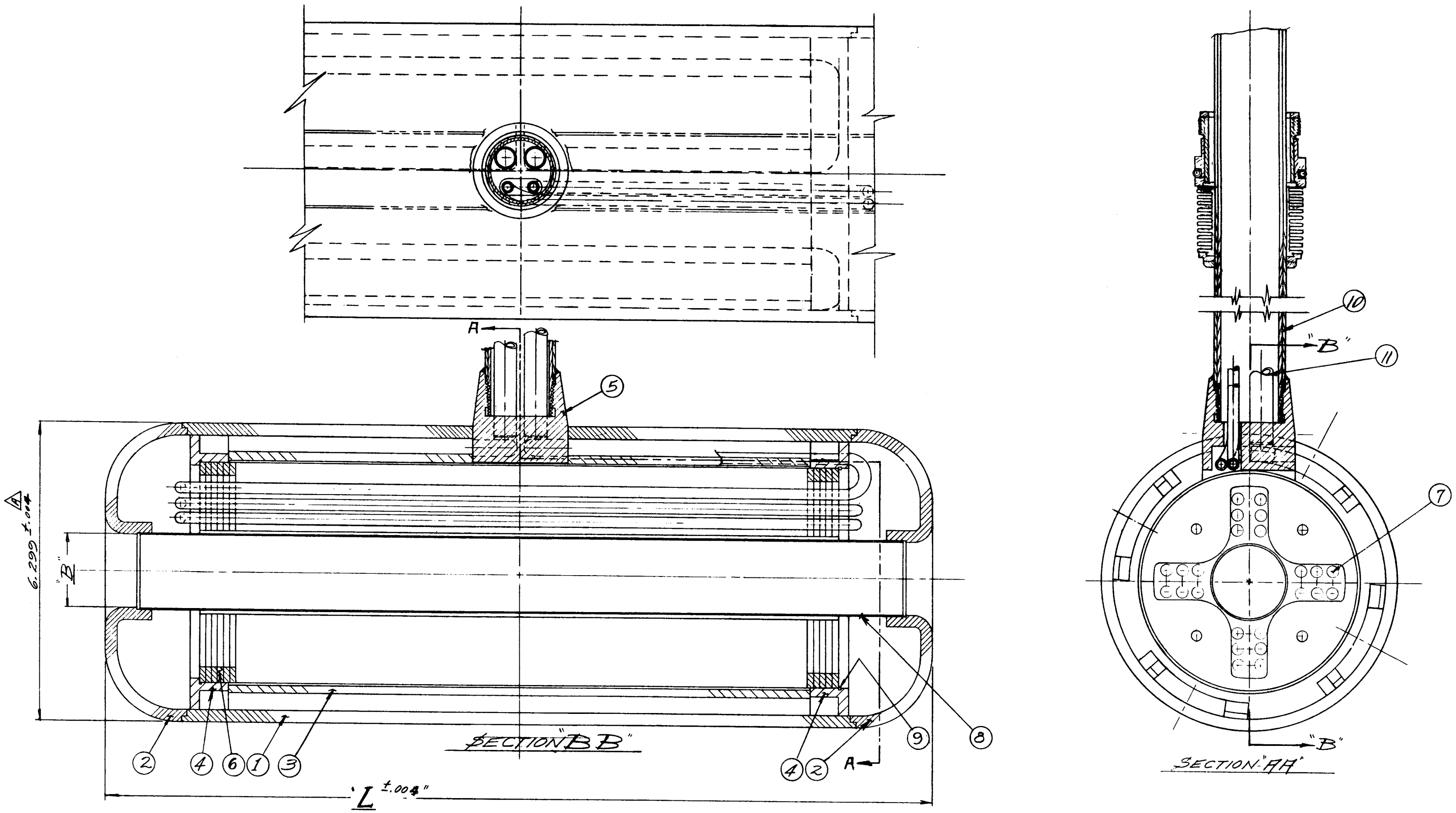

FIG. 22 200 MeV DRIFT TUBE

The bore tube is inserted and the end caps are positioned. The joints are then electron beam welded for vacuum tight service.

The drift tube stem is stainless steel with copper cladding on the outside. The stainless is the strength member and is screwed into the drift tube with the copper being soldered to the adapter to provide an rf connection and a vacuum seal. The bellows arrangement provides for rf continuity from the stem to the cavity wall, means of establishing a vacuum seal, and flexibility during alignment.

From this design, drawings were sent to potential commercial suppliers and Argonne National Laboratory Central Shops for cost estimates and feasibility. A review of the cost estimates appears later in the cost section.

A number of companies were visited and this design was discussed with their engineers. From these discussions evolved variations in the over-all concept of fabrication and this has resulted in drawings being generated as shown in Figs. 24, 25, and 26. These drawings are to record the various ideas and no single arrangement is advocated over another. Figure 23 is an isometric view of the original design in Fig. 22. A final design might include features from any of these.

Drift Tube Cylinder Body

The body is made of OFHC tubing as shown in Fig. 23. This is finish machined on the O. D. and bored on the inside if necessary for liner fit.

A suggestion has been made that the body be made of stainless steel. This would provide a body that is stiffer and less likely to sag with time. A stainless steel body also has less chance of being damaged during handling.

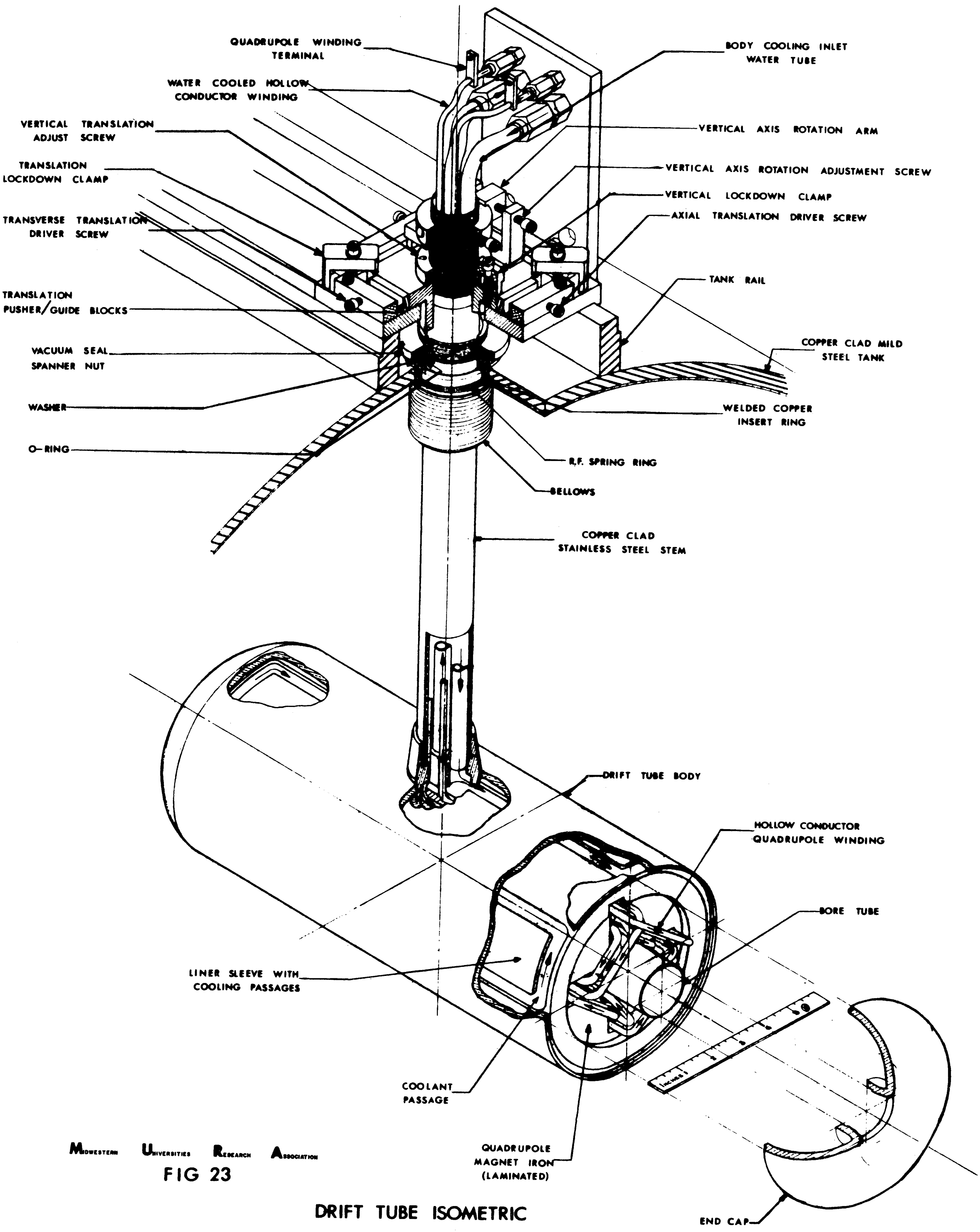

Midwestern Universities Research Association

FIG 23

DRIFT TUBE ISOMETRIC
HOLLOW COILS

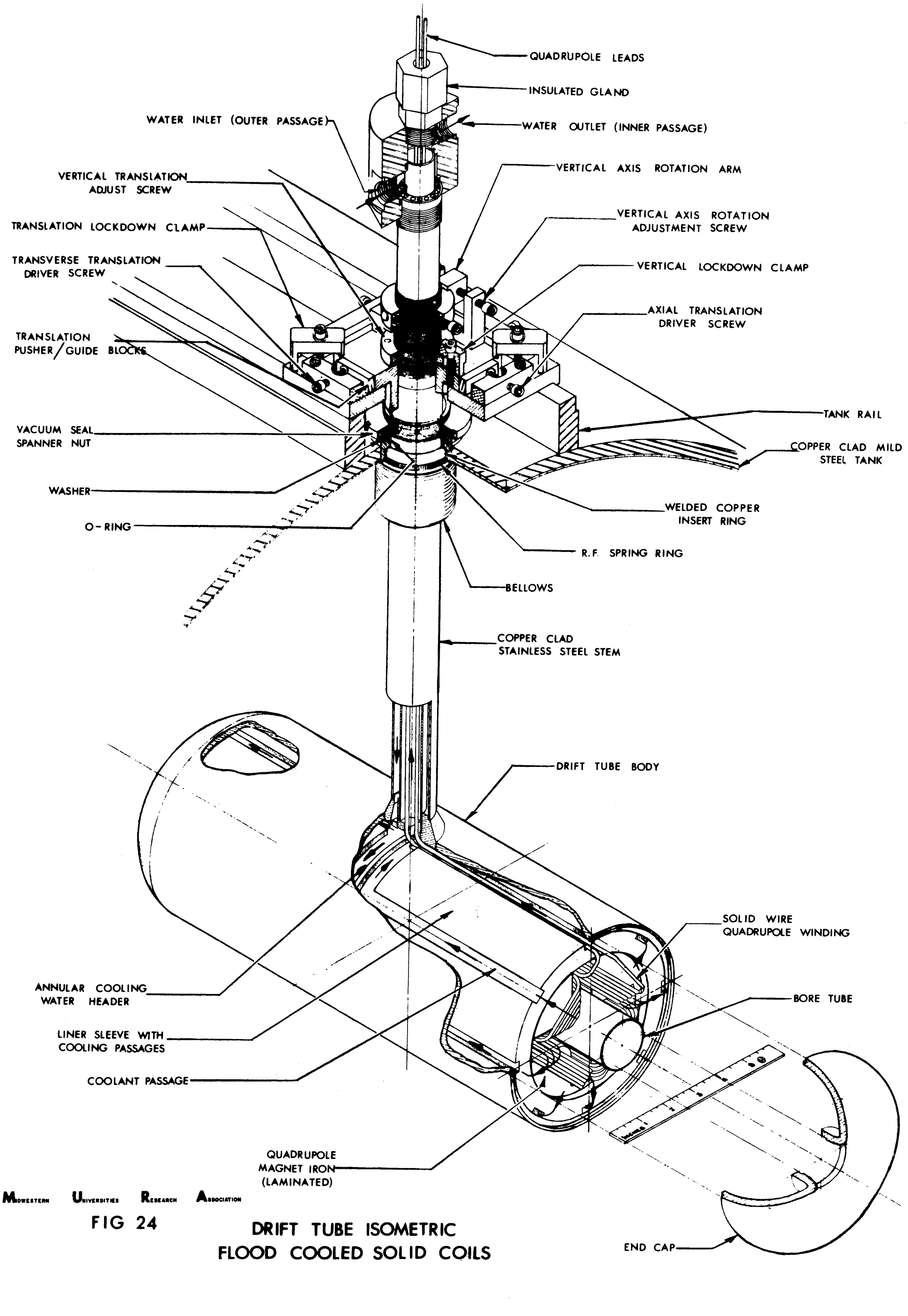

MIDWESTERN UNIVERSITIES RESEARCH ASSOCIATION

FIG 24

DRIFT TUBE ISOMETRIC
FLOOD COOLED SOLID COILS

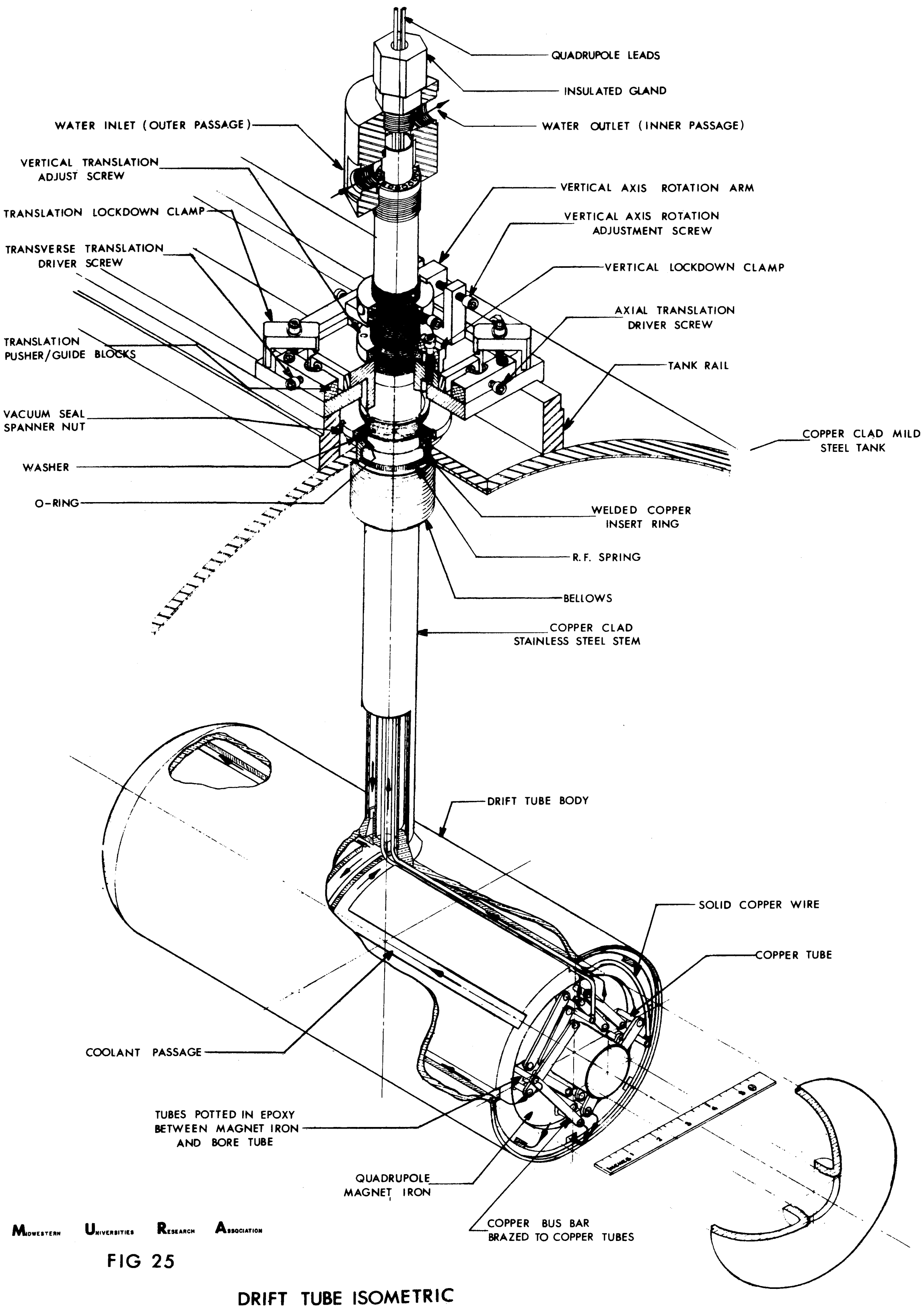

Midwestern **U**niversities **R**esearch **A**ssociation

FIG 25

DRIFT TUBE ISOMETRIC
FLOOD COOLED BUSBAR/TUBE COILS

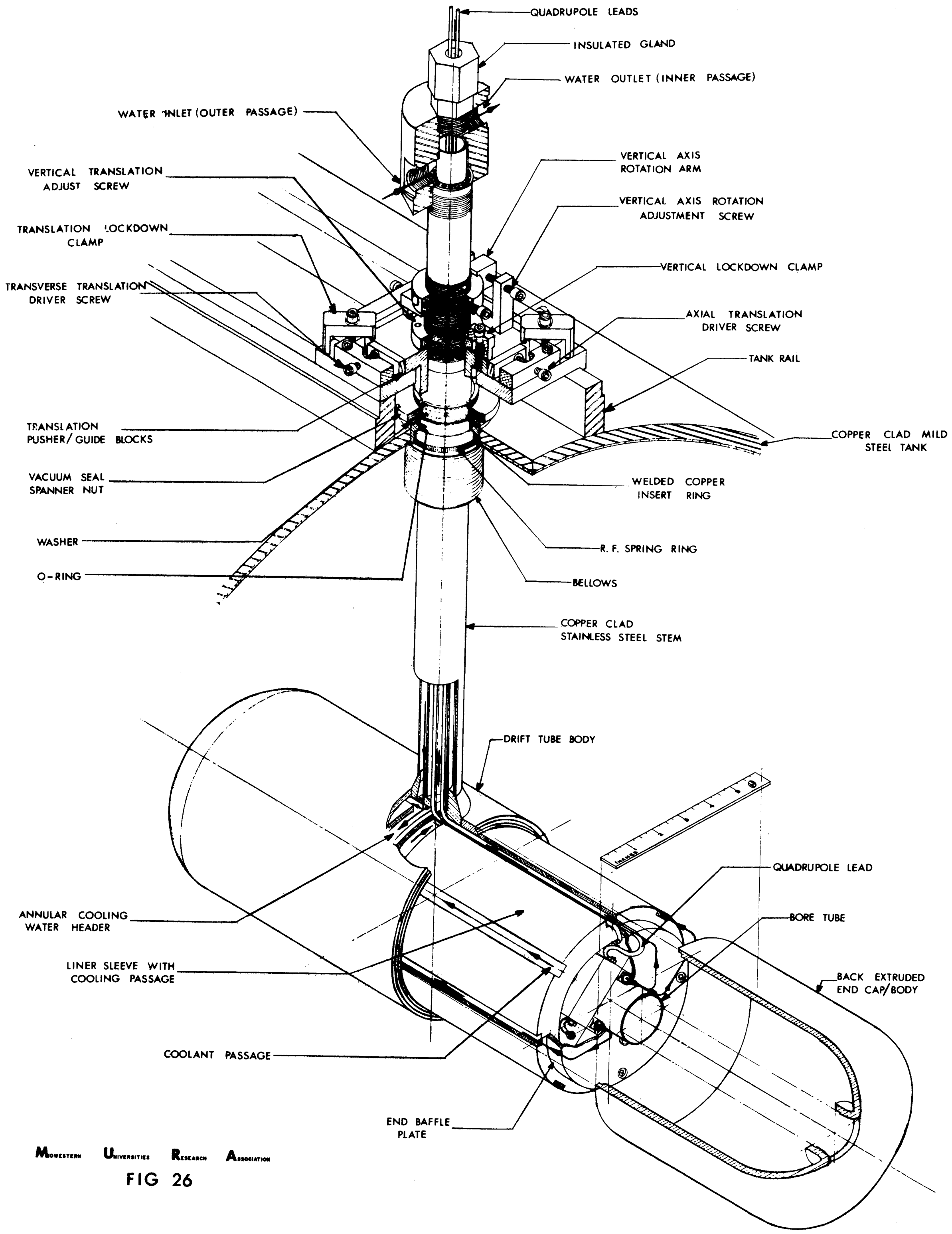

MIDWESTERN UNIVERSITIES RESEARCH ASSOCIATION

FIG 26

DRIFT TUBE ISOMETRIC

FOIL COILS AND BACKWARD EXTRUDED CAP BODY

In this case, the external surface would be copper plated after final assembly. The plating could be eliminated on the end cap areas if stainless steel proves to have better sparking tolerance than the copper. The stainless steel end caps could be brazed to the body by a high capacity induction heater that would melt the solder before sufficient heat was induced to cause damage to the quadrupole winding insulation. This would eliminate electron beam welding of the end caps as required for copper.

Cooling for Cylinder Body

The liner sleeve in Fig. 23 has a heavy wall so that coolant passages may be milled in it. The cross section of the passages are selected to insure turbulent flow conditions with sufficiently high flow rates so that the coolant temperature rise is acceptable. This liner is slid into the drift tube body. The stem adapter, drift tube cylinder, and coolant liner are all brazed in one operation to provide a sealed water chamber.

Use of electrodeposition was investigated as a means of providing the drift tube body with integral cooling passages. The liner sleeve passages are filled with wax and then the outer body copper is electrodeposited. This eliminates machining and brazing of the two parts. A price quotation from Elmore's Schladern/Sieg, West Germany, who specialize in this method, was received but it appeared considerably more expensive than brazing.

An investigation was made for casting the liner sleeve with the cooling passages. It appears that this is competitive pricewise with an adjustable pattern for changing lengths. The main disadvantage is the problem of a sound casting without porosity that might leak.

In Figs. 24, 25, and 26 the coolant passages are designed so that the coolant for the body flows into the end cap and passes axially along the quadrupole windings to the other end. Thus only one water system is required to handle the cooling of the drift tube body and the quadrupole windings and the problems of isolating the two systems are eliminated. This is particularly advantageous when the stem is made of concentric cooling tubes to prevent movement of the drift tube axis due to unsymmetrical cooling of the stem. This distortion is discussed later under "Drift Tube Stem."

Drift Tube End Caps

The end caps in Fig. 23 are OFHC copper plate. With a number of end caps of the same shape, there is an excellent opportunity for savings in fabrication costs. A two-piece die for pressing a plate into this shape is nominal in cost and the operation is fast. Removable centers for piercing and forming the bore and radius would be used to provide for the two bore sizes. Additional forming dies would be used to bring the part to size and finish so that no machining on the outside surface would be needed.

The use of spinning methods were investigated. The forming of the material at the bore is difficult and the companies contacted declined to quote.

Figure 26 shows the end cap and half the body as one part. This part can be fabricated by Janney Cylinder Company, Philadelphia, Pennsylvania. It would be made from OFHC copper by backward extrusion and finish machining except for the length and the stepped joint to the other half. This company has done work of this type with good sizing and excellent finish. The advantages of this method is that there is only one joint on the body and it is not on the end where irregularities and surface finish are important from sparking considerations. The backward extrusion method of forming results in a denser material with better vacuum integrity. The setup and electron beam welding cost and the possibility of leakage is reduced since there is only one weld. For this fabrication method it would be necessary to use flooded cooling since it would be difficult to provide a water-tight seal for the liner sleeve.

Quadrupole Magnet Coils

Three general approaches to magnet coil design were considered. The AGS linac currently uses hollow conductor windings and this is shown in Figs. 22 and 23. Two alternate methods are to use flood-cooled solid wire and edge-cooled foil coils. All three of these methods and their respective power consumptions are discussed in Appendix C. The general calculation of the number of ampere turns also appears in Appendix C. It would appear that all three methods would work and that the final decision would probably be on the basis of cost. The edge-cooled foil magnet has a significantly lower power consumption but may well be the most costly in terms of initial cost.

The quadrupole windings of Fig. 24 are solid copper wire with insulation. This is dependent on the flooded cooling method. In this case the cooling liquid moves from the center headers through passages along the body into the end cap and then axially, cooling the quadrupole windings, to the opposite end cap and then returns to the center header. The advantages of this system are that the windings are easier to make and the danger of permanent damage due to pinching the tube is eliminated. This is particularly true when the quadrupole is being installed in the body and the leads are being worked through the adapter and up the stem. With the coolant in the complete cavity a number of internal sealing problems are eliminated, particularly at the stem-to-body joint which is difficult with concentric tube cooling. A disadvantage is the possibility of a leak in the body or joints resulting in the coolant entering the cavity and the vacuum system. The tightness of the adapter joint, however, is a problem for all the designs considered.

The quadrupole windings of Fig. 25 require the same cooling system used in Fig. 24. Copper tubes are cut to the length needed for a drift tube and positioned in a fixture vertically. Stamped copper strips are positioned over the tubes and a preformed solder ring placed around the tube on top of the strip. The complete assembly is then furnace brazed. The magnet iron stampings are then assembled around the tubes. It is also possible to assemble the iron first and then to furnace braze the tube assembly in position inside the iron. The tubes are then potted in epoxy between the iron which holds the tube assembly in position and seals the axial passage. The coolant will have to flow through the conductor tubes, cooling as in the system in Fig. 23. The leads from the coil windings through the stem are solid wire and provide the advantages of assembly as in the Fig. 24 system.

The problem of quadrupole windings in drift tubes is providing sufficient ampere turns in the limited space with minimum power loss and adequate cooling. With tube conductors having internal cooling there is a considerable waste of space due to the geometry with the corresponding high current density and power losses. Using smaller solid wire permits more turns but there is a problem of supporting many turns in position and still providing a flow of coolant without hot spots. Another approach that provides many turns in a confined space is an edge-cooled foil coil. Figure 26 shows a drift tube with such a coil.

The coil in Fig. 26 is fabricated from copper foil with intermediate layers of mylar. In this design it is possible to devote a high percentage of the available cross section to conductor; i.e., a high "packing factor" is achieved. An analysis of this coil is included in Appendix C.

In Fig. 27 it can be seen that there is only one thermal insulator between any foil and the cooling bar. Using either a "header plate" or encapsulating in epoxy, one can force coolant to pass down the cooling tubes which are attached to each coil.

With new developments on permanent magnet materials, it is possible to fit a magnet of sufficient field strength into the space available. Geometric centering of the field could be accomplished with the use of reluctance adjustment and operating variations could be made by use of a fine tuning coil. Depending on the range of operating adjustment necessary, a separate quadrupole cooling system might not be required since the heat could be absorbed by the drift tube body cooling.

Quadrupole Magnet Iron

The magnet iron of Fig. 22 is made by using iron stampings as shown in the end view. Each layer is composed of two identical halves with two locating holes in each half. Each layer has the joint rotated 90 degrees from the previous layer. The selection of the lamination thickness will depend upon a given vendor's preference. Various fabricators indicated preferences ranging from 1/8 inch

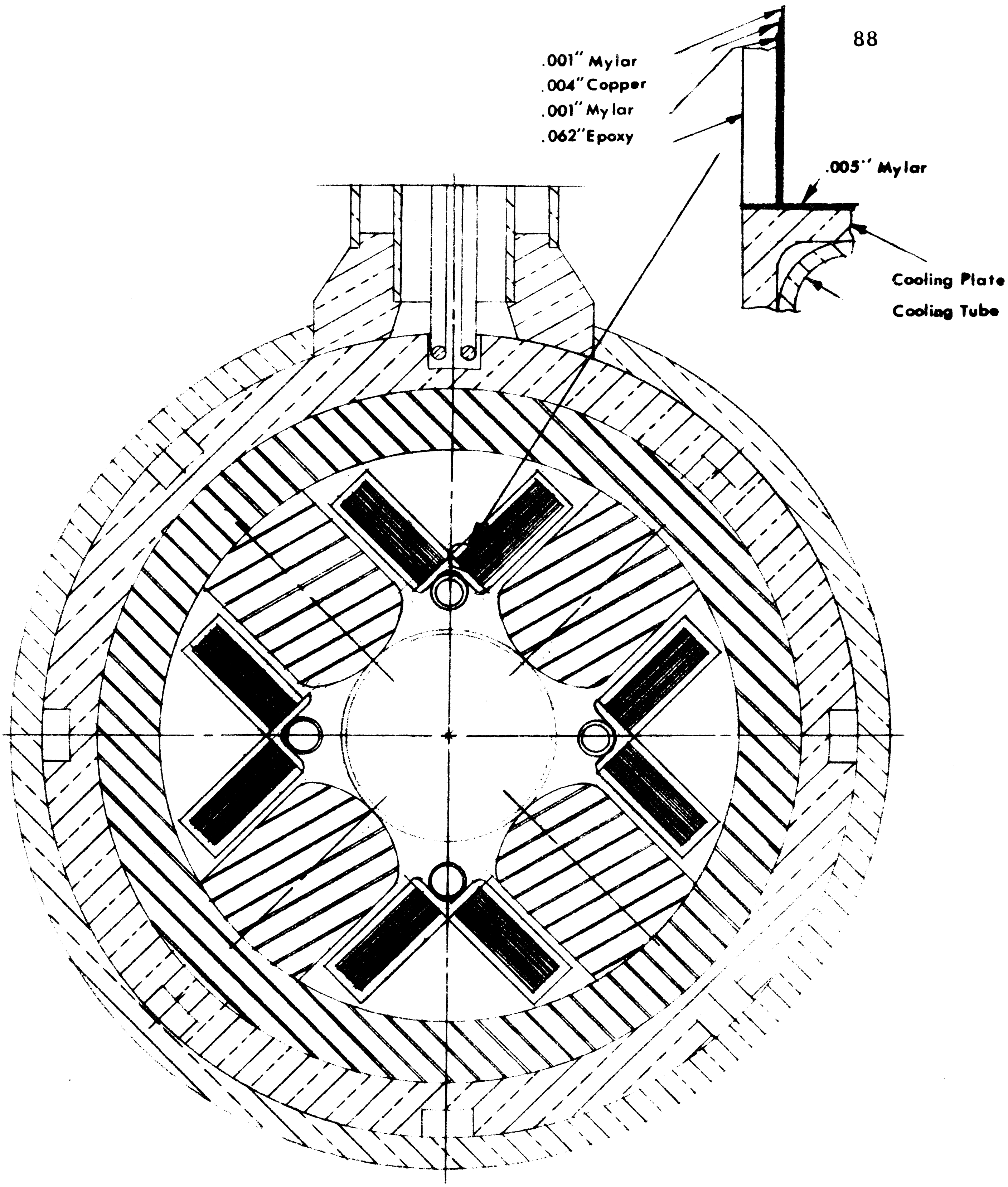

FOIL WOUND QUADRUPOLE COIL

FIG 27

to less than 1/16 inch. With a rod inserted into each pole the complete stack is tied together around the preformed coil. While the contemplated magnets are dc and would not require lamination, the ease of stacking the stampings to achieve the necessary magnet length appears to be a cost saving. The cylindrical drift tube design provides justification for die cost that can be spread over many thousands of pieces and would warrant making a die that would make accurate parts. Accurate stamping might be a two-step operation with a blanking die followed by a shaving die to bring the part to size.

Another method of magnet iron fabrication is to machine four pole pieces to shape from a solid iron bar with each piece of sufficient length for a particular drift tube. The four pole pieces are then positioned at the correct distance from the bore center and turned on the outside to fit into a retaining tube. The four pieces are then positioned in the prewound conductor coil, the retaining tube slid over, and the pole pieces bolted to the retaining tube. This construction is shown in Fig. 27.

Drift Tube Stem

The stem is a stainless steel tube to support the drift tube with an outer copper tube, either clad or loose, as an rf conductor. In Figs. 22 and 23 the copper is clad on the stainless steel and soldered at the adapter to the drift tube body to make a vacuum seal and rf connection. The cooling tubes and quadrupole winding leads pass through the inside of the stainless tube. A copper bellows is welded to the copper clad and makes rf contact to the cavity copper wall lining through a spring ring. The stainless steel tube is held at the upper end through the threaded connection to the support and adjusting mechanism.

It is desired to maintain the drift tube bore axis within 2 mils of the reference axis from all causes of misalignment. The dissipation of rf power in the drift tube stem will cause elongation and an investigation was made to determine if cooling was necessary (see Appendix C).

Drift Tube Support and Adjusting Mechanism

The support mechanism must provide a rigid mounting for the drift tube that will not allow shifting with time and still provide easy adjustment. In some existing linacs the support mechanism has been mounted on longitudinal rails welded to the cavity. The use of a supporting frame independent of the cavity was investigated. It was assumed that the alignment and relative position of each drift tube was the controlling factor rather than the precise location of the drift tube in the cavity.

Figure 28 shows the use of a supporting frame for mounting drift tubes. While this assembly separates the two fabrication problems, the main disadvantage is that the external structure is subject to movement due to temperature changes. Since the cavity must be water jacketed to provide cooling for rf power dissipation, a method is provided for maintaining constant temperature and dimensional stability which maintains the drift tube location in space when the mounting is on the cavity. Another cooling system to maintain stability would be necessary if the supporting frame system is used. While costs have not been investigated, it is believed that the external support method, with a temperature control system added, would cost more than the cavity-mounted system.

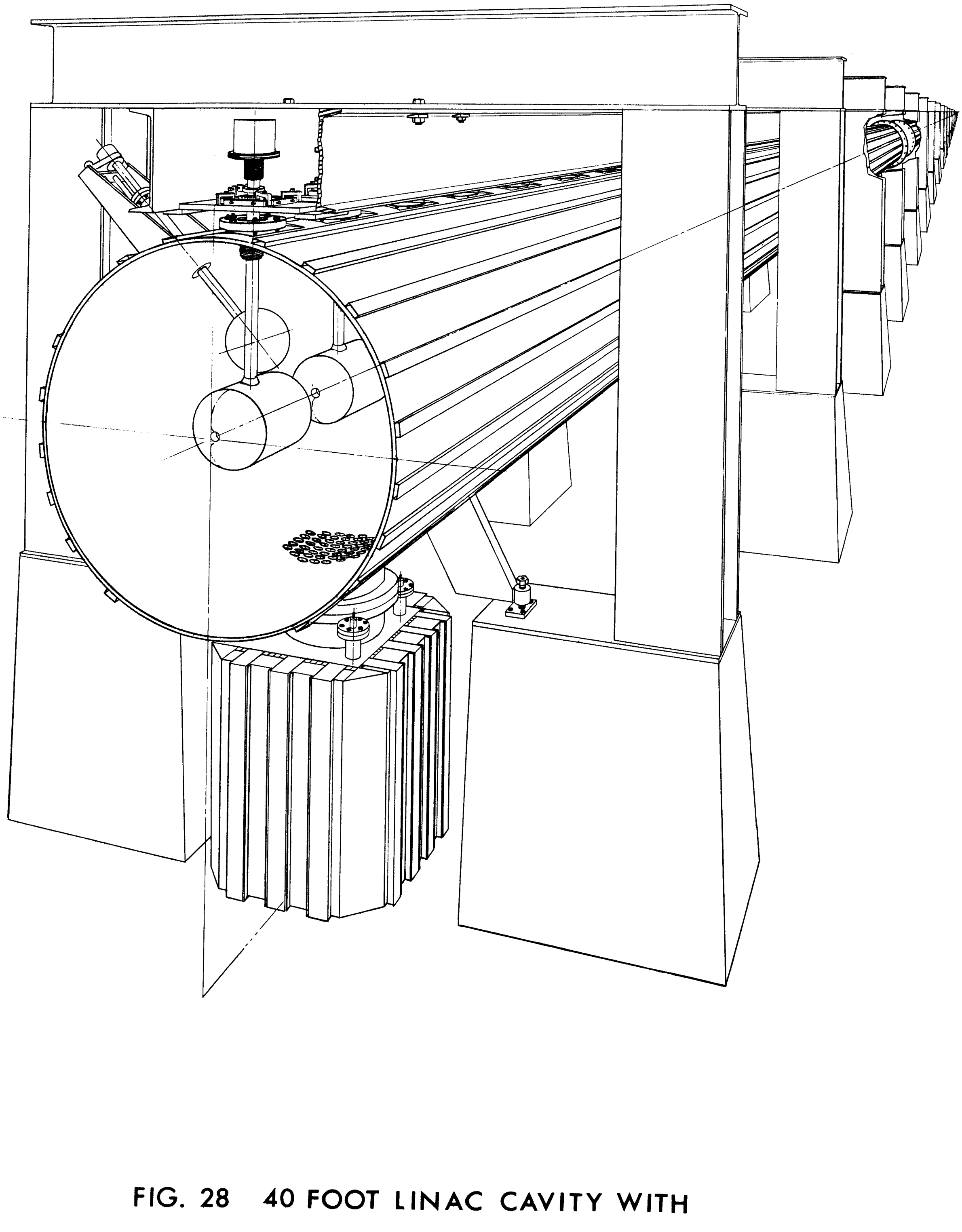

FIG. 28 40 FOOT LINAC CAVITY WITH EXTERNAL DRIFT TUBE SUPPORT

To precisely align each drift tube in the line of sight with the center of the quadrupole field within 2 mils from end to end and the axial location of drift tubes from the reference plane within 2 mils, an adjusting mechanism with 6 degrees of movement is required. If the support rails on the cavity are accurately machined parallel to the drift tube axis and the drift tube axis is made at 90 degrees to the stem mounting, one degree of movement (rotation about a transverse axis) can be eliminated. The mountings shown in Figs. 23 through 26 are so constructed. However, expensive machining is required on a long cavity if this is done. Further, drift tubes would have to be removed and machined or straightened if accumulated errors bring the drift tube centers off more than an allowed amount during assembly.

To provide the adjustment capability for drift tube alignment, it is desired to be able to move in any one direction without involving movement along another axis. Referring to the mechanism in Fig. 23, the angular rotation about the vertical axis is achieved by adjusting screws working on a collar arm that is clamped and pinned to the stem. Below this is the screw collar used for vertical adjustment. The locking clamps hold the screw collar to the slide plate. The slide plate sits on the base plate and is located between four guide blocks. Two opposite blocks are used as guides while the other two are used to translate. Thus, the axial and transverse adjustments can be made independently. After movement the slide plate is clamped to the base plate with four translation lock clamps.

To eliminate the precision rail machining required with the system shown in Fig. 23, it is possible to position the base plate by using threaded adjustment posts with locking nuts. This allows six degrees of movement on the mechanism. If a three-screw adjustment system is used, adjustment can be made with one screw using the other two for a pivot, but in this case there is motion about more than one reference axis or plane. This makes alignment more time consuming. This is particularly so when the man making the adjustment is on the outside, the target in the drift tube is inside the cavity, and another man is on the line of sight at the end of the tank. A four-screw adjustment system is therefore preferred.

Cavity Construction

"Single-wall" construction is recommended for cavity fabrication utilizing OFHC copper clad mild steel. Care must be taken to protect the copper surface during rolling, welding, stress relieving, and machining. When a paper covering was used during the rolling process of the cavity models, wrinkles appeared in the copper surface. If the rolls can be kept free from dirt and metal chips, it is preferable not to use the paper. Stress relieving of the tank is necessary after welding. The copper surface oxidation can be minimized by flooding the interior of the tank with forming gas (15% H_2, 85% N_2 mixture). In spite of these precautions, it is necessary to do further chemical (activated chromic acid) and mechanical cleaning prior to installation.

The cavity welds must meet vacuum and rf requirements. The welds must be porosity free and leak tight. In addition, it is necessary that they cause as little an increase in cavity-wall resistance as possible. The two longitudinal seams that were necessary in the three-cell experimental cavity were made with a monel barrier between the mild steel and the copper overlay.

The purpose of the monel barrier is to prevent iron dilution into the copper with the resulting copper embrittlement. The sequence of welds can be seen in Fig. 29.

End covers are placed on each end of the cavity. It is necessary that an rf contact be made with the copper walls of the cavity. An OFHC copper ring was welded into each end of the cavity to provide for a seating area for the spring rings on the end cover. The OFHC ring welding was done by MIG* process with argon backing of the weld area and a preheat of 350°F. It is recommended in future designs that the end plate be set into the end of the cavity in a fashion similar to the one-cell cavity (see Fig. 30). This eliminates the costly welding and precision machining of end plates.

It appears that considerable savings in cavity fabrication costs might be realized if a single weldment for each cavity were made rather than cavities fabricated from 10-ft flanged sections. When the cavities are made up of many short sections, the over-all length and squareness of end flanges becomes important. Also, a copper insert in each end must be provided for spring ring contacts. In long single cavities this machining would be eliminated.

Experience on the three-cell model linac cavity has convinced us that machined rails are not needed. A preferable support would permit leveling of the drift tube adjustment mechanism. This leveling would also preclude the necessity of insuring squareness between the drift tube bore axis and the stem axis. Since it is necessary to position drift tubes for alignment in any case, the degree of precision of mounting surface is not important.

---

*Metal Inert Gas.

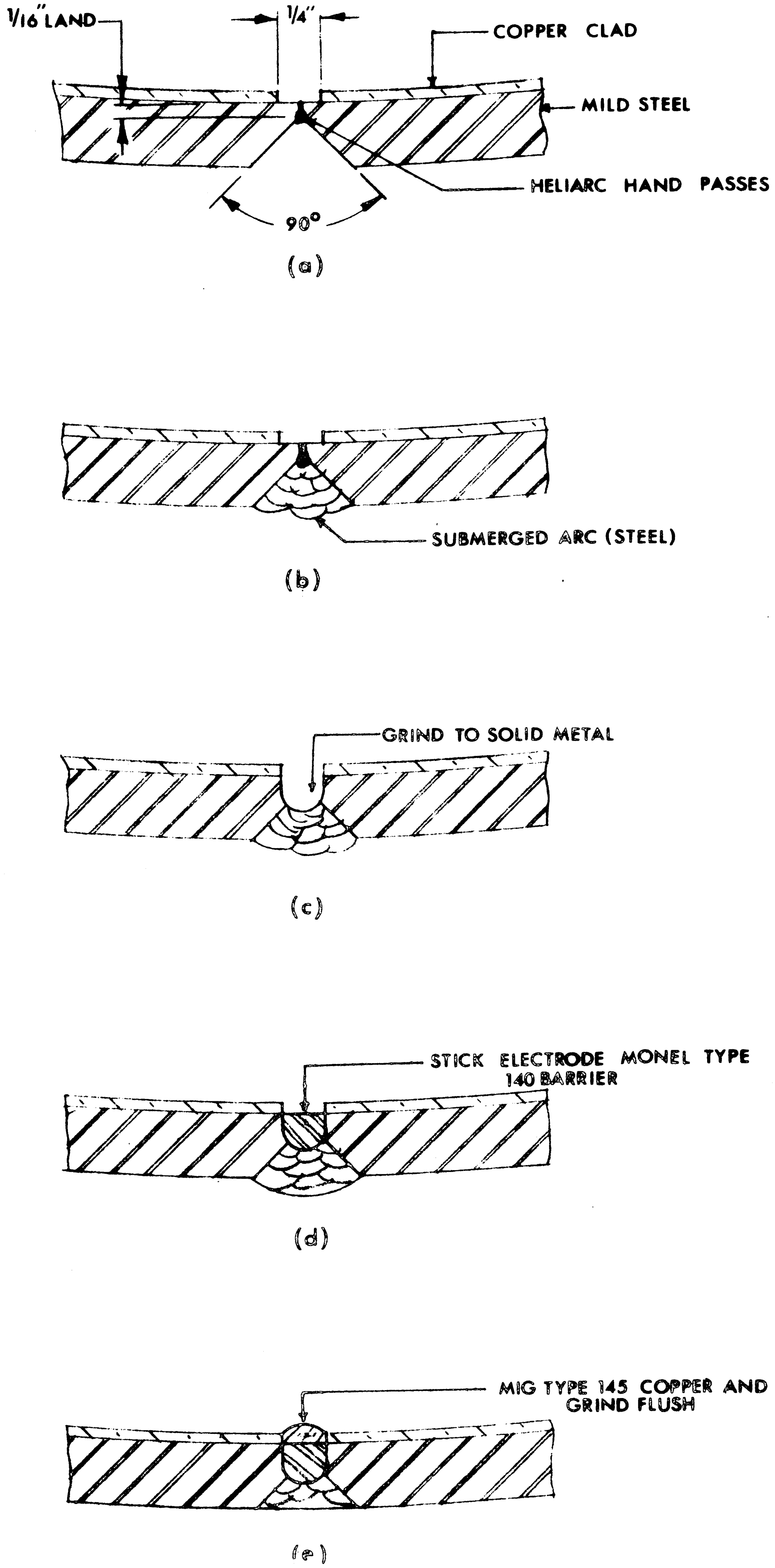

(a)

(b)

(c)

(d)

(e)

COPPER CLAD CAVITY WELDING SEQUENCE

FIG 29

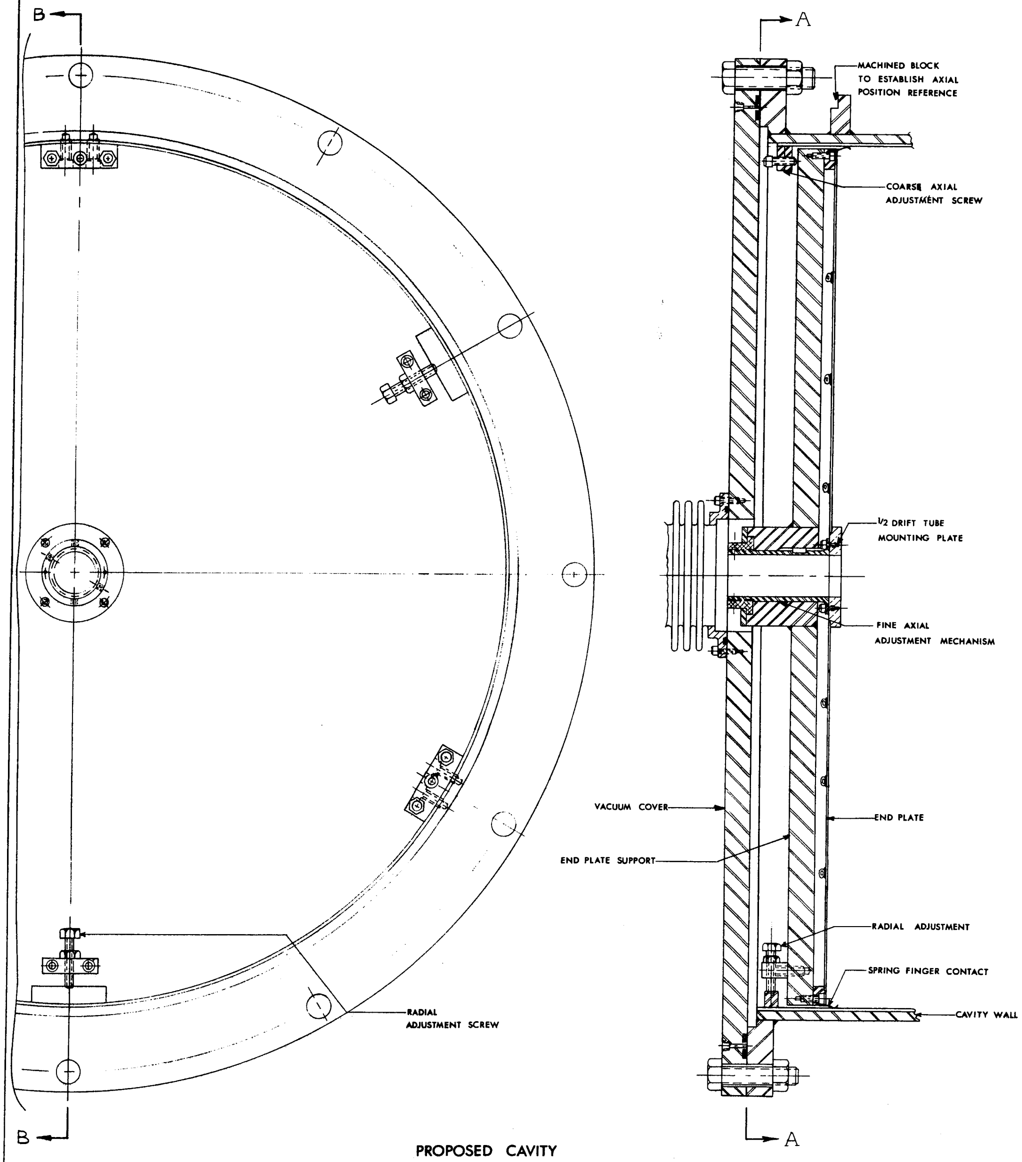

PROPOSED CAVITY
END PLATE DESIGN

FIG. 30

In the event that minor leaks develop in drift tube stem seals, it is desirable to rough vacuum "backstop." Although the drawings do not illustrate a roughing box for this purpose, it is felt that individual cans could be used to provide a back-up for leaks in the stem-to-cavity sealing area.

The selection of wall thickness for the cavity can be made based upon a stress and deflection analysis of externally loaded cavities. Such an analysis has been made for the three-cell model. It appears that a cavity-wall thickness of 1/2 inch is acceptable from a stress point of view. However, large deflections in cavity walls will occur (or the order of several mils). These deflections will cause misalignments of drift tubes since they are supported by the cavity wall. In Fig. 31 deflections that one might expect in a typical cavity are plotted. These curves are based upon the University of Illinois Engineering Experiment Station Bulletin #329. It can be seen that frequent stiffener rings would be required if deflections are to be kept to less than 1 mil. Present alignment tolerances for quadrupoles indicate that this is necessary.

Vacuum Considerations

Experience obtained from the three-cell cavity indicates that outgassing rates of 10^{-9} mml/sec/cm^2 can be readily obtained for unbaked copper surfaces. It is anticipated that this figure can be reduced by at least a factor of 10 by mild baking and prolonged pumping.

Diffusion pumps are used on the model cavity, providing a pumping speed of approximately 100 liter/sec/foot of cavity. A diffusion system has been used to permit rapid start up after the system has been brought up to atmospheric pressure. It is not recommended that a diffusion system be used on a

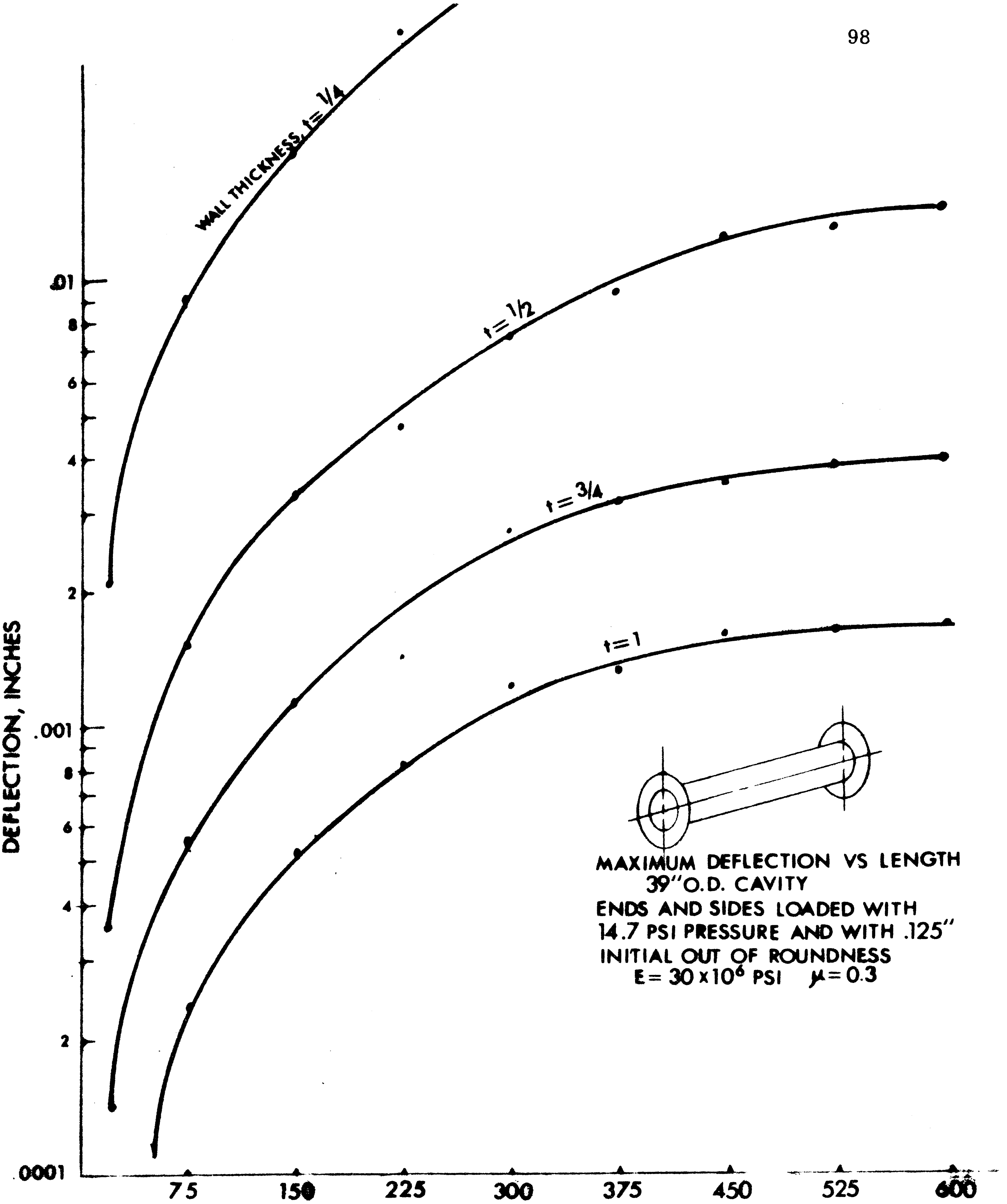

CAVITY WALL DEFLECTIONS

FIG. 31

"working" linac. Getter-ion pumps are recommended due to their lower cost and simplicity of operation.

Cooling

Two general objectives in the design of a linac cooling system are: (1) to operate the cavities at or near room temperature, and (2) to limit variations in temperature so that excessive drifts in resonant frequency do not occur. Operation at room temperature permits the coolant to be the dominant factor in determining the cavity temperature. Slight variations in room temperature are not significant under this condition.

Dimensional stability is necessary to maintain resonant conditions. The maximum tolerable drift due to temperature (dimensional) drift was set at 5 kc. Dimensional stability is also necessary for maintaining alignment of the quadrupoles mounted in each drift tube. An analysis of the methods of stem cooling is given in Appendix C.

In addition to rf losses, it is necessary to remove heat generated by quadrupole magnet coils. Analysis of cooling requirements for several different quadrupole coil designs has been discussed in the quadrupole section.

A detailed analysis of the water-cooling scheme used on the three-unit cell cavity illustrates how these design objectives were met. The power losses on each component and the coefficients for frequency drift as function of various cavity dimensions are given in Appendix C.

Cost Estimation

After a workable design of a drift tube had been made, an assembly drawing (Fig. 22) and part drawings with sufficient detail for cost estimation were sent to fabricators for cost estimates. The fabricators contacted were vacuum tube manufacturers or other manufacturers with vacuum fabrication capabilities. Cost estimates were based on the fabricator procuring the material, developing any tooling required and fabricating all the drift tubes needed between 20 MeV and 200 MeV (approximately 188). These estimates were not firm but were only used to determine the general level of cost as a comparison with previous cost figures. The previous cost figures were based on an estimate supplied by ANL for the contoured drift tube design used in their present 50 MeV linac.

Price estimates from most of the companies were well grouped. Based on the estimated cost of present contoured drift tubes, the price reduction ranged from 37% to 42% for a single set of linac drift tubes.

The engineers and process people from the fabricators who had submitted estimates were contacted as a follow up to determine design simplification and cost reduction. The component parts were reviewed to determine where design changes could be made to reduce cost without reducing the effectiveness of the end product. As a result, there have been a number of changes and these are included in Figs. 24, 25, and 26. No attempt has been made to evaluate these changes costwise but they are considered feasible from a mechanical standpoint.

Studies have shown that the cost of fabricating a larger number of drift tubes, say for two or three linacs, will reduce the cost per drift tube by spreading the fixture cost over more components. If parts common to a larger number of drift tubes can be fabricated simultaneously, the costs will be further reduced.

APPENDIX A: MESSYMESH PROGRAM

The calculation of electromagnetic eigenvectors and eigenvalues in linear accelerator-type cavities containing stemless drift tubes whose meridian plane cross sections are piecewise simply describable, as illustrated in Fig. A-1, can be accomplished by solving finite difference approximations to the wave equation. The resulting eigenvectors and eigenvalues allow quantitative determination of relevant auxiliary electromagnetic quantities and subsequently of particle dynamic phenomena.

Maxwell's equations, when expressed in cylindrical coordinates, admit two linearly and azimuthally independent sets of solutions; one with a vanishing E_φ, the other with a vanishing H_φ (TM or TE modes respectively). The former type of solution or mode has a nonvanishing E_z and hence permits an axial acceleration of particles, whereas the latter type does not.

The modes of interest are hence the TM modes, for which:

$$E_z = \frac{i}{\omega \epsilon} \frac{1}{r} \frac{\partial (r H_\varphi)}{\partial r} , \quad E_r = \frac{-i}{\omega \epsilon} \frac{1}{r} \frac{\partial (r H_\varphi)}{\partial z} , \qquad \text{(A-1)}$$

and

$$\frac{1}{r} \frac{\partial}{\partial r} \left(r \frac{\partial H_\varphi}{\partial r} \right) + \frac{\partial^2 H_\varphi}{\partial z^2} + (k^2 - \frac{1}{r^2}) H_\varphi = 0 , \qquad \text{(A-2)}$$

such that

$$k^2 = \omega^2 \mu \epsilon = \frac{\omega^2}{c^2} = \left(\frac{2\pi}{\lambda} \right)^2 . \qquad \text{(A-3)}$$

The boundary conditions applicable to the solution of Eq. (A-2) must be such that the tangential component of E vanishes on all metallic surfaces and is expressable as

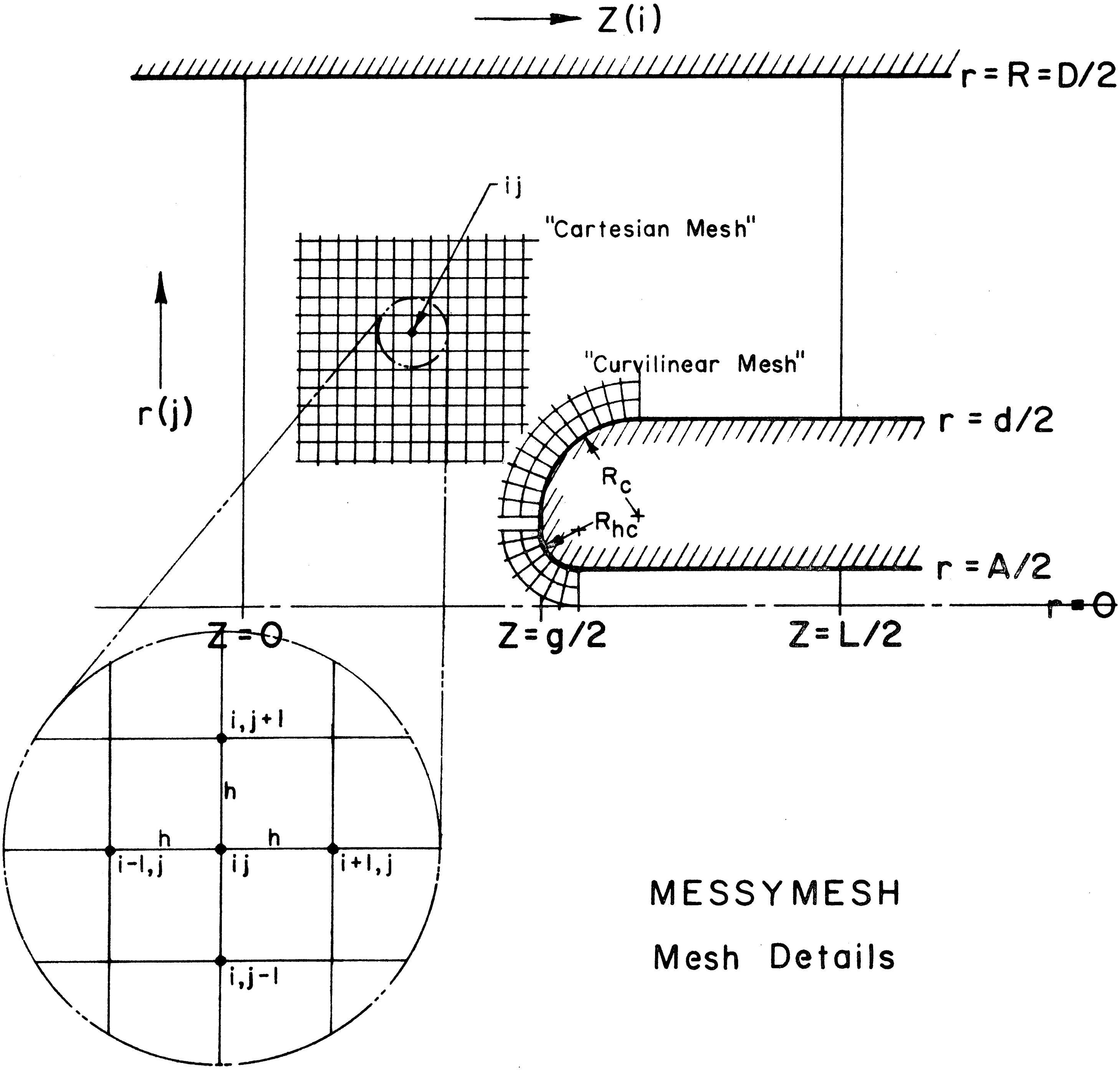

MESSYMESH
Mesh Details

Fig. A-1

$$\epsilon \frac{\partial}{\partial t} (\hat{n} \times \bar{E}) = \hat{n} \times \frac{\partial \bar{D}}{\partial t} = \hat{n} \times (\bar{\nabla} \times \bar{H}_{\varphi}) = 0, \qquad \text{(A-4)}$$

whereupon it follows from $(\hat{n} \cdot \hat{u}_{\varphi}) = 0$, that

$$\hat{n} \cdot \bar{\nabla} (r\, H_{\varphi}) = \frac{\partial}{\partial n} (r\, H_{\varphi}) = 0\,. \qquad \text{(A-5)}$$

Because of the comparative simplicity of the boundary condition, Eq. (A-5), it seems to be advantageous to formulate the problem in terms of the dependent variable $F = r\, H_{\varphi}$, whereupon the field components, Eq. (A-1), and the scalar wave equation, Eq. (A-2), become

$$E_z = \frac{i}{\omega \epsilon} \frac{1}{r} \frac{\partial F}{\partial r}, \quad E_r = \frac{-i}{\omega \epsilon} \frac{1}{r} \frac{\partial F}{\partial z}, \qquad \text{(A-6)}$$

and

$$r \frac{\partial}{\partial r} \left(\frac{1}{r} \frac{\partial F}{\partial r} \right) + \frac{\partial^2 F}{\partial z^2} + k^2 F = 0\,, \qquad \text{(A-7)}$$

subject to the boundary condition

$$\frac{\partial F}{\partial n} = 0\,, \qquad \text{(A-8)}$$

on metallic surfaces and planes of symmetry.

At the onset of the numerical solution of Eq. (A-7), subject to the boundary condition, Eq. (A-8), neither the eigenvector F, nor the eigenvalue k, are known. However, if an approximate "trial eigenvector" and "trial eigenvalue" are available, a convergent process to calculate the true eigenvector and eigenvalue may be developed. To see that this is so, it is known that any trial eigenvector ϕ, may always be expanded in terms of the complete set of true eigenvectors ϕ_n, in the form

$$\phi = \sum_n A_n \phi_n, \text{ where } \quad \mathcal{L} \phi_n + k_n^2 \phi_n = 0\,, \qquad \text{(A-9)}$$

where in the present instance the symbolic operator $\mathcal{L}$ may be identified with that operator of Eq. (A-7). Upon computing the scalar product $\langle \phi, \mathcal{L} \phi \rangle$ it may be readily seen that the lowest eigenvalue satisfies the inequality

$$k_1^2 \leq - \frac{\langle \phi, \mathcal{L}\phi \rangle}{\langle \phi, \phi \rangle} = - \frac{\iint_S \frac{F}{r}\left[r \frac{\partial}{\partial r}\left(\frac{1}{r}\frac{\partial F}{\partial r}\right) + \frac{\partial^2 F}{\partial z^2}\right] dr\, dz}{\iint_S \frac{F^2}{r}\, dr\, dz} . \qquad \text{(A-10)}$$

It is furthermore demonstrable that this leads to a stationary or variational principle, such that if ϕ differs from an eigenvector ϕ_n, by a small amount proportional to λ, then the generalized form of the inequality Eq. (A-10) is proportional to λ^2. This may be observed by expanding the ratio of scalar products of Eq. (A-10) in Taylor series

$$\frac{\langle \phi, \mathcal{L}\phi \rangle}{\langle \phi, \phi \rangle} = \frac{\langle (\phi_n + \lambda \psi), \mathcal{L}(\phi_n + \lambda \psi) \rangle}{\langle (\phi_n + \lambda \psi), (\phi_n + \lambda \psi) \rangle} = \frac{\langle \phi_n, \mathcal{L}\phi_n \rangle}{\langle \phi_n, \phi_n \rangle} +$$

$$+ \lambda \left\{ \frac{\langle \phi_n, \mathcal{L}\phi_n \rangle \left[\langle \phi_n, \psi \rangle + \langle \phi_n, \psi \rangle \right]}{\left[\langle \phi_n, \phi_n \rangle \right]^2} - \frac{\left[\langle \phi_n, \mathcal{L}\psi \rangle + \langle \mathcal{L}\phi_n, \psi \rangle \right]}{\langle \phi_n, \phi_n \rangle} \right\} + \mathcal{O}(\lambda^2) + \ldots . \qquad \text{(A-11)}$$

The numerator of the first-order term in Eq. (A-11) may be seen to vanish if the operator $\mathcal{L}$ is self-adjoint, i.e., if

$$\langle \phi_n, \mathcal{L}\psi \rangle = \langle \mathcal{L}\phi_n, \psi \rangle = - k_n^2 \langle \phi_n, \psi \rangle . \qquad \text{(A-12)}$$

Thus the final variational principle is

$$\frac{\langle \phi, \mathcal{L}\phi \rangle}{\langle \phi, \phi \rangle} = - k_n^2 + \mathcal{O}(\lambda^2) + \ldots , \qquad \text{(A-13)}$$

and a convergent process is realized if, alternately, better "trial eigenvectors" ϕ or F are chosen, and if successively better eigenvalue approximations are calculated, each choice and/or calculation employing the best known results from the previous calculation or choice.

The calculation of improved trial eigenvectors may conveniently be accomplished by the technique of (over)relaxation. Upon constructing a cartesian two-dimensional array or mesh (see Fig. A-1) of discrete values of F at various coordinates r and z, the problem can be formulated as a "matrix" problem rather than as the continuous problem expressed by Eq. (A-7). The fundamental equations, Eqs. (A-7) and (A-10) may then be written in finite difference form by expanding the matrix elements of the trial eigenfunction F surrounding a central element F_{ij}, in Taylor series with respect to F_{ij}. If only the four nearest neighbors of the central element F_{ij} are employed, the resulting approximations to Eq. (A-7) and Eq. (A-10), become, respectively

$$\begin{aligned} &F_{i,j+1}\left(1 - \frac{h}{2\,r_j}\right) + F_{i,j-1}\left(1 + \frac{h}{2\,r_j}\right) + F_{i+1,j} + F_{i-1,j} + \\ &\quad (k^2\,h^2 - r)\,F_{ij} + O(h^4) = 0\,, \end{aligned} \tag{A-14}$$

and

$$k_1^2\,h^2 \simeq -\frac{\sum\limits_i \sum\limits_j \left\{ \frac{F^n_{ij}}{r_j} \left[F^n_{i,j+1}\left(1 - \frac{h}{2\,r_j}\right) + F^n_{i,j-1}\left(1 + \frac{h}{2\,r_j}\right) + F^n_{i+1,j} + F^n_{i-1,j} - 4\,F^n_{ij} \right] \right\} \Delta S_{ij}}{\sum\limits_i \sum\limits_j \left[\frac{(F^n_{ij})^2}{r_j} \right] \Delta S_{ij}} \tag{A-15}$$

where i and j are matrix indices referring to the z and r coordinates, respectively, and where h is the common interelement coordinate difference. The finite difference equation, Eq. (A-14) may be written as a Liebmann four-point algorism

$$\begin{aligned} F^{n+1}_{ij} - F^n_{ij} = \alpha \Bigg\{ &F^n_{ij}\left(\frac{k^2\,h^2}{4} - 1\right) + \frac{1}{4}\Bigg[F^n_{i,j+1}\left(1 - \frac{h}{2\,r_j}\right) + F^{n+1}_{i,j-1}\left(1 + \frac{h}{2\,r_j}\right) + \\ &+ F^n_{i+1,j} + F^{n+1}_{i-1,j} \Bigg] \Bigg\}\,, \end{aligned} \tag{A-16}$$

where it is assumed that the matrix is repetitively traversed in a regular manner, such that upon improving F^n_{ij} into F^{n+1}_{ij}, the matrix elements $F^{n+1}_{i-1,j}$ and $F^{n+1}_{i,j-1}$ will already have been processed on the current $(n + 1)^{th}$ traversal, whereas the matrix elements $F^n_{i,j+1}$ and $F^n_{i+1,j}$ are those remaining from the previous n^{th} traversal. It is, however, expedient to calculate successive improvements of the eigenvalue via Eq. (A-15) using everywhere values of F^n_{ij}, i.e., from the n^{th} traversal only.

The boundary condition, Eq. (A-8), corresponds to a reflection effect which is easily applicable to all boundaries which coincide with a row or column of matrix elements. For example, $F^n_{i,j+1}$ can be replaced by $F^{n+1}_{i,j-1}$ in Eq. (A-16) if a metallic boundary or plane of symmetry is coincident with the j^{th} row of matrix elements. However, for boundaries that are not parallel with a row or column of matrix elements, such a procedure is not easily accomplished in applying the requisite boundary condition. For this latter case, an auxiliary "curvilinear matrix" can be constructed, as shown in Fig. A-1, which follows the contour of the boundary and sufficiently overlaps the principal "cartesian matrix" described above. The application of the boundary condition to this auxilairy matrix is then easily accomplished by a reflection of the form indicated above.

If, for example, the curvilinear mesh is (locally) polar in form, then the scalar wave equation, Eq. (A-7) may be transformed to the (local) polar form by the transformations

$$r = r_c + \rho \sin \theta, \quad z = z_c + \rho \sin \theta \,, \tag{A-17}$$

with the result

$$\frac{\partial^2 F}{\partial \rho^2} + \left[\frac{r_c}{\rho(r_c + \rho \sin \theta)}\right] \frac{\partial F}{\partial \rho} + \frac{1}{\rho^2}\frac{\partial^2 F}{\partial \theta^2} - \left[\frac{\cos \theta}{\rho\,(r_c + \rho \sin \theta)}\right] \frac{\partial F}{\partial \theta} + k^2 F = 0 \,. \tag{A-18}$$

Similarly the expression for the eigenvalue, Eq. (A-10), becomes

$$k_1^2 \leq - \frac{\iint_s \frac{F}{(r_c + \rho \sin\theta)} \left\{ \frac{\partial^2 F}{\partial \rho^2} + \left[\frac{r_c/\rho}{(r_c + \rho \sin\theta)} \right] \frac{\partial F}{\partial \rho} + \frac{1}{\rho^2} \frac{\partial^2 F}{\partial \theta^2} - \left[\frac{\cos\theta/\rho}{(r_c + \rho \sin\theta)} \right] \frac{\partial F}{\partial \theta} \right\} \rho \, d\rho \, d\theta}{\iint_s \frac{F^2}{(r_c + \rho \sin\theta)} \rho \, d\rho \, d\theta} \tag{A-19}$$

The finite difference expressions analogous to Eqs. (A-15) and (A-16) become

$$\begin{aligned} k_1^2 h^2 \simeq - \sum_{\ell} \sum_{m} \Bigg\{ & \frac{F^n_{\ell m}}{(r_c + \rho \sin\theta)} \Bigg[\left(\frac{h}{h_\rho}\right)^2 (F^n_{\ell+1,m} + F^n_{\ell-1,m}) + \\ & + \left(\frac{h}{h_\theta}\right)^2 (F^n_{\ell,m+1} + F^n_{\ell,m-1}) + \left(\frac{h}{h_\rho}\right) \frac{(F^n_{\ell+1,m} - F^n_{\ell-1,m})}{2\left(\frac{\rho}{r_c}\right)\left(\frac{r_c}{h} + \frac{\rho}{h} \sin\theta\right)} + \\ & + \left(\frac{h}{h_\theta}\right) \frac{\cos\theta \, (F^n_{,m-1} - F^n_{,m+1})}{2\left(\frac{r_c}{h} + \frac{\rho}{\sin\theta}\right)} + \\ & - 2\left(\frac{h^2}{h_\rho^2} + \frac{h^2}{h_\theta^2}\right) F^n_{\ell m} \Bigg] \Bigg\} \Delta S_{\ell m} \Bigg/ \sum_{\ell} \sum_{m} \frac{(F^n_{\ell m})^2}{(r_c + \rho \sin\theta)} \Delta S_{\ell m} , \end{aligned} \tag{A-20}$$

and

$$\begin{aligned} F^{n+1}_{\ell m} - F^n_{\ell m} = \alpha \Bigg\{ & F^n_{\ell m} \left[\frac{k^2}{\left(\frac{2}{h_\rho^2} + \frac{2}{h_\theta^2}\right)} - 1 \right] + \frac{1}{\left(\frac{2}{h_\rho^2} + \frac{2}{h_\theta^2}\right)} \Bigg[F^n_{\ell+1,m} \left\{ \frac{1}{h_\rho^2} + \frac{1}{2h_\rho} \left[\frac{r_c/\rho}{(r_c + \rho \sin\theta)} \right] \right\} + \\ & + F^{n+1}_{\ell-1,m} \left\{ \frac{1}{h_\rho^2} - \frac{1}{2h_\rho} \left[\frac{r_c/\rho}{(r_c + \rho \sin\theta)} \right] \right\} + F^n_{\ell,m+1} \left\{ \frac{1}{h_\theta^2} - \frac{1}{2h_\theta} \left[\frac{\cos\theta}{(r_c + \rho \sin\theta)} \right] \right\} + \\ & + F^{n+1}_{\ell,m-1} \left\{ \frac{1}{h_\theta^2} + \frac{1}{2h_\theta} \left[\frac{\cos\theta}{(r_c + \rho \sin\theta)} \right] \right\} \Bigg] \Bigg\} . \end{aligned} \tag{A-21}$$

where ℓ and m are curvilinear matrix indices referring to the ρ and θ coordinates, respectively, and where h_ρ and h_θ are the (local) interelement coordinate differences.

The factor α appearing in Eqs. (A-16) and (A-21) is the (over)relaxation factor. If $\alpha = 1$, these algorisms are rigorous. By judicious choice of $\alpha > 1$, however, accelerated convergence may be obtained. Although some attempts have been made to calculate an optimum value of α for algorisms derivable from Laplace's equation, little is known in connection with wave equations such as Eq. (A-7). Empirically, a value between 1.4 and 1.9, increasing as the number of cartesian matrix elements increases from about 1000 to 8000 has been found best.

In order to make full use of both the cartesian matrix and the curvilinear matrix, it is necessary to interpolate "trial eigenvector" matrix elements from one form of matrix to the other. Such interpolation formulae as are required may be deduced, for example, by expanding several matrix elements F_{ij} in two-dimensional Taylor series about the unknown matrix element $F_{\ell m}$, and requiring that a weighted sum of a sufficient number of such Taylor expansions be consistent with the fundamental identity, Eq. (A-7). It follows easily that five such F_{ij} are required to maintain the same order of accuracy as already indicated in Eq. (A-14), for example, and that the corresponding weights w_{ij} for the various F_{ij} are determined by a 5 x 5 matrix problem:

$$\begin{bmatrix} (z_1 - z) & (z_2 - z) & (z_3 - z) & (z_4 - z) & (z_5 - z) \\ (r_1 - r) & (r_2 - r) & \cdots & \cdots & (r_5 - r) \\ \frac{1}{2}(z_1 - z)^2 & \frac{1}{2}(z_2 - z)^2 & \cdots & \cdots & \frac{1}{2}(z_5 - z)^2 \\ (z_1 - z)(r_1 - r) & (z_2 - z)(r_2 - r) & \cdots & \cdots & (z_5 - z)(r_5 - r) \\ \frac{1}{2}(r_1 - r)^2 & \frac{1}{2}(r_2 - r)^2 & \frac{1}{2}(r_3 - r)^2 & \frac{1}{2}(r_4 - r)^2 & \frac{1}{2}(r_5 - r)^2 \end{bmatrix} \begin{bmatrix} w_1 \\ w_2 \\ w_3 \\ w_4 \\ w_5 \end{bmatrix} = \begin{bmatrix} 0 \\ -\frac{1}{r_{\ell m}} \\ 1 \\ 0 \\ 1 \end{bmatrix} \tag{A-22}$$

where $(F_{ij})_u$ and $F_{\ell m}$ differ in z and r coordinates by the amounts $(z_u - z)$ and $(r_u - r)$, respectively. The solution of this matrix problem, for the various w's, permits use of the associated interpolation formula

$$F_{\ell m} = \sum_{u=1}^{5} w_u (F_{ij})_u / (\sum_{u=1}^{5} w_u - k^2) . \qquad \text{(A-23)}$$

Care must be exercised in the choice of the different (F_{ij})'s so that the resulting matrix in Eq. (A-22) is not singular, and so that the various w's are as nearly equal as possible. It is found that the appropriate (F_{ij})'s are usually those nearest the unknown $F_{\ell m}$.

In practice, it is advantageous to use the best initial "trial eigenvector" possible, since the number of iterations necessary to achieve final convergence is dependent upon the amount by which this initial trial eigenvector must be altered. Initially the initial trial eigenvector may conveniently be chosen as an analytic approximation of the true eigenvector if the geometry is not too far removed from that for which the approximation is exact. However, after a repertoire of solutions of interest has been developed, a reasonably good initial trial eigenvector may be obtained from an eigenvector previously calculated for approximately the same geometry.

Furthermore, care must be taken to assure final convergence of the eigenvector, the eigenvalue and various auxiliary quantities. It has been found that three criteria are sufficient to insure full convergence. These criteria, in the order in which they are best satisfied, are

1) Eigenvalue convergence $(k^2)^{n+1} - (k^2)^n \lesssim 10^{-3}$,

2) Eigenvector convergence $\left[\sum(\Delta F_{ij})^2\right]^{n+1} - \left[\sum(\Delta F_{ij})^2\right]^n \lesssim 10^{-7} N$,

3) Auxiliary quantity convergence $(ZT^2)^{n+1} - (ZT^2)^n \lesssim 10^{-3}$,

where N is the total number of cartesian matrix elements. It has also been found expedient to hold the (over)relaxation factor α, in Eqs. (A-16) and (A-21), at its rigorous value, namely unity, for several iterations near the end of a mesh calculation in order to damp out the eigenvector changes.

An indication of the flow of MESSYMESH during the calculation of the final eigenvector, eigenvalue, and auxiliary quantities is shown in Fig. A-2.

In order to meaningfully compare eigenvectors of two slightly dissimilar geometries, it is necessary to maintain some standard(s) of normalization with respect to the amplitude of the eigenvector and/or with respect to scalability of relative geometrical dimensions. A convenient quantity which meets both requirements is the stored energy per unit volume W/V, which, for a hollow cylindrical cavity has a known solution, i.e.

$$W/V = \frac{1}{\pi R^2 L} \cdot \frac{\mu}{2} \iiint_V H^2 \, dV = \cdots = \frac{\mu}{2} F_o^2 J_1^2 (kR)/R^2 , \qquad \text{(A-24)}$$

where μ is the permeability of the cavity medium, R and L are the radius and length, respectively, of the cavity volume, and where the amplitude factor F_o is defined by

$$F = r H_\varphi = H_o r J_1 (kr) = F_o \frac{r}{R} \cdot J_1 (kr) . \qquad \text{(A-25)}$$

This form of normalization easily permits successive renormalization to a fixed cavity size or frequency and to any desired excitation level, for example, to a given average axial accelerating field.

The eigenvectors and eigenvalues so calculated may be used to compute several auxiliary electromagnetic quantities, including:

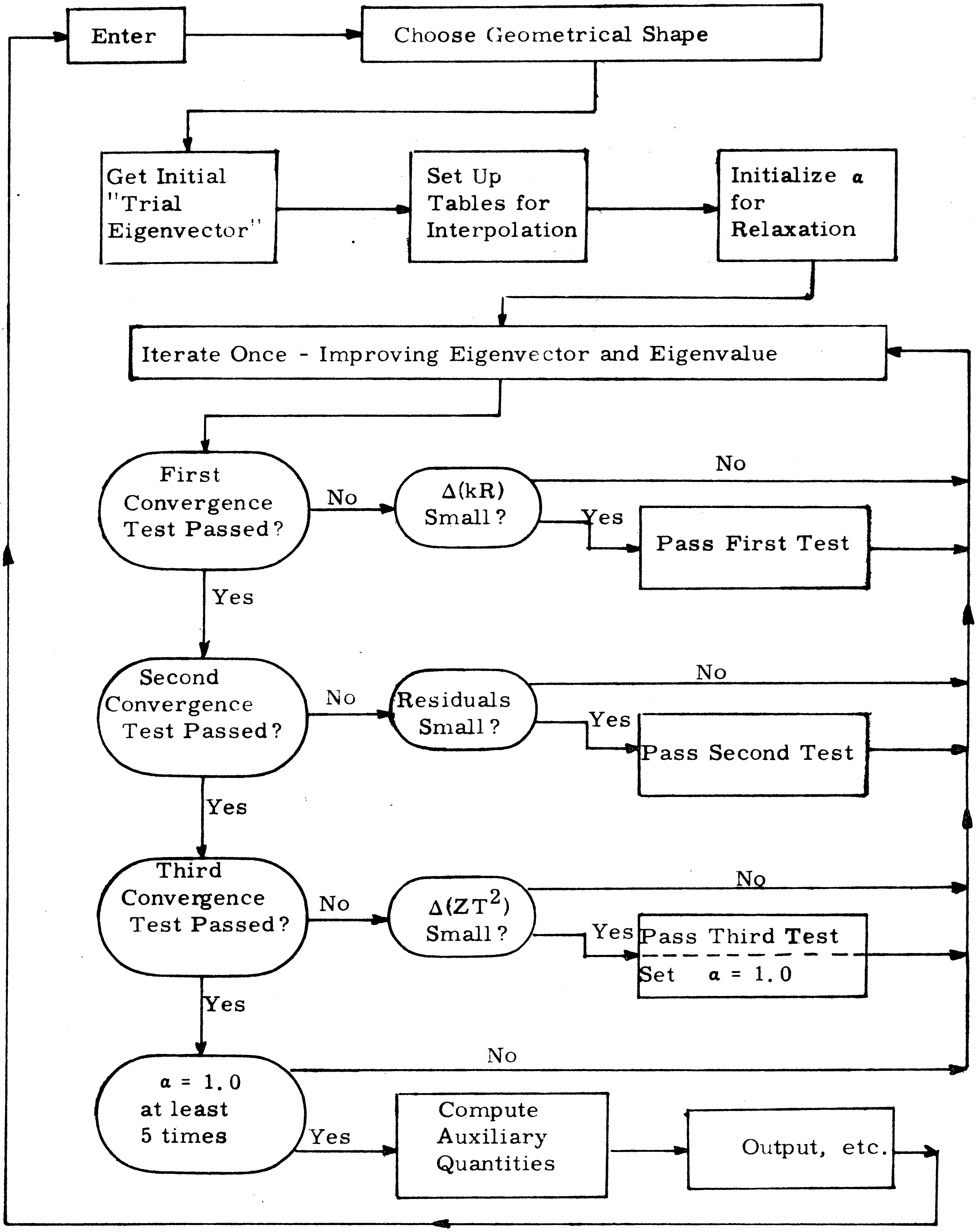

MESSYMESH Flow Chart

Fig. A-2

1) Energy Stored Per Unit Volume:

$$\frac{W}{V} = \frac{\mu}{2}\,\frac{\iint_s \frac{F^2}{r}\,dr\,dz}{\iint_s r\,dr\,dz} = 2\pi \times 10^{-7}\,\frac{\iint_s F^2\left(\frac{R}{r}\right) dr\,dz}{\iint_s \left(\frac{r}{R}\right) dr\,dz} \cdot \frac{1}{R^2}\,, \qquad \text{(A-26)}$$

2) Power Lost to Cavity Walls Per Unit Area:

$$\frac{P_W}{A} = \frac{\pi R_S}{2\pi}\,\frac{\oint \frac{F^2}{r}\,d\ell}{\oint r \cdot d\ell} = 9.01 \times 10^{-4}\sqrt{kR}\,\frac{\oint F^2\left(\frac{R}{r}\right) d\ell}{\oint \left(\frac{r}{R}\right) d\ell} \cdot \frac{1}{R^{5/2}}\,, \qquad \text{(A-27)}$$

3) Quality Factor:

$$Q = \frac{\omega\mu}{R_S}\,\frac{\iint_s \frac{F^2}{r}\,dr\,dz}{\oint \frac{F^2}{r}\,d\ell} = 2.09 \times 10^{5}\sqrt{kR}\,\frac{\iint_s F^2\left(\frac{R}{r}\right) dr\,dz}{R\oint F^2\left(\frac{R}{r}\right) d\ell} \cdot R^{1/2}\,, \qquad \text{(A-28)}$$

4) Average Axial Accelerating Field:

$$\mathcal{E}_o = \frac{1}{\omega\epsilon L}\int_z \left(\frac{1}{r}\frac{\partial F}{\partial r}\right)_{o,z} dz = 120\pi \cdot \frac{1}{kR}\int_z \left(\frac{R^2}{r}\frac{\partial F}{\partial r}\right)_{o,z} \frac{dz}{L} \cdot \frac{1}{R}\,, \qquad \text{(A-29)}$$

$$\mathcal{E}_o = \frac{\omega\mu}{L}\iint_s \left(\frac{F}{r}\right) dr\,dz = 120\pi \cdot kR \iint_s F \cdot \left(\frac{R}{r}\right)\frac{dr}{R}\,\frac{dz}{L} \cdot \frac{1}{R}\,, \qquad \text{(A-30)}$$

5) Shunt Impedance:

$$Z_s = \frac{\mathcal{E}_o^{\,2}}{P_W/L} = 2.51 \times 10^{7} \cdot \frac{1}{(kR)^{5/2}}\,\frac{\left[\int_z \left(\frac{R^2}{r}\frac{\partial F}{\partial r}\right)_{o,z} \frac{dz}{L}\right]^2}{\oint F^2\left(\frac{R}{r}\right)\frac{d\ell}{L}} \cdot \frac{1}{R^{1/2}}\,, \qquad \text{(A-31)}$$

6) Transit Time Factor

$$T = \frac{1}{\omega\epsilon L\,\mathcal{E}_o}\int_z \left(\frac{1}{r}\frac{\partial F}{\partial r}\right)_{o,z} \cos\frac{2\pi z}{L}\,dz = \frac{\int_z \left(\frac{R^2}{r}\frac{\partial F}{\partial r}\right)_{o,z} \cos\frac{2\pi z}{L} \cdot \frac{dz}{L}}{\int_z \left(\frac{R^2}{r}\frac{\partial F}{\partial r}\right)_{o,z} \frac{dz}{L}}\,,$$

(A-32)

7) Coupling Coefficient:

$$S = \frac{1}{\omega \epsilon L^2 \mathcal{E}_o} \int_z \left(\frac{1}{r}\frac{\partial F}{\partial r}\right)_{o,z} z \sin\frac{2\pi z}{L}\, dz = \frac{\int_z \left(\frac{R^2}{r}\frac{\partial F}{\partial r}\right) \cdot \frac{z}{L} \sin\frac{2\pi z}{L} \cdot \frac{dz}{L}}{\int_z \left(\frac{R^2}{r}\frac{\partial F}{\partial r}\right)_{o,z} \cdot \frac{dz}{L}}, \quad \text{(A-33)}$$

where R.M.K.S. units have been assumed throughout, and where the numerical coefficients, etc., arise from considering copper cavity walls ($\sigma = 5.8 \times 10^7$ mhos/m) and a vacuum cavity medium, together with the definition for the surface resistance R_S :

$$R_S = \sqrt{\frac{\omega \mu}{2\sigma}} = \sqrt{\frac{kR}{R}} \cdot \sqrt{\frac{c\mu}{2\sigma}} \; . \quad \text{(A-34)}$$

It has been found that the calculation of the average axial accelerating field is more precisely accomplished by employing Eq. (A-30) than by Eq. (A-29), since, as a general rule, numerical integration is more precise than numerical differentiation. However, calculation of the transit time factor and the coupling coefficient are conveniently accomplished by obtaining the axial values:

$$\left(\frac{1}{r}\frac{\partial F}{\partial r}\right)_{o,z} = \frac{1}{r}\frac{\partial}{\partial r}\left[a(z)\, r^2 + b(z)\, r^4 + c(z)\, r^6 + \cdots\right]_{o,z} = 2\, a(z) \; . \quad \text{(A-35)}$$

The output of MESSYMESH is normalized in two ways: 1) according to the latter forms of (A-26) to (A-33) which show the dependence of the various derived auxiliary quantities on relative size of the cavity, and 2) according to the amplitude of the eigenvector necessary to maintain a constant stored energy per unit volume as given in (A-24).

The SUMMARY program renormalizes the eigenvector, eigenvalue, and various auxiliary quantities to a specific size cavity and to a specific average accelerating field.

In the SUMMARY program the value of the electric field is calculated along the metallic surface of the drift tube according to:

$$|\bar{E}| = \left|\frac{1}{i\omega\epsilon}\left(\bar{\nabla} \times H_\phi\right)\right| = \frac{1}{\omega\epsilon}\cdot\frac{1}{r}\left|\bar{\nabla}\left(r\, H_\phi\right)\right| = \frac{120\pi}{k\,R}\left[\frac{R^2}{r}\,\frac{\partial F}{\partial t}\right]\cdot\frac{1}{R}\,, \quad (A\text{-}36)$$

where because of the boundary condition (A-5), the last form involving the tangential derivative is deduced from the second form. The maximum of these values is determined and the location of this peak electric field is given.

APPENDIX B

COMPUTER PROGRAM FOR LINAC PARTICLE DYNAMICS

I. INTRODUCTION

A computer program entitled PARMILA has been written to trace the phase motion and the transverse motions of particles through a proton linear accelerator. The name of the program is derived from the phrase "phase and radial motion in linear accelerators." The program is prepared to simulate a linac of standard design, namely a linac composed of a set of resonant linac cavities (tanks), each containing a series of drift tubes, each of which contains a quadrupole focusing magnet.

The program proceeds by transforming the coordinates of a collection of particles through a set of transformations representing the linac. The transformations are chosen to represent the important effects of the linac accelerating and focusing structure on the particles.

Each particle has six coordinates, namely x, x', y, y', W and ϕ where x, x', y and y' are the transverse displacements and angles of the particle trajectories in two transverse directions, W is the energy and ϕ is the phase of the particle with respect to the rf accelerating voltage.

II. COUPLING BETWEEN PHASE AND TRANSVERSE MOTION

If one ignores the coupling between the x, x' motion, the y, y' motion and the W, ϕ motion, one can study each of the three motions independently. This has been done on many occasions, both analytically and digitally and is well described in the literature.[18, 19, 20, 21]

In order to describe the nature of the coupling terms included in the program, the sequences of transformation performed by the program must be outlined, and the functional dependence of each transformation described.

The linac is treated as a series of cells, each cell beginning at the center of one drift tube and ending at the center of the next. The main loop of the program transforms the coordinates of the particles through one cell. The main loop is described in detail in the next section.

The first transformation is denoted on Fig. B-1 as T1 and simulates the action of the quadrupole magnet on the transverse coordinates x, x', y and y'. The x, x' motion is independent of the y, y' and ϕ coordinates, but is a function of the particle energy W. This is one of the terms which couple the transverse motions to the phase motion.

The second transformation is denoted on Fig. B-1 as T2 and simulates a free-space drift to the electrical center of the accelerator gap. There are no coupling terms present here.

Before proceeding to the transformation T3 at the center of the gap, it should be noted that transformations T4 and T5 are similar, except in magnitude, to transformations T2 and T1, respectively.

The transformation T3 at the center of the gap simulates the change in energy of the particle, and the net defocusing experienced by the particle on crossing the gap.

The change in ϕ from the previous gap is a simple function of the length of the cell and the longitudinal component of the particle velocity. The change in ϕ per cell is calculated in two steps. It is calculated once to prepare the coordinates for output at the end of the unit cell and once to prepare for the phase-dependent calculations at the center of the gap. The difference between the actual velocity and the longitudinal component is a possible coupling between

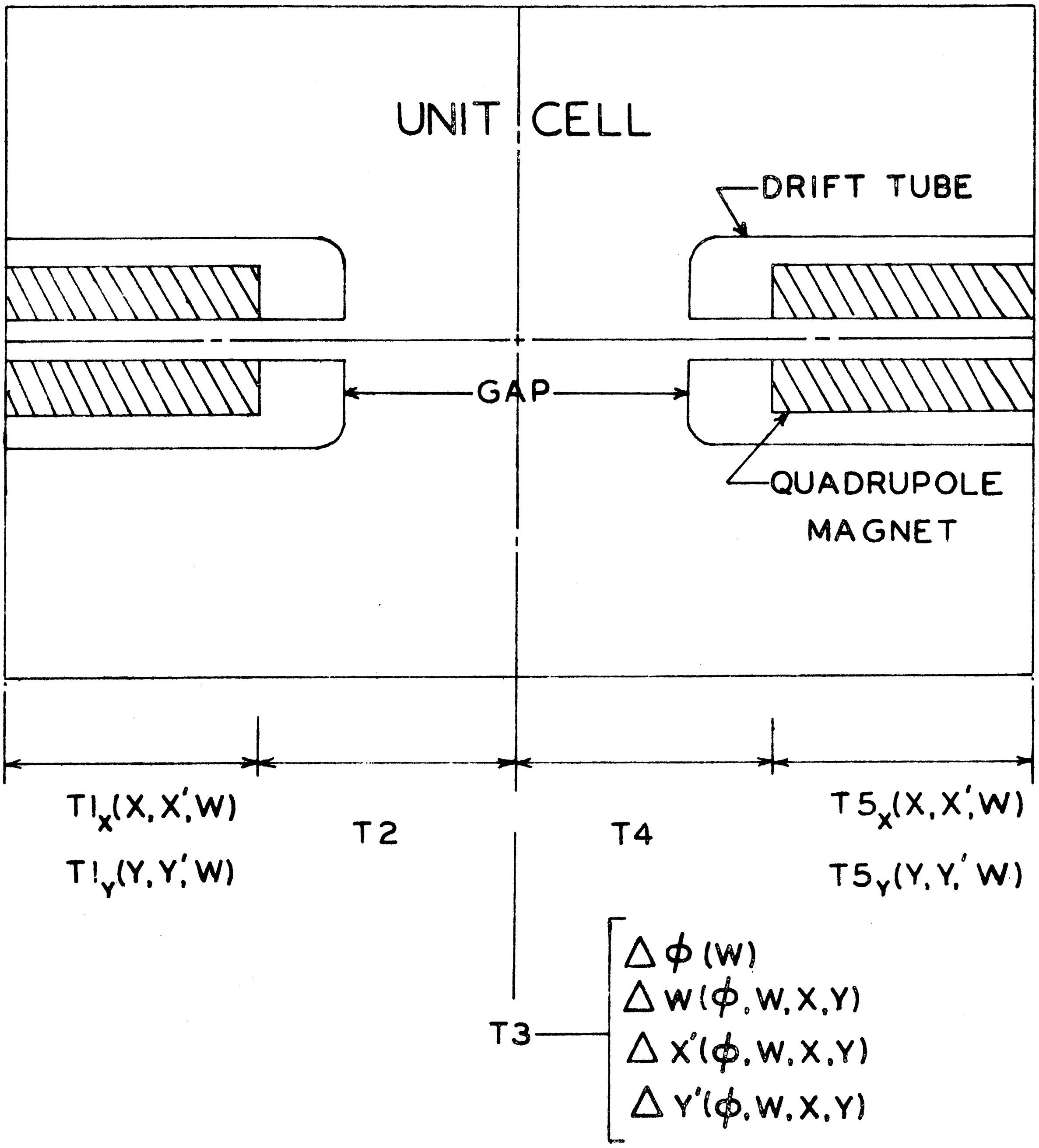

FUNCTIONAL DEPENDENCE OF TRANSFORMATION

Figure B1

the phase motion and the transverse motion. This effect is very small and is ignored. The change in energy for each particle on crossing the gap is a function of ϕ, of the effective transit time factor, and of the transverse coordinates x, x', y and y'. Hence this represents a strong coupling between the phase and transverse motion.

The defocusing action of the x' or y' coordinate of a particle on crossing the gap is a function of ϕ, x or y, the effective transit time factor and the velocity.

III. MAIN LOOP OF COMPUTATION

A block diagram of the main loop of the PARMILA program is shown in Fig. B-2. The loop is entered at Block C, where transformations T1 and T2 are accomplished. Following this block, the cell number is increased by unity, and the program proceeds to Block A where the transformations T3 and T4 are accomplished. From Block A the program proceeds to Block B where the transformation T5 is accomplished. A check is made to see if output is desired before completing the loop by proceeding to Block C.

These blocks are described in detail below.

Block A.

The phase of a particle at the beginning of the n^{th} cell $\phi_{n-1/2}$ is transformed to its value at the center of the gap ϕ_n by the relation

$$\phi_n = \phi_{n-1/2} + \left(\frac{\beta_{s,n-1}}{\beta_{n-1}} - 1 \right)$$

where $\beta_{s,n-1}$ is the value of β for the synchronous particle at the end of the $n - 1^{st}$ cell. At this point the energy of each particle is increased by δW where (see Eq. (B-4) in Section V)

MAIN COMPUTATIONAL LOOP

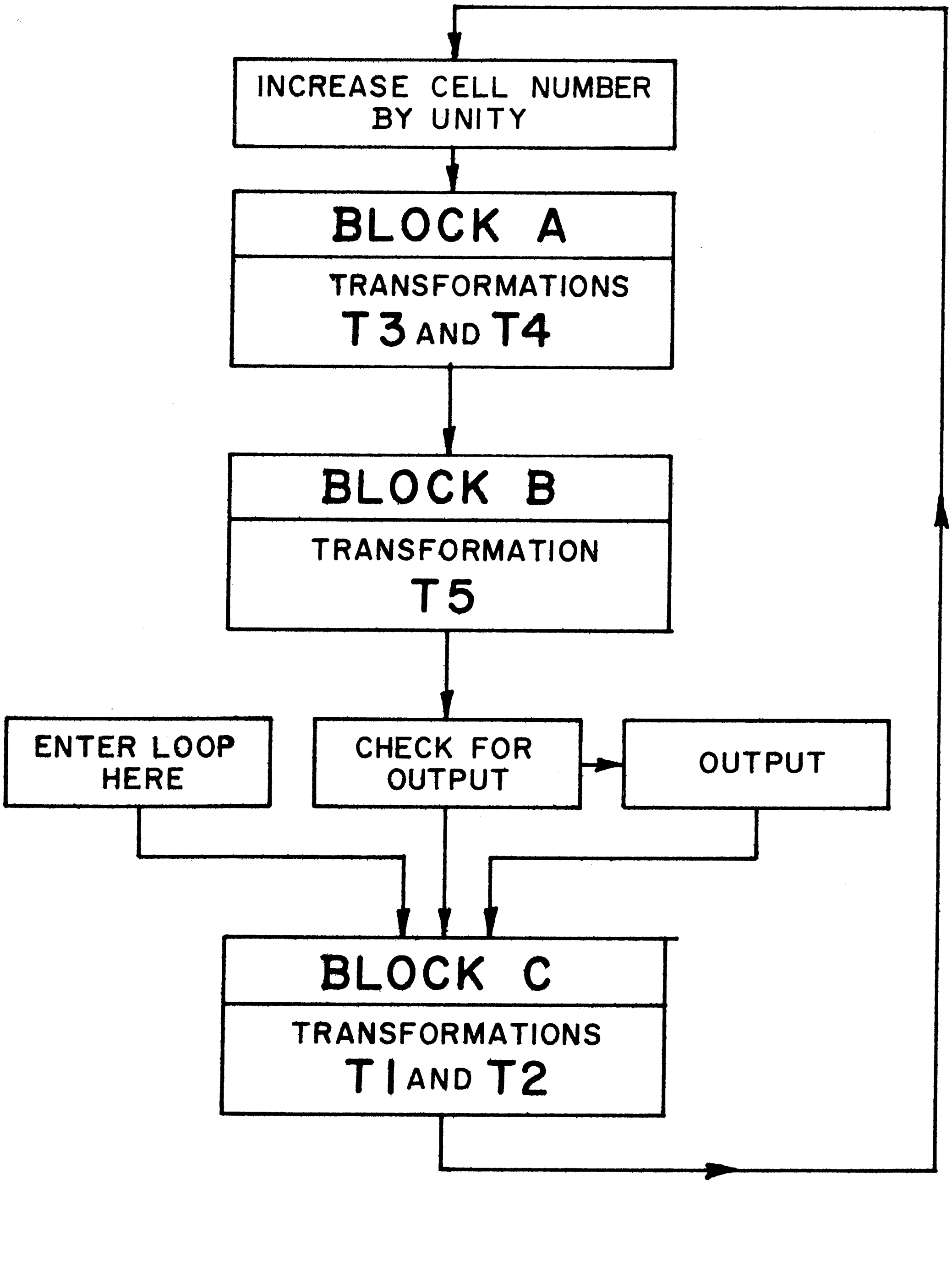

Figure B2

$$\delta W_n = e\,E_o\,L_n \left\{ \left(\frac{1 + \pi^2 (x^2 + y^2)}{\lambda^2 \beta^2 \gamma^2} \right) T_{eff,\,n} \cos \phi_n - \frac{(x\,x' + y\,y')\pi}{\beta\lambda}\, T_n \sin \phi_n \right\}$$

where E_o is the average axial electric field, L_n is the length of the n^{th} cell, λ is the wavelength (the velocity of light divided by the frequency of rf), and $T_{eff,\,n}$ is the effective transit time factor for a particle entering the n^{th} cell with velocity β_{n-1}. $T_{eff,\,n}$ is defined as

$$T_{eff,\,n} = T_n - 2\pi \left(\frac{\beta_{s,\,n-1}}{\beta_{n-1}} - 1 \right) S_n$$

where T_n and S_n are simple quadratic functions of $\bar{\beta}_{s,\,n}$. The coefficients of the quadratic functions are part of the input, and are chosen so that the values of T and S correspond to values determined by MESSYMESH for different values of $\bar{\beta}$.

The following transformations are now performed on both pairs of transverse coordinates x, x' and y, y' to simulate the action of the rf fields for a single gap on these transverse coordinates.

$$\begin{pmatrix} x_a & \text{or} & y_a \\ x_a' & \text{or} & y_a' \end{pmatrix} = \begin{pmatrix} 1 & 0 \\ -\Delta/\beta\lambda & 1 \end{pmatrix} \begin{pmatrix} 1 & 0 \\ 0 & \frac{(\beta\gamma)_{n-1}}{(\beta\gamma)_n} \end{pmatrix} \begin{pmatrix} x & \text{or} & y \\ x' & \text{or} & y' \end{pmatrix}$$

where the subscript "a" denotes the coordinates <u>after</u> crossing the gap and where Δ is the unitless quantity* in the relation between the net deflections $\delta x'$ or $\delta y'$ and the transverse displacement x or y. This relation is

$$\frac{\delta x'}{x} = \frac{\delta y'}{y} = -\frac{\Delta}{\beta\lambda}\,.$$

---

*The quantity Δ of this report is identical to the quantity Δ of the Smith and Gluckstern paper.

The formula for Δ is partially derived in Section V of this appendix, giving the relation

$$\Delta = \frac{\pi e\, E_o\, \lambda\, T_{eff}\, \sin\phi}{m_o\, c^2 \beta\, \gamma^3}$$

where $m_o\, c^2$ is the rest energy of the proton.

x and y now get the ordinary drift transformation $\begin{pmatrix} 1 & D \\ 0 & 1 \end{pmatrix}$ where D is the distance from the center of the gap to the entrance of the quadrupole magnet. The value of $x^2 + y^2$ is checked at this point to see that it is within the aperture of the n^{th} drift tube.

Block B.

The phase of the particle at the end of the cell is calculated by the relation

$$\phi_{n+1/2} = \phi_n + \left(\frac{\beta_{s,n}}{\beta_n} - 1 \right) \pi \ .$$

A transformation to simulate the action of the quadrupole magnet is now performed. The transformation shown below transforms the coordinate pairs x, x' and y, y' at the entrance to the quadrupole magnet into the coordinate pairs x_c, x_c' and y_c, y_c' at the center of the quadrupole magnet. The quadrupole field is defined in terms of the field gradient B' in gauss per centimeter and its length Q. The orientation of the field is given by the algebraic sign of B'. If B' is positive, the quadrupole is oriented to focus the x motion, and if negative, it is oriented to focus the y motion.

The transformation in the focusing plane is

$$\begin{pmatrix} x_c & \text{or} & y_c \\ x_c' & \text{or} & y_c' \end{pmatrix} = \begin{pmatrix} \cos K\ell & \frac{1}{K} \sin K\ell \\ -K \sin K\ell & \cos K\ell \end{pmatrix} \begin{pmatrix} x & \text{or} & y \\ x' & \text{or} & y' \end{pmatrix}$$

and in the defocusing plane is

$$\begin{pmatrix} x_c \quad \text{or} \quad y_c \\ \\ x_c' \quad \text{or} \quad y_c' \end{pmatrix} = \begin{pmatrix} \cosh K\ell & \frac{1}{K}\sinh K\ell \\ \\ K\sinh K\ell & \cosh K\ell \end{pmatrix} \begin{pmatrix} x \quad \text{or} \quad y \\ \\ x' \quad \text{or} \quad y' \end{pmatrix}$$

where ℓ is the half length of the quadrupole magnet in centimeters, and

$K = \sqrt{\frac{|B'|}{B\rho}}$ where $B\rho = \frac{m_o c^2}{e} \beta\gamma$ is the magnetic rigidity of the particle in gauss-centimeter.*

Check for Output

The six coordinates of each particle now have values which represent the situation at the center of the quadrupole magnet. Output of these coordinates is available at this point in one of many possible formats, as specified by the user.

Block C.

Here the transverse coordinates undergo transformation through the second half of the quadrupole magnet in a fashion identical to that used in Block B, followed by a transformation representing a drift to the center of the gap in the next cell. This marks the end of the main loop. The cell number is increased by unity and the program transfers to Block A.

IV. GENERATING THE LINAC

The geometry of each unit cell and the dynamical properties of the synchronous particle are generated by the GENLIN subroutine at the beginning of each series of runs. The nature of the linac to be generated is based on the input of the following quantities:

---

*The θ and θ_o of Smith and Gluckstern are equivalent to $K\ell$ and $K\beta\lambda$ respectively as defined here.

1. NTT, number of linac cavities (total)
2. W_o, initial kinetic energy of synchronous particle in MeV
3. f, resonant frequency in Mc
4. Periodicity of quadrupole fields (i.e., + - + -, or + + - - , or ···)

and the following information on each cavity:

5. Ordinal number of cavity
6. W_f, the kinetic energy in MeV, which when exceeded, marks the last unit cell of the cavity
7. D, the drift distance in centimeters separating the cavity from the next cavity
8. E_{field} in MV/cm, C_1 and C_2, which are used to specify the average axial electric field E_o. E_o is equal to $E_{field} \cdot$ TILT. TILT is the linear function $C_1 + C_2 \cdot D$, where D is defined as the total distance in centimeters from the low energy end of the cavity. If C_1 is zero, the computer will set $C_1 = 1$ and $C_2 = 0$.
9. ϕ_s, the stable phase angle in degrees
10. C_3 and C_4, an alternative procedure for specifying the acceleration rate. If the input value of ϕ_s is zero, the acceleration rate is set equal to RATE = $C_3 + C_4 \cdot D$ in MeV/cm where D is defined above. ϕ_s is then calculated from the relation

$$\text{RATE} = \mathcal{E}_{field} \cdot \text{TILT} \cdot T \cdot \cos \phi_o$$

where

$$\frac{3\pi}{2} \leq \phi_s \leq 2\pi$$

11. C_5 and C_6, where the radius of the drift tube hole A in centimeters is $C_5 + C_6 \cdot D$, again a linear function of D. Alternatively, if $C_5 < 0$, the ratio of A to the cell length L is set equal to $|C_5|$.

12. Q/L, the ratio of the quadrupole length to cell length.

13. $\delta\phi$, the difference in rf phase in degrees between the cavity and the next cavity.

14. C_7 and C_8, which are used to determine the magnetic field gradient B' such that $\left(\frac{Q/L}{0.5}\right)\theta_o^2$ is the linear function $C_7 + C_8\,\Delta$ for the synchronous particle where

$$\theta_o^2 = K^2\beta^2\lambda^2 = \frac{e\,B'\beta\lambda^2}{m_o\,c^2\gamma}$$

and

$$\Delta = \frac{\pi e\,E_o\,\lambda\,T_n\sin\phi_s}{m_o\,c^2\,\beta\gamma^3} .$$

This results in the equation for the field gradient

$$B' = \frac{0.5}{Q/L}\;\frac{\gamma_s}{\beta_s}\left(\frac{m_o\,c^2}{e\,\lambda^2}\,C_7 + \frac{\pi E_o\,T_n\sin\phi_s}{\lambda\beta_s\,\gamma_s^3}\,C_8\right)$$

15. C_9, C_{10}, and C_{11}, the coefficients of the quadratic relation for $T_n = C_9 + C_{10}\,\overline{\beta}_{s,n} + C_{11}\,\overline{\beta}_{s,n}^{\,2}$. T_n is used in the evaluation of the effective transit time factor.

16. C_{12}, C_{13}, and C_{14}, the coefficients of the quadratic relation for $S_n = C_{12} + C_{13}\,\overline{\beta}_{s,n} + C_{14}\,\overline{\beta}_{s,n}^{\,2}$. S_n is used in the evaluation of the effective transit time factor.

Given the above information for every cavity, the parameters of the linac are generated in the following way and stored in the memory for use in the main computational loop.

The n^{th} cell begins at the center of the $n - 1^{st}$ drift tube and extends to the center of the n^{th} drift tube. The electrical center of the gap is taken to be $\beta_{s,n-1}\ \lambda/2$ from the low energy end of the cell and $\beta_{s,n}\ \lambda/2$ from the other end of the cell, where $\beta_{s,n}$ is the velocity of the synchronous particle within the n^{th} drift tube.

The effective transit time factor, $T_{eff,n}$ is a quadratic function of the average value of β within the cell, which for the synchronous particle is taken to be $\beta_{s,n-1} - \beta_{s,n-2}$ since $\delta\beta$ does not change rapidly. Given the average value of β_s for the n^{th} cell $\overline{\beta}_{s,n}$, $T_{eff,n}$ for the synchronous particle is set equal to $C_9 + C_{10}\ \overline{\beta}_{s,n} + C_{11}\ \overline{\beta}_{s,n}^{\,2}$.

The average axial electric field E_o is the constant E_{field} times TILT, a linear function of the distance from the low energy end of the cavity to the electrical center of the n^{th} gap. This distance is $\sum_{i}^{n-1} L_i + \beta_{s,n-1}\ \lambda/2$ which does not involve $\beta_{s,n}$ and hence presents no problem in calculation.

The change of momentum δp_n for the synchronous particle as a result of the acceleration through the n^{th} cell is then evaluated as

$$\frac{\delta p_n}{m_o\, c} = \frac{e\, E_o\ \lambda T_{eff,n} \cos\phi_s}{m_o\, c^2} .$$

The momentum for the n^{th} cell is then

$$p_n = p_{n-1} + \delta p_n .$$

From p_n the quantities β_n, γ_n, W_n, and L_n are calculated.

$$L_n = (\beta_{n-1} + \beta_n)\ \lambda/2 .$$

If the alternative description of the acceleration rate is used, $\frac{\delta p_n}{m_o\, c}$ is set equal to $\text{RATE}_n\ \lambda/m_o\, c^2$.

The gradient of the quadrupole field in the n^{th} drift tube is calculated at this point, from the relation described earlier in this section. At this point the evaluation of the parameters pertinent to the n^{th} cell is complete and the subroutine proceeds to the $n + 1^{st}$ cell.

V. APPLICATION OF CALCULATED FIELDS TO PARTICLE DYNAMICS

The MESSYMESH program described in Appendix A makes available the actual distribution of fields for an entire linac cell. These fields can be reduced to two quantities, T and S, that reflect most precisely the effect of these fields on the particle motion. With the use of these quantities the energy gain δW and the radial impulse Δ can be calculated.[22]

Let $\vec{\mathcal{E}}(r, z, t)$ be the electric field vector at radius r, longitudinal position z, and time t. The fields through which the particles travel, that is, the fields near the axis of the linac, can be expressed in terms of the axial component of the electric field on the axis, $\mathcal{E}_z(0, z, t)$. The time dependence is taken to be sinusoidal and $E_z(z)$ is defined so that

$$\mathcal{E}_z(0, z, t) = E_z(z) \cos(\omega t + \phi) .$$

It is assumed that the fields on the axis of the linac are known $\left[\text{i.e., } \mathcal{E}_z(0, z, t)\right]$, and it is necessary to get a satisfactory expression for the fields off the axis in terms of $\mathcal{E}_z(0, z, t)$. An iterative procedure is used to get the n^{th} order field in terms of the $n - 1^{st}$ order solution. This procedure yields the following expression for $\mathcal{E}_z(r, z, t)$, $\mathcal{E}_r(r, z, t)$, and $B_\theta(r, z, t)$.

$$\mathcal{E}_z(r,z,t) = \mathcal{E}_z(0,z,t) - \frac{r^2}{4}\left(\frac{\partial^2 \mathcal{E}_z(0,z,t)}{\partial z^2} - \frac{1}{c^2}\frac{\partial^2 \mathcal{E}_z(0,z,t)}{\partial t^2}\right) \tag{B-1}$$

+ terms in r^4 and higher

$$\mathcal{E}_r(r,z,t) = -\frac{r}{2}\frac{\partial \mathcal{E}_z(0,z,t)}{\partial z} + + \frac{r^3}{16}\frac{\partial}{\partial z}\left(\frac{\partial^2 \mathcal{E}_z(0,z,t)}{\partial z^2} - \frac{1}{c^2}\frac{\partial^2 \mathcal{E}_z(0,z,t)}{\partial t^2}\right) \tag{B-2}$$

+ terms in r^5 and higher

$$B_\theta(r,z,t) = \frac{r}{2c}\frac{\partial \mathcal{E}_z(0,z,t)}{\partial t} - - \frac{r^3}{16c}\frac{\partial}{\partial t}\left(\frac{\partial^2 \mathcal{E}_z(0,z,t)}{\partial z^2} - \frac{1}{c^2}\frac{\partial^2 \mathcal{E}_z(0,z,t)}{\partial t^2}\right) \tag{B-3}$$

+ terms in r^5 and higher.

The energy gain δW is

$$\delta W = e\int_{\text{path}} \vec{\mathcal{E}} \cdot ds = e\int_{\text{path}} (\mathcal{E}_z\, dz + \mathcal{E}_r\, dr)$$

which can be written from the fields above as

$$\delta W = e\int \mathcal{E}_z(0,z,t)\, dz - \frac{er^2}{4}\int\left(\frac{\partial^2 \mathcal{E}_z(0,z,t)}{\partial z^2} - - \frac{1}{c^2}\frac{\partial^2 \mathcal{E}_z(0,z,t)}{\partial t^2}\right) dz - e\int \frac{r}{2}\frac{\partial \mathcal{E}_z(0,z,t)}{\partial z}\, dr\ . \tag{B-4}$$

The origin of z is defined by requiring

$$\int E_z(z) \sin\frac{2\pi z}{L}\, dz = 0\ .$$

The transit time factor T for the synchronous particle is defined by the relation

$$\int E_z(z) \cos \frac{2\pi z}{L} \, dz = E_0 L T$$

and the coefficient of the velocity dependent term of the transit time factor S is defined by the relation

$$\int z \, E_z(z) \sin \frac{2\pi z}{L} \, dz = E_0 L^2 S .$$

The evaluation of the first integral on the right-hand side of Eq. (B-4) will be outlined to illuminate the meaning of the terms α and S.

$$\int \mathcal{E}_z(0, z, t) \, dz = \int E_z(z) \cos (\omega t + \phi) \, dz$$

where $t = \frac{z}{V}$. Let $\frac{1}{V} = \frac{1}{V_s} (1 + \alpha)$, where V_s is the velocity of the synchronous particle. Noting that $\omega t = \frac{2\pi z}{L} (1 + \alpha)$, then

$$\int \mathcal{E}_z(0, z, t) \, dz = \int E_z(z) \cos \left(\frac{2\pi z}{L} + \phi + \frac{2\pi z\alpha}{L} \right) dz$$

$$= \int E_z(z) \left[\cos \left(\frac{2\pi z}{L} + \phi \right) \cos \frac{2\pi z\alpha}{L} - \sin \left(\frac{2\pi z}{L} + \phi \right) \sin \frac{2\pi z\alpha}{L} \right] dz$$

$$= \int E_z(z) \left[\left(\cos \frac{2\pi z}{L} \cos \phi - \sin \frac{2\pi z}{L} \sin \phi \right) - \right.$$

$$\left. - \frac{2\pi z\alpha}{L} \left(\sin \frac{2\pi z}{L} \cos \phi + \cos \frac{2\pi z}{L} \sin \phi \right) \right] dz$$

where

$$\cos \frac{2\pi z\alpha}{L} = 1 \qquad \text{and} \qquad \sin \frac{2\pi z\alpha}{L} = \frac{2\pi z\alpha}{L} .$$

The second term of the four terms is zero by definition of the origin of z and for a symmetric gap where $E_z(z)$ is an even function of z, the fourth term integrates to zero, leaving

$$\int \mathcal{E}_z(0, z, t)\, dz = E_o L (T - 2\pi \alpha S) \cos\phi \ .$$

The factor $(T - 2\pi\alpha S)$ can be interpreted as the effective transit time factor for particles of all velocities. The expression reduces to T for the synchronous velocity.

When the other two integrals on the right-hand side of Eq. (B-4) are evaluated, the expression for the energy gain for one linac cell is

$$\delta W = e E_o L \left\{ \left(1 + \frac{\pi^2 r^2}{\lambda^2 \beta^2 \gamma^2}\right) (T - 2\pi \alpha S) \cos\phi - \frac{r r' \pi}{\beta \lambda} T \sin\phi \right\} .$$

The radial impulse imparted to the particle on crossing a gap is

$$\delta p_r = \int_{\text{path}} |\vec{F}_r| dt = \int_{\text{path}} e\left(\mathcal{E}_r - \frac{V B_\theta}{c}\right) dt \ .$$

Using the expression for the fields given in Eqs. (B-2) and (B-3), and eliminating third and higher orders in the variable r, the expression for $\delta r'$ becomes

$$\delta r' = - \frac{e\pi}{m_o c^2 \lambda} \frac{E_o L}{\beta^3 \gamma^3} r \sin\phi \, (T - 2\pi \alpha S)$$

where

$$\delta r' = \frac{\delta p_r}{m_o c \beta \gamma} .$$

If $\frac{\delta r'}{r}$ is defined as $-\frac{\Delta}{\beta\lambda}$, Δ reduces to

$$\Delta = \frac{\pi e E_o \lambda \, T_{eff} \sin\phi}{m_o c^2 \beta \gamma^3} .$$

The equations above for δW and $\delta r'$ are used in Block A of the Main Computation Loop to simulate the effect of the rf fields on each particle of the beam.

APPENDIX C: ENGINEERING CALCULATIONS

Calculation of Ampere-Turns Required for Quadrupole Coil

The design equation for a quadrupole coil is

$$NI = \frac{0.398\ G\ b^2}{n} \qquad (C.1)$$

N = number of turns per pole

I = current in turns, amperes

G = flux gradient, gauss/cm

b = half circle aperture, cm

n = an efficiency term which will usually be about 90% for pole tip fluxes of less than 12.5 kG.

The computed quadrupole magnet strength for a 200 MeV linac varies from about 500 gauss/cm at 20 MeV to about 175 gauss/cm at 200 MeV for a quadrupole system with a periodicity of two (i.e., +, +, -, -).* For the maximum case of 500 gauss/cm and a half circle aperture of 2.22 cm

$$NI = \frac{0.398\ (500)(2.22)^2}{0.9} = 1090 \text{ ampere-turns} .$$

Calculation for a Coil Using a Thin Wall Hollow Conductor

Using the 1/8-in. minimum tube I.D., 1/32-in. wall copper and 5 mil thick formvar insulation, there is room for four turns.

A_c = cross-sectional area of a 3/16-in. O.D. x 1/32-in. wall tube conductor = 0.0153 in.^{2}

$$I = \frac{1090}{4} = 272.5 \text{ amperes}$$

$$I/A_c = \text{current density} = \frac{272.5}{0.0153} = 17{,}800 \text{ amp/in.}^2$$

which is below the density limit of 25,000 amp/in.^{2}.

---

*It should be noted that the periodicity of the quadrupole strengths in Table X, System I, is one.

The power per quadrupole including loss through the drift tube stem leads is

$$P = I^2/A_c \, R_t \, L \tag{C.2}$$

where

P = power, watts

R_t = resistivity of conductor, μ ohm in.^{2}/ft (8.33×10^{-6})

B = conductor length per turn per pole, feet

T = turns of conductor per pole, turns/pole

ℓ = drift tube stem lengths, feet

L = total length of conductor in quadrupole and stem, feet

$= 4\,B\,T + 2\ell$

$$P = \frac{272.5^2}{0.0153}\,(8.33 \times 10^{-6})\left[\left(4 \times \frac{14.8}{12} \times 4\right) + \left(2 \times \frac{25}{12}\right)\right] = 966 \text{ watts} .$$

The quadrupole for the drift tube at the 200 MeV level has a flux gradient of about one-third of the 20 MeV gradient. Since the conductor used above is minimal, the same size will be used for all quadrupoles resulting in simpler material procurement and fabrication with corresponding lower cost. The length of the coils will be made to suit the drift tube with the number of turns remaining the same. Adjustment of the current will be used to achieve the computed flux density.

Calculation for a Coil Using Flood-Cooled Solid Wire

Using #9 solid copper wire with heavy formvar insulation, there is room for six turns in a single layer. For the case of 500 gauss/cm and half-circle aperture of 2.22 cm, 1090 ampere-turns are required.

$$I = \frac{1090}{6} = 181.5 \text{ amperes}$$

$$\frac{I}{A_c} = \frac{181.5}{1.02 \times 10^{-2}} = 17,800 \text{ amp/in.}^2$$

$$P = \frac{181.5^2}{1.02 \times 10^{-2}} \quad 8.33 \times 10^{-6} \left[(4 \times \frac{14.8}{12} \times 6) + (2 \times \frac{25}{12})\right] = 908 \text{ watts.}$$

Calculations for a Foil-Wound Coil

Figure 27 shows a section view through the coil and the magnet poles.

For a quadrupole magnet with the same flux gradient and space limitations as for the quadrupole magnet using the thin copper tubes, the computations are:

The space available is 3/8 in. x 7/8 in. and with 1/16 in. allowed for potting epoxy on three sides; there is 1/4 in. x 13/16 in. available space for each coil. Using 4-mil copper foil and 1-mil mylar film between foil, there is space for 50 turns in the 1/4-in. width. For 1090 ampere-turns

$$I = \frac{1090}{50} = 21.8 \text{ amperes}$$

$$I/A_c = \frac{21.8^2}{(0.004 \text{ in.})(0.8125 \text{ in.})} = 6,700 \text{ amp/in.}^2$$

substituting in Eq. (C. 2)

$$P = \frac{21.8^2}{(0.004 \text{ in.})(0.8125 \text{ in.})} (8.33 \times 10^{-6}) \left[(4 \times \frac{14.8}{12} \times 50) + (2 \times \frac{25}{12})\right]$$

$$P = 306 \text{ watts .}$$

With the increased number of turns, the current requirement is down and so is the current density. The power required has been appreciably reduced.

Neglecting any benefit of heat transfer of the 1-mil mylar film between foil, the temperature rise between the cooling strip and the opposite side of the foil is

$$\theta = \frac{1}{2} \frac{Z R_1 h^2}{k_1 A_2} . \qquad (C.3)$$

For a one-foot length of foil, i.e., $Z = 1$, $A_2 = 1\delta$

$$\theta = \frac{1}{2} \frac{R_1 h^2}{k_1 \delta} \qquad (C.4)$$

where

θ = temperature rise, °F

R_1 = heat transmission coefficient, $\frac{\text{Btu/hr/ft length}}{\text{ft}^2\text{/ft length}}$

h = width of foil, feet

k_1 = thermal conductivity of foil $\frac{\text{Btu-ft}}{\text{ft}^2\ {}^{\circ}\text{F hr}}$, 226 for copper

A_2 = cross-sectional area for heat flow per foot of length, $\text{ft}^2\text{/ft}$

δ = thickness of foil, feet

Z = length of conductor, feet.

Substituting for R_1

$$R_1 = \frac{306 \text{ watts } (3.413 \text{ Btu/hr/watt})/251 \text{ ft}}{\frac{0.8125 \text{ in. x } 12 \text{ in./ft}}{144 \text{ in.}^2/\text{ft}^2}} .$$

$$= 61.5 \text{ Btu/hr/ft}^2 .$$

Substituting in Eq. (C.4)

$$\theta = \frac{61.5\left(\frac{0.8125}{12}\right)^2}{2 \times 226\left(\frac{0.004}{12}\right)} = 1.87\ {}^{\circ}\text{F} .$$

The temperature rise across the 5-mil mylar insulator to the cooling plate is

$$T = \frac{\ell_2 Q}{k_2 A_2} \qquad \text{(C. 5)}$$

where

T = temperature difference, $^{\circ}F$

ℓ_2 = thickness of mylar film, feet

Q = heat loading per foot, $\frac{\text{Btu/hr}}{\text{ft}}$

k_2 = thermal conductivity of mylar film, $9.7 \times 10^{-2} \frac{\text{Btu-ft}}{\text{ft}^2\ ^{\circ}\text{F hr}}$

A_2 = cross-sectional area for heat flow per foot of length, ft^2/ft

$$Q = \frac{306 \text{ watt}}{251 \text{ ft}}\ 3.41 \text{ Btu/hr/watt} = 4.15 \frac{\text{Btu/hr}}{\text{ft}} .$$

Substituting in Eq. (C. 5)

$$T = \frac{\frac{0.005}{12}\ 4.15}{9.7 \times 10^{-2}\ \frac{0.004 \times 12}{144}} = 53.5\ ^{\circ}F .$$

The temperature rise across the copper foil is negligible and while the temperature gradient from the foil across the mylar to the cooling plate is appreciable, it is well within the property limit of mylar.

DRIFT TUBE STEM ELONGATIONS WITH NO STEM COOLING

Assume 30 watts of average rf power dissipated in the stem, which is 1-1/2-in. O. D. copper clad stainless steel, and cooling is from one end of the stem at the cavity wall.

A stem is shown in Fig. C1 with an elemental length Δx, with heat flow in the upward direction defined as negative. Assuming all heat transfer is by conduction up the stem, then

$$Q_u = Q_{in} + Q_L \qquad \text{(C. 6)}$$

where Q_u is heat flow through the upper face and Q_L is the heat flow through the lower face. Q_{in} is the heat dissipated on the cylindrical surface of element Δx .

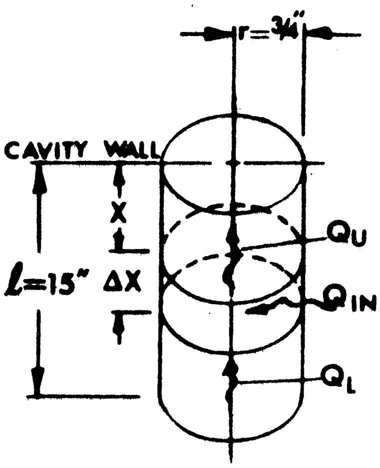

FIG. C1

$$Q_u = - k_1 A \left(\frac{dt}{dx}\right)_x \tag{C.7}$$

$$Q_L = - k_1 A \left(\frac{dt}{dx}\right)_{x+\Delta x} \tag{C.8}$$

$$Q_{in} = - 2 \pi r \Delta x R \tag{C.9}$$

where

k_1 = thermal conductivity of the rod, $\frac{\text{Btu-ft}}{\text{ft}^2\ \text{hr}\ ^\circ\text{F}}$

A = cross-sectional area of rod, sq ft

$\frac{dt}{dx}$ = thermal gradient, $^\circ$F/ft

R = power dissipation, $\frac{\text{Btu}}{\text{sq ft hr}}$

r = radius of rod, feet

t = temperature rise, $^\circ$F

ℓ = length of stem, feet

by substitution of (C. 7), (C. 8), and (C. 9) in Eq. (C. 6).

$$-k_1 A \left(\frac{dt}{dx}\right)_x = -2\pi r \Delta x R - k_1 A \left(\frac{dt}{dx}\right)_{x+\Delta x}$$

$$\frac{\left(\frac{dt}{dx}\right)_{x+\Delta x} - \left(\frac{dt}{dx}\right)_x}{\Delta x} = \frac{2\pi r R}{k_1 A}$$

$$\Delta x \rightarrow 0, \quad \frac{d^2 t}{dx^2} = -\frac{2\pi r R}{k_1 A}$$

$$\frac{dt}{dx} = -\frac{2\pi r R x}{k_1 A} + C_1$$

when

$$x = \ell, \quad \frac{dt}{dx} = 0$$

$$\therefore C_1 = +\frac{2\pi r R \ell}{k_1 A}$$

$$t = -\frac{2\pi r R x^2}{2 k_1 A} + \frac{2\pi x r R \ell}{k_1 A} + C_2$$

when

$$x = 0$$

$$t = 0$$

$$\therefore C_2 = 0 .$$

The temperature rise at ℓ becomes

$$t = \frac{1}{2}\,\frac{2\pi\; r\,R\,\ell^2}{k_1\,A} = \frac{\pi r\,R\,\ell^2}{k_1\,A}\ .$$

The mean temperature rise is

$$t_m = \frac{\int_0^{\ell} t}{\ell}$$

$$\frac{1}{k_1\,A}\int_0^{\ell} t = \frac{2\;\pi\;\, r\,R\,\ell x^2}{2} - \frac{2\,\pi\; r\,R\,x^3}{6}\Bigg]_0^{\ell}$$

$$t_m = \frac{2\;\pi\;\; r\,R\,\ell^2}{3\,k_1\,A}\ . \qquad \text{(C. 10)}$$

The increase in the length of the stem

$$\Delta\ell = t_m\,k_2\,\ell \qquad \text{(C. 11)}$$

where k_2 = coefficient of thermal expansion, $\frac{1}{{}^{\circ}F}$.

For 30 watts dissipation on the stem

$$R = \frac{30 \text{ watts} \times 3.413\ \frac{\text{Btu}}{\text{watt hr}}}{2\,\pi\;\, r\,\ell} = \frac{102.4 \text{ Btu/hr}}{2\;\pi\;\, r\;\,\ell \text{ sq ft}}$$

$$k_1 \text{ for copper } = 226\ \frac{\text{Btu-ft}}{\text{ft}^2\text{ hr }{}^{\circ}\text{F}}$$

$$k_2 \text{ for copper } = \frac{9.8 \times 10^{-6}}{{}^{\circ}\text{F}}$$

$$A \text{ (for 1-1/2 in. O.D. } \times \tfrac{1}{16} \text{ wall tube)} = 2\,\pi\;\, r\;\frac{1}{16} = \frac{\pi\,r}{8}$$

$$= 2.05 \times 10^{-3} \text{ sq ft}$$

$$\ell = 1.25 \text{ ft}\ .$$

Substitution of these values in Eq. (C. 10)

$$t_m = \frac{2\pi r \frac{102.4}{2\pi r \ell}\ell^2}{3\,(226)(2.05 \times 10^{-3})} = 92.3\ ^{\circ}F,$$

then

$$\Delta \ell = (92.3)(1.25)(9.8 \times 10^{-6}) = 1.13 \times 10^{-3}\ \text{ft or } 13.6\ \text{mils}.$$

If we assume that the stem is cooled at its junction with the drift body as well as cooled at the cavity wall, the equation for t_m becomes

$$t_m = \frac{2\pi r R \ell^2}{12\, k_1 A}$$

i.e., the mean temperature rise and therefore the elongation are reduced by a factor of 4. Hence, for this example the elongation would be approximately 3.5 mils. It is to be noted that if either end of the stem at the point of cooling exceeds room temperature, further elongation would result.

In conclusion, it appears that if 0.002 in total drift tube (quadrupole) misalignments from all causes are all that can be tolerated, it is essential that the stems be directly and uniformly cooled over their entire length.

DISTORTIONS IN UNSYMMETRICALLY COOLED DRIFT TUBES

It has been demonstrated in a previous calculation that drift tube stem cooling is necessary. The following is an analysis of the distortion in copper clad stainless steel stem where a water-cooling tube has been joined to one wall.

Figure C2 shows a cross section of the stem with the water-cooling tube attached. It is assumed that the rf power is dissipated uniformly on the stem exterior surface and the water flow rate is sufficiently high that the temperature rise along the stem is negligible. Since no heat flow takes place across the plane immediately opposite the cooling tube, the cooling analysis is the same as it would be for a flat plate cooled at its center as shown in Fig. C3.

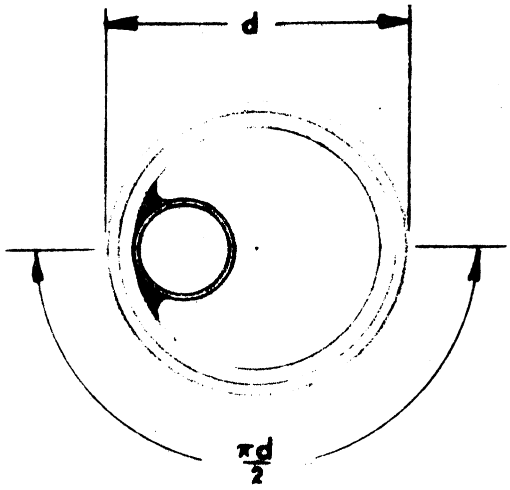

FIG. C2

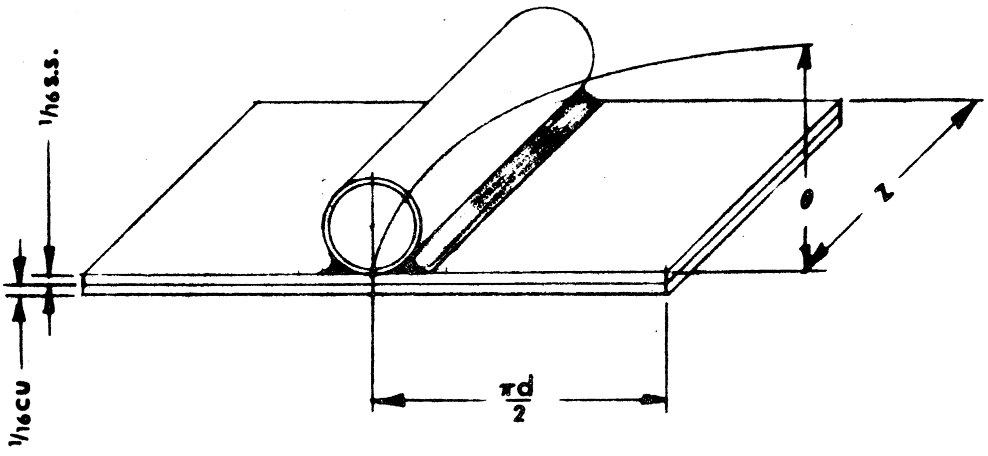

FIG. C3

Figure C4 shows the preferred orientation of the cooling in tube in the stem, if this scheme is to be used. Figure C5 illustrates the further displacement of the end of the drift tube with the orientation of cooling tube moved 90° in the stem.

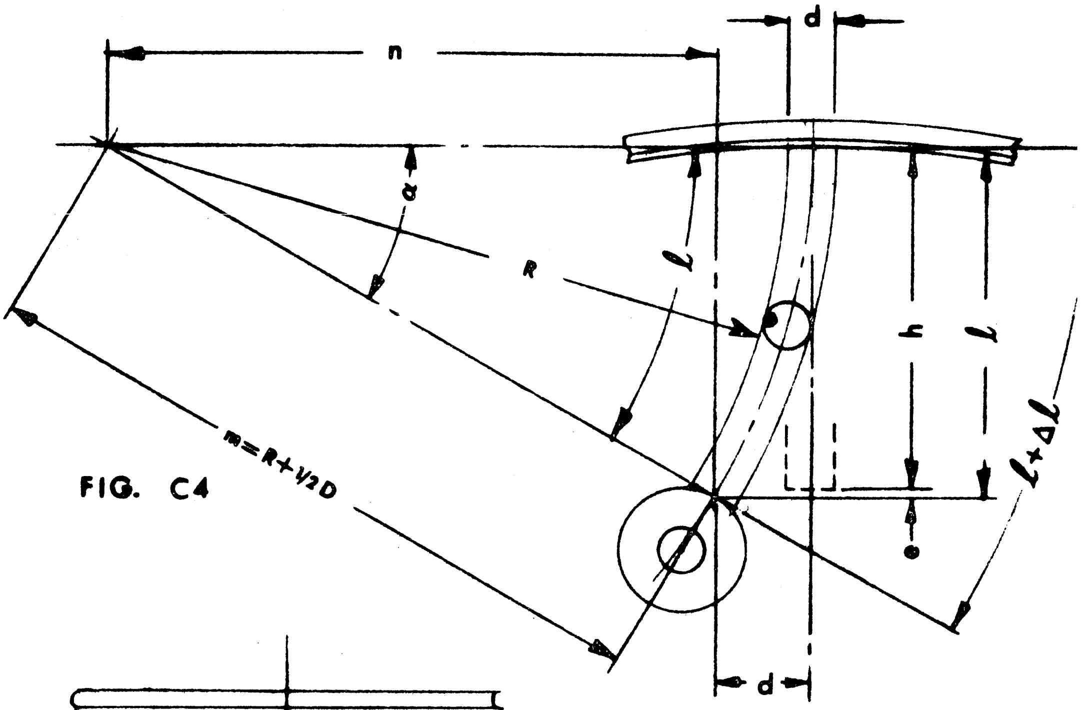

FIG. C4

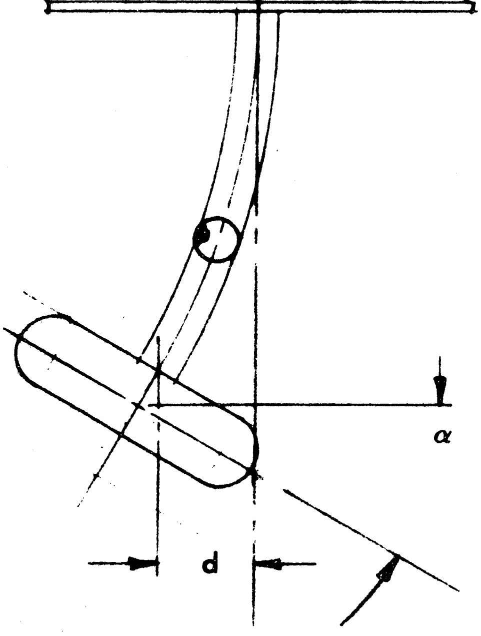

FIG. C5

Since the stem is fabricated from a copper clad stainless steel tube, it is necessary to consider the overall heat conductance of the tube wall in the direction of heat flow. The thermal conductivity of copper is $226 \frac{\text{Btu-ft}}{\text{ft}^2 \text{ hr } {}^\circ\text{F}}$ compared to a value of 9.4 for stainless steel.

The stainless steel is of the same thickness as the copper and therefore contributes less than 5% to the circumferential thermal conductance and will be neglected.

The temperature rise on the opposite face of the tube can be expressed as

$$\theta = \frac{1}{2} \frac{z R \ell^2}{k_1 A_1} = \frac{R \left(\frac{\pi D}{2}\right)^2}{2 k_1 A_1} \qquad \text{(C. 12)}$$

where

R = heating rate, Btu/sq ft-hr

k_1 = thermal conductivity, $\frac{\text{Btu-ft}}{\text{ft}^2 \, {}^\circ\text{F hr}}$

A_1 = cross-sectional area normal to direction of heat flow, sq ft

z = length of surface, feet .

For a copper stem 1-1/2 in. O.D. x $\frac{1}{16}$ wall and 30 watts of rf average power dissipated on the entire stem, the following values are obtained.

$$R = \frac{\text{total power on stem}}{\text{area of stem}} = 209 \frac{\text{Btu/hr}}{\text{ft}^2}$$

$$k_1 = 226 \frac{\text{Btu-ft}}{\text{ft}^2 \, {}^\circ\text{F hr}}$$

$$A_1 = 5.21 \times 10^{-3}$$

$$\ell = \frac{\pi D}{2} = 0.196 .$$

Then

$$\theta = \frac{(1)(209)(0.196)^2}{2\,(226)(5.21 \times 10^{-3})}$$

$$= 3.42 \, {}^\circ\text{F}$$

then

$$\Delta \ell = (t)\,(\ell_{in})\,(k_2) \qquad (C.13)$$

where

k_2 = coefficient of thermal expansion, $9.8 \times 10^{-6}/^{o}F$ for copper

ℓ_{in} = length of drift tube stem, inches

α = angular displacement of drift tube, radians

$\Delta \ell = (3.42)(15)(9.8 \times 10^{-6}) = 5.03 \times 10^{-4}$ in..

$$\alpha = \frac{\ell}{R} = \frac{\ell + \Delta \ell}{R + D}$$

$$\alpha = \frac{15}{R} = \frac{15.000503}{R + 1.5}$$

$\therefore R = 4.47316103 \times 10^{4}$ in.

$$\therefore \alpha = \frac{15}{4.4732 \times 10^{4}} = 3.3533 \times 10^{-4} \text{ radians} = 0^{o}\ 1'\ 9.167''.$$

In Fig. C4, $m = R + \frac{1}{2} D$ or 44732.360 in.

$\sin \alpha = 3.353311 \times 10^{-4}$, $\cos \alpha = 0.9999999436$

$h = m \sin \alpha = 15.00015$.

Therefore the end of the drift tube has been displaced 0.00015 in. vertically.

$n = m \cos \alpha = 44,732.357$

the horizontal displacement $d = m - n$

$= 0.003$ in..

Since this horizontal displacement of the drift tube (quadrupole) exceeds the misalignment tolerances, a stem should not be cooled in this fashion.

It may be noted that if the return water tube were to be brazed to the stem, i.e., a location immediately opposite the inlet water tube, that the distortion would be aggravated for any case where the temperature rise exceeded 3.4 ^{o}F.

We may conclude then that a uniform cooling scheme must be used for any stem which provides mechanical support for the drift tube body. If a mechanical support member is independent of an rf conducting surface, as shown in Fig. 6C, then it is only necessary to maintain constant temperature on the support member. Another approach is to use a coaxial cooling tube approach where the support member receives the cool inlet water as in Fig. C7.

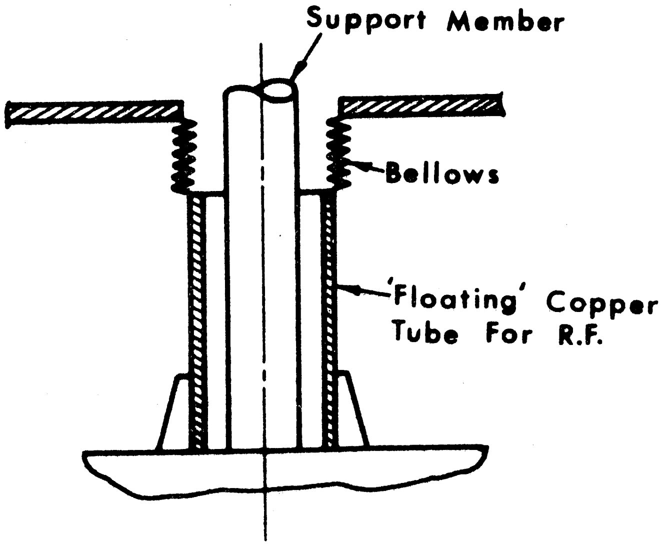

FIG C6

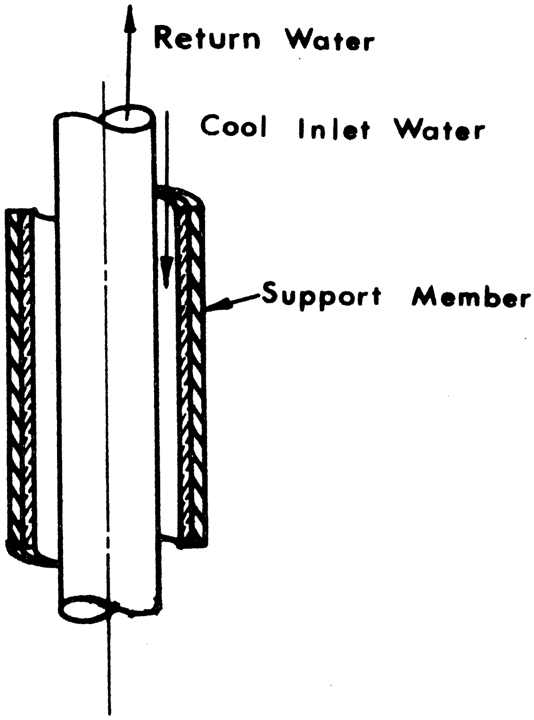

FIG C7

In conclusion, it is essential that the member of the stem which provides the mechanical support of the drift tube be maintained at room temperature. Cooling schemes that permit circumferential temperature gradients on the support member are not acceptable where quadrupole alignments must be maintained to a fraction of a mil. Hence the attachment of a cooling tube to one wall of a stem should not be used.

DESIGN FOR COOLING A 200 MEV LINAC CAVITY

Summary

The purpose of this section is to present a scheme for water cooling an 8.3-ft long experimental linac cavity.* The general approach is applicable to full-scale linacs.

Dimensional changes in the linac cavity and the drift tubes affect the operating frequency of the cell and for this reason should be kept to a minimum. The criteria used to determine the temperature control tolerance were the following (at 200 MeV):

$$\left(\frac{\Delta \ell}{\Delta f}\right)_{D,\, d,\, L,\, R_c,\, A} = -\ 0.38 \text{ cm/Mc}$$

$$\left(\frac{\Delta D}{\Delta f}\right)_{d,\, \ell,\, L,\, A,\, R_c} = -\ 0.79 \text{ cm/Mc}$$

$$\left(\frac{\Delta d}{\Delta f}\right)_{D,\, \ell,\, L,\, A,\, R_c} = -\ 0.63 \text{ cm/Mc}$$

$$\left(\frac{\Delta L}{\Delta f}\right)_{D,\, \ell,\, d,\, A,\, R_c} = +\ 2.17 \text{ cm/Mc}$$

where the tolerable $\Delta f = 5$ kc, ℓ is the drift tube length, D the cavity diameter, d the drift tube diameter and L the cell length. Using the above

---

*These calculations are based on similar calculations done by Igor Sviatoslavsky, MURA.

TABLE I

No.	Item		Linac Component		
			Linac Cavity	Drift Tube	End Plate
1	Power Dissipated (watts)		2500	1600	750
2	Type of Water Cond. (in.)	Size	2 x 1 x 3/16	3/8 D	3/8 D
		Length	180	150	220
3	Total Heat Transfer Area (ft^2)		20	0.6	1.0
4	Water Flow (gpm)		11.4	2.73	2.56
5	Inlet Water Temp. ($^{\circ}$F/$^{\circ}$C)		73/22.8	73/22.8	73/22.8
6	Outlet Water Temp. ($^{\circ}$F/$^{\circ}$C)		74.5/23.6	77/25	75.0/23.9
7	Operating Temp. of Comp. ($^{\circ}$F/$^{\circ}$C)		75/24.4	79/26	75.2/24.4
8	Heat Transfer Coeff. (Btu/hr ft^2 $^{\circ}$F)		560	3160	2337
9	Water Velocity (F.P.S.)		0.7	12	11.3
10	Reynold's Number		6000	29,000	26,000
11	Pressure Drop (psi)		10	20	20
12	Heat Exchanger: 16 ft^2 heat transfer area is needed				
13	Pump: A centrifugal pump which will deliver 40-50 gpm at 100 ft is required.				

criteria, it appears that the maximum tolerable dimensional changes and the corresponding temperature differences needed to produce them are:

$\Delta \ell = 0.75 \times 10^{-3}$ in.

$\Delta D = 1.57 \times 10^{-3}$ in.

$\Delta d = 1.2 \times 10^{-3}$ in.

$\Delta L = 4.33 \times 10^{-3}$ in.

The required temperature stability for the drift tube length can be calculated in the following manner:

$$\Delta T_{s\ell} = \frac{\Delta \ell}{\ell k_{cu}}$$

where

$\Delta \ell =$ allowable dimensional change

$\Delta T_{s\ell} =$ allowable thermal drift, $^{\circ}F$

$\ell =$ drift tube length, 17.523 in.

$k_{cu} =$ coefficient of thermal expansion for copper, 9.8×10^{-6} in./in. $^{\circ}F$

For the cavity calculations the coefficient of expansion for steel is used (8.4×10^{-6} in./in. $^{\circ}F$).

The following temperature stability requirements are obtained.

$\Delta T_{s\ell} = 4.37\ ^{\circ}F$

$\Delta T_{sD} = 5.59\ ^{\circ}F$

$\Delta T_{sd} = 19.4\ ^{\circ}F$

$\Delta T_{sL} = 15.6\ ^{\circ}F$.

The limiting tolerance is that on the drift tube length. With a safety factor of 2 in mind, it appears that the water temperature will have to be controlled within 2 $^{\circ}F$.

Drift Tube Cooling

Figure C8 illustrates the cooling passages for the drift tubes.

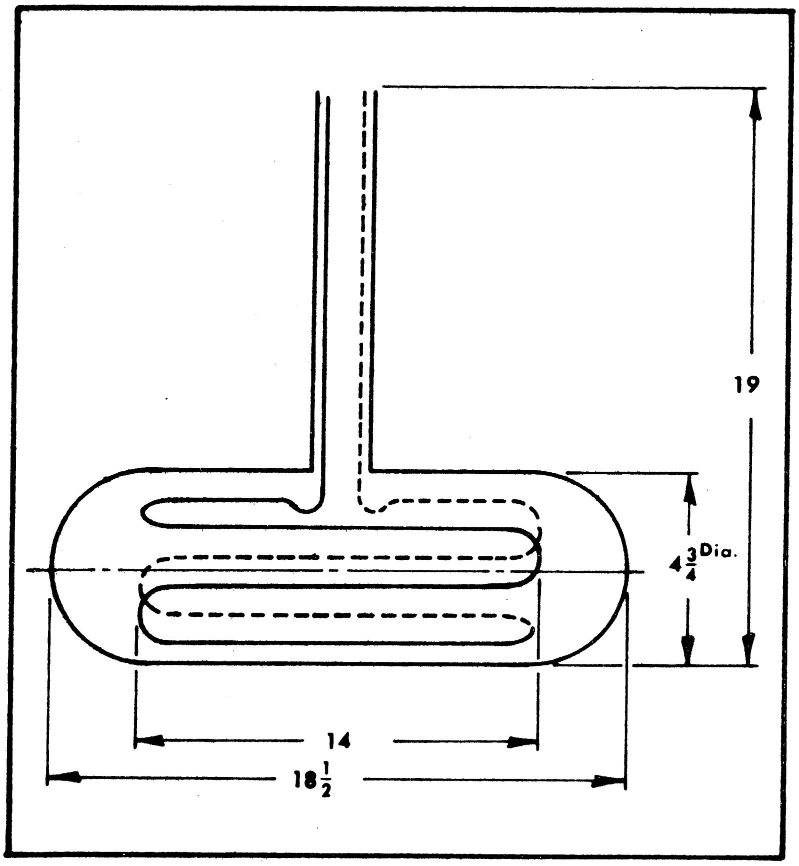

FIG. C8

Power dissipated in each drift tube is 1.6 kW. A temperature rise in the water of not more than 4 °F is desirable. The flow is then

$$W = \frac{Q}{C_p \Delta T} \qquad (C.14)$$

where

W = flow rate, lb/hr

C_p = specific heat, Btu/lb ^{o}F

Q = heat rate, $\frac{\text{Btu}}{\text{hr}}$

ΔT = temperature change, ^{o}F

for our example

$$Q = 1.6 \text{ kW} \times 3413 \frac{\text{Btu}}{\text{kW hr}}$$

$$C_p = 1$$

$$\therefore W = \frac{1.6 \times 3413}{1 \times 4} = 1365 \text{ lb/hr}$$

for gallons per minute

$$\frac{1365}{60 \frac{\text{min}}{\text{hr}} \; 8.34 \frac{\text{lb}}{\text{gal}}} = 2.73 \text{ gpm} .$$

The size of the tubing is 3/8 in. O.D. x 0.035 in. wall, which gives a velocity of 12 fps and a pressure drop of 20 psi.

In order to determine the operating average temperature of the drift tube, one has to calculate a "heat transfer coefficient h ." This coefficient is the predominant resistance to the flow of heat and is large compared to the resistance of the copper tubing. We will then, for simplicity, neglect the resistance of the copper.

For turbulent flow, the heat transfer coefficient can be determined with sufficient accuracy by McAdams equation[23]

$$\frac{hs}{k} = 0.023 \, (N_{RE})^{0.8} \, (N_{PR})^{0.4} \, , \tag{C. 15}$$

where

h = coefficient of heat transfer, $\frac{\text{Btu}}{\text{ft}^2\ \text{hr}\ {}^\circ\text{F}}$

s = tube diameter, ft

k = thermal conductivity of fluid, $\frac{\text{Btu}}{\text{hr ft}\ {}^\circ\text{F}}$

N_{RE} = Reynold's number, $\frac{v\ s\ \rho}{}$

N_{PR} = Prandtl number, $\frac{\mu C_p}{k}$

v = velocity, $\frac{\text{ft}}{\text{sec}}$

ρ = weight density, $\frac{\text{lb}}{\text{ft}^3}$

μ = dynamic viscosity, $\frac{\text{lb}}{\text{hr ft}}$.

When $N_{RE} > 3000$, the flow is turbulent. In this example

$$N_{RE} = \frac{v\ s\rho}{\mu} = \frac{12\ \frac{0.305}{12}\ 62.4\ (3600)}{2.36}$$

$$= 29,000 \text{ and Eq. (C.15) applies}$$

N_{PR} is a function of fluid property and in this case is 6.86

$$h = \frac{k}{s}\ (0.023)\ (29,000)^{0.8}\ (6.86)^{0.4}$$

$$h = 2500\ \frac{\text{Btu}}{\text{hr ft}^2\ {}^\circ\text{F}}\ .$$

The length of tube is estimated to be 90 in. Area in contact with the fluid is then $\frac{3.142 \times 0.305 \times 90}{144} = 0.6\ \text{ft}^2$.

Total power transferred to coolant is

$$Q = hA\ \Delta T_m \ \text{Btu/hr}$$

where ΔT_m is the logarithm mean temperature difference and is defined as

$$\Delta T_m = \frac{(T_a - Tw_i) - (T_a - Tw_o)}{\ln \dfrac{T_a - Tw_i}{T_a - Tw_o}} \qquad \text{(C.16)}$$

where

ΔT_m = mean temperature differences, ^oF

T_a = average temperature of drift tube, ^oF

Tw_i = inlet water temperature, ^oF

Tw_o = outlet water temperature, ^oF

$$\Delta T_m = \frac{1.6 \times 3413}{0.6 \times 2500} = 3.64\ ^oF .$$

The process on a temperature diagram is shown in Fig. C9.

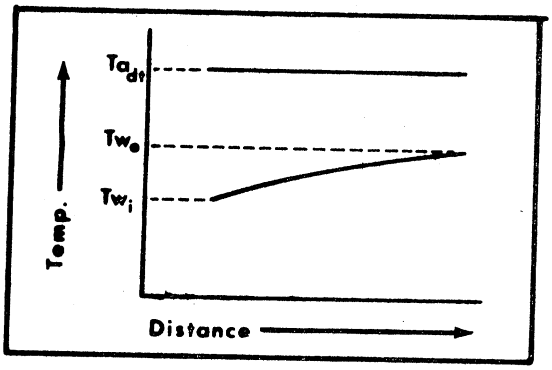

FIG. C9

For the drift tube

$$\Delta T_m = \frac{(T_a - 73) - (T_a - 77)}{\ln\left(\frac{T_a - 73}{T_a - 77}\right)} = 3.64\ ^oF$$

solving for T_a, $T_a = 79\ ^oF$. The average drift tube temperature will be $79\ ^oF$.

Cooling the Linac Cavity

The total power dissipated in the cavity is 2.5 kW. It is cooled by water circulating in 2 x 1 x 3/16 channels which are welded along the length of the cavity. There are four loops, each loop consisting of five passes so that all the inlet connections are at one end of the cavity and the outlet connections at the other. This way 0.625 kW are dissipated in each loop. Water flow, F_w in gpm, can be calculated from the following:

$$F_w = \frac{Q}{\Delta T \times 8.34 \text{ Btu}/{}^\circ\text{F gal } 60 \text{ min/hr}} \qquad \text{(C.17)}$$

where

Q = total power dissipated, Btu/hr

8.34 = Btu's required per $^\circ$F rise per gallon

ΔT = temperature change per $^\circ$F .

If a temperature rise of 1.5 $^\circ$F/loop is desired, the flow is

$$F_w = \frac{0.625 \times 3413}{1.5 \times 8.34 \times 60} = 2.84 \text{ gpm} .$$

To be able to use the same heat transfer equations for rectangular channels, we calculate a hydraulic diameter which is 1.08 in. in this case. This value gives

Velocity = 0.7 fps

$N_{RE} = 6000$

$h = 560 \frac{\text{Btu}}{\text{hr ft}^2 \, {}^\circ\text{F}}$

$\Delta T_m = 1 \, {}^\circ\text{F}$

and the average temperature of the cavity is 75 $^\circ$F.

It is of interest to note that the warmest region on the cavity is on the inside radius between cooling channels and is ~2.5 °F over the temperature calculated above.

Cooling the Linac Cavity End Plates

The end plates of the cavity are cooled with 3/8 in. copper tubing which is coiled and soldered on the plate. The tube length is 220 in.; power dissipated is 0.75 kW. The temperature rise in the water was picked to be 2 °F in an attempt to match the average temperature of the plates to the cavity.

Water flow = 2.56 gpm

Velocity = 11.3 fps

$N_{RE} = 26,000$

$h = 2.337 \frac{\text{Btu}}{\text{hr ft}^2\ {}^{\circ}\text{F}}$

$\Delta T_m = 0.75\ {}^{\circ}\text{F}$.

The average temperature of the end plate will be 75.2 °F .

The total water flow for three drift tubes, two end plates and one cavity is 24.7 gpm and the temperature rise is ~2.2 °F. In Fig. C10 a schematic of the cooling loop is presented.

Heat Exchanger Size

Assume a 5 gpm flow on the shell side, with a ΔT of 12 °F .

$$T_m = \frac{18 - 8}{\ln \frac{18}{8}} = 12.34\ {}^{\circ}\text{F}$$

$$Q = UA\Delta T_m \frac{\text{Btu}}{\text{hr}} \quad \text{where } U \approx 150 \frac{\text{Btu}}{\text{hr ft}^2\ {}^{\circ}\text{F}} \quad \text{and } Q = 8.8 \frac{\text{Btu}}{\text{hr}}$$

$$A = \frac{8.8 \times 3413}{150 \times 12.34} \approx 16 \text{ ft}^2 .$$

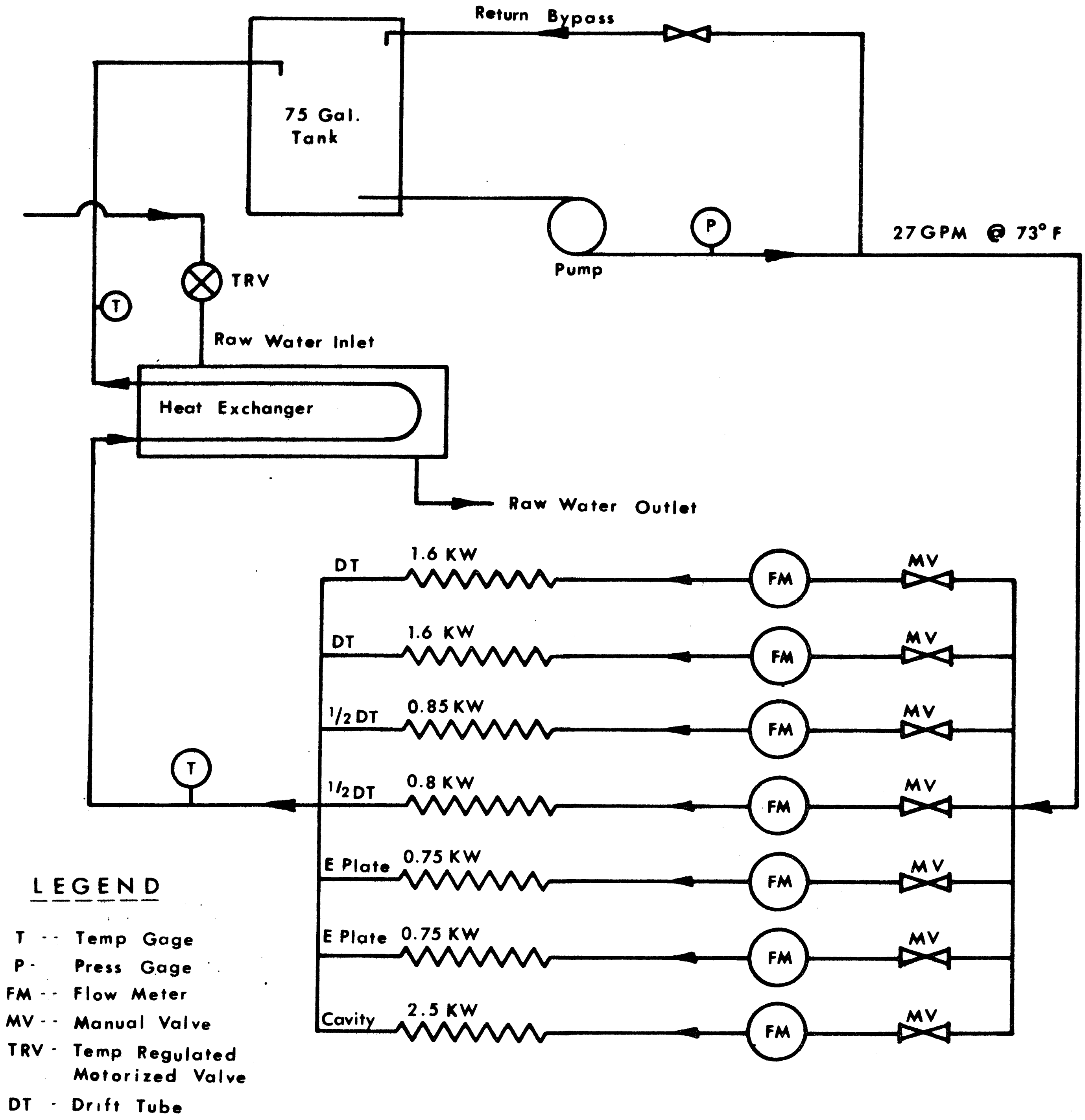
Return Bypass
75 Gal. Tank
Pump
P
27GPM @ 73° F
TRV
T
Raw Water Inlet
Heat Exchanger
Raw Water Outlet
DT 1.6 KW
DT 1.6 KW
1/2 DT 0.85 KW
1/2 DT 0.8 KW
E Plate 0.75 KW
E Plate 0.75 KW
Cavity 2.5 KW
FM
MV
LEGEND
T -- Temp Gage
P - Press Gage
FM -- Flow Meter
MV -- Manual Valve
TRV - Temp Regulated Motorized Valve
DT - Drift Tube

FIG C10

Time Needed for Reaching Operating Temperature

It is interesting to calculate the length of time it will take the linac to reach operating temperature after it is turned on. The approximate mass and pertinent quantities involved are:

Item	Mass (lb)	C_p (Btu/lb $^{\circ}$F)	Q (ΔT of 1 $^{\circ}$F)
Steel	4,500	0.11	495
Copper	500	0.094	47
Water	800	1.00	800
		Total	1342 Btu/$^{\circ}$F

Assume 20% is lost due to connection and radiation, then $\approx$ 1600 Btu are needed to raise the temperature 1 $^{\circ}$F. If the raw water in the heat exchanger is not turned on until the closed loop water reaches 73 $^{\circ}$F, then the time it will take the linac cavity to warm up 1 $^{\circ}$F is

$$\frac{1600 \times 60}{8.8 \times 3413} = \frac{1600}{500} \approx 3 \text{ min} .$$

STRESS ANALYSIS OF THE MURA 8.3-FT LONG, 200 MEV LINAC CAVITY[*]

Dimensional changes of a linac cavity are of particular importance, because they affect the resonance and electrical characteristics of the cavity. Since the cavity is under vacuum, it is important to determine the collapsing pressure, maximum stress and maximum deflection.

Analysis

The following assumptions are made:

---

[*] These calculations are based on similar calculations done by Igor Sviatoslavsky, MURA.

1. The shell is a round cylinder before buckling.
2. It is of uniform thickness throughout.
3. The material is homogeneous, isotropic and elastic according to Hooke's law.
4. Thickness of the shell is small compared to the diameter.
5. Radial stresses are negligible compared to circumferential and longitudinal stresses.
6. Deflections are small compared to the thickness.

The cylinder will be constructed from copper clad steel 0.5-in. thick, copper thickness being 0.063 in. Length is 99.96 in. and I.D. is 33.46 in.

Critical collapsing pressure is calculated with data obtained by the University of Illinois Engineering Experiment Station.

$$W_c = K E \left(\frac{t}{D}\right)^3 \qquad (C.18)$$

where K is a constant obtained from a graph in Report No. 12 (November 11, 1941) of the Illinois Engineering Experiment Station and is a function of $\frac{D}{t}$ and $\frac{L}{R}$, and where

E = Young's modulus, 30×10^6 psi for steel

t = wall thichness, in.

D = diameter of the cavity, in.

K = 8.0

$$W_c = (8)(30 \times 10^6)(0.0131)^3$$

$$= 540 \text{ psi};$$

from the same graph we obtain $N = 3$ which is the number of nodes into which the cylinder tends to collapse. These values are for simply supported edges and for $\mu = 0.30$ (Poisson's ratio). We further assume that the copper lends no support.

Assuming an out of roundness (A_o) of ± 0.125, total deflection (A) is given by

$$A = \frac{W\,A_o}{W_c - W} \tag{C.19}$$

$$A = \frac{(14.7)\,(0.125)}{540 - 14.7} = \frac{1.837}{525.3} = 0.0035 \text{ in.}$$

where W is atmospherical pressure = 14.7 psi. Maximum out of roundness is then

$$0.125 + 0.0035 = 0.1285 \text{ in.}$$

Maximum moment is given by

$$M_s = \frac{EI}{1 - \mu^2}\left[\frac{N^2 - 1}{R^2} + \mu\frac{\pi^2}{L^2}\right] A \tag{C.20}$$

$$= \frac{30 \times 10^6}{12}\;\frac{(0.437)^3}{1 - (0.3)^3}\left[\frac{3 - 1}{(17)^2} + (0.3)\,\frac{(3.142)^2}{(99.9)^2}\right]\;0.0035$$

where

$R = D/2$

$I = \frac{bd^3}{12}$

where

I = moment of inertia for the wall

b = a unit length, in.

d = thickness of the steel .

M_s = 23 in. lb from which the maximum bending stress is

$$S_2 = \frac{M_s\, t}{2\, I}$$

$$= \frac{23\ (0.437)}{2\ (0.0835)}\ (12) = 722 \text{ psi} .$$

Maximum hoop stress is

$$S_1 = \frac{WR}{t}$$

$$= \frac{(14.7)\ (17.2)}{(0.437)} = 578.6 \text{ psi} .$$

Total stress

$$S_1 + S_2 = S = 1300.6 \text{ psi} .$$

Assuming a 10 °F temperature gradient in the wall of the cylinder, a thermal stress can be obtained from

$$S_{TH} = \frac{\alpha E\ (\Delta T)}{2\ (1 - \mu\ )} \qquad (C.21)$$

where α is coefficient of expansion.

$$S_{TH} = \frac{(8.4 \times 10^{-6})\ (30 \times 10^{6})\ (10)}{2\ (1 - 0.3)} = 1800 \text{ psi} .$$

Maximum total stress is then 3100 psi .

Results and Conclusions

1. Critical collapsing pressure = 540 psi .
2. Maximum stress (including thermal) = 3100 psi .
3. Maximum deflection assuming a ± 0.125 in. out of roundness = 0.0035 in.

The cylinder has a wide margin of safety in regards to collapsing pressure and since drift tube alignment in this model is not critical, the deflection is acceptable.

REFERENCES

1. Considerable activity in this area existed with the group at Harwell, England who had been designing a 600 MeV linac, e.g., J. J. Wilkins, "Design of RF Resonant Cavities for Acceleration of Protons from 50 to 150 MeV", P.L.A.C. 11 (1955).
2. J. Van Bladel, MURA Report No. 481 (1959) or, IRE Transactions on Microwave Theory and Techniques MTT-8, 309 (1960).
3. T. Edwards, "Proton Linear Accelerator Cavity Calculations", MURA Report No. 622 (1961, unpublished).
4. F. J. Kriegler and T. Edwards, "Comparison of Linear Accelerator Calculations", MURA Report TN-429 (1963, unpublished).
5. D. Swenson, B. Austin, and D. Stauffacher, "'LINDY', A Linac Ion Dynamics Program", MURA Report TN-517 (1964, unpublished).
6. L. Smith, Handbuch der Physik, Vol. 44, 368 (1959).
7. D. E. Young et al., Proceedings of the International Conference on High Energy Accelerators (Dubna, USSR 1963), p. 454.
8. G.W. Wheeler, "The Electric Field and Cost Minimization in Linear Accelerators", Yale Internal Report GW-1 (1962, unpublished).
9. A. Carne, "Cost Optimization in the Design of a 200 - 250 P.L.A.", P.L.A. Acc. Phys. 14 (unpublished).
10. A. Carne and K. Batchelor, "Design of a High Current 200 MeV Proton Linear Accelerator", NIRL/R/55 (1964).
11. Private communication from BNL on the AGS injector costs.
12. Private communication from ANL on the ZGS injector costs.

REFERENCES (continued)

13. See for example, "Informal Discussion of Sparking Phenomena", 1964 Linear Accelerator Conference MURA Report 714, p. 606 (1964).

14. W. D. Kilpatrick, "A Criterion for Vacuum Sparking Designed to Include Both R. F. and D. C.", UCRL-2321 (1953).

15. C. W. Owen, C. A. Radmer, and D. E. Young, "Preliminary Sparking and X-Ray Phenomena in a 200 Mc Linac Cavity", MURA Report TN-535 (1965, unpublished).

16. LASL private communication from Freyman to D. Hagerman, "Review of Frequency Assignments."

17. Minutes of the Meeting of the Drift Tube Subcommittee of the Linac Coordination Committee held at MURA May 27, 1964.

18. J. P. Blewett, "Phase Acceptance and Bunching in the AGS Linac", Internal BNL Report JPB-18 (1963).

19. L. Smith and R. L. Gluckstern, "Focussing in Linear Ion Accelerators", Rev. Sci. Instr. 26, 220 (1955).

20. D. Cohen, "Radial Motions in the 50 MeV Linear Accelerator", Internal ANL Report, ANLAD-57 (1959).

21. J. C. Slater, Rev. Mod. Phys. 20, 473 (1948).

22. D. A. Swenson, "Application of Calculated Fields to the Study of Particle Dynamics", 1964 Linear Accelerator Conference Proceedings MURA Report 714, p. 328 (1964).

23. Heat Transmission, McGraw-Hill (1954).